ABSTRACT

TEMPORAL SYNCHRONIZATION OF CA1 PYRAMIDAL CELLS BY HIGH-FREQUENCY, DEPRESSING INHIBITION, IN THE PRESENCE OF INTRACELLULAR NOISE

by
Stephen A. Kunec

The Sharp Wave-associated Ripple is a high-frequency, extracellular recording observed in the rat hippocampus during periods of immobility. During the ripple, pyramidal cells synchronize over a short period of time despite the fact that these cells have sparse recurrent connections. Additionally, the timing of synchronized pyramidal cell spiking may be critical for encoding information that is passed on to post-hippocampal targets. Both the synchronization and precision of pyramidal cells is believed to be coordinated by inhibition provided by a vast array of interneurons. This dissertation proposes a minimal model consisting of a single interneuron which synapses onto a network of uncoupled pyramidal cells. It is shown that fast decaying, high-frequency, depressing inhibition is capable of rapidly synchronizing the pyramidal cells and modulating spike timing. In addition, these mechanisms are robust in the presence of intracellular noise. The existence and stability of synchronous, periodic solutions using geometric singular perturbation techniques are proven. The effects of synaptic strength, synaptic recovery, and inhibition frequency are discussed. In contrast to prior work, which suggests that the ripple is produced by homogeneous populations of either pyramidal cells or interneurons, the results presented here suggest that cooperation between interneurons and pyramidal cells is necessary for ripple genesis.

TEMPORAL SYNCHRONIZATION OF CA1 PYRAMIDAL CELLS BY HIGH-FREQUENCY, DEPRESSING INHIBITION, IN THE PRESENCE OF INTRACELLULAR NOISE

by
Stephen A. Kunec

A Dissertation
Submitted to the Faculty of
New Jersey Institute of Technology and
Rutgers, The State University of New Jersey – Newark
in Partial Fulfillment of the Requirements for the Degree of
Doctor of Philosophy in Mathematical Sciences

Department of Mathematical Sciences
Department of Mathematics and Computer Science, Rutgers-Newark

May 2002

APPROVAL PAGE

TEMPORAL SYNCHRONIZATION OF CA1 PYRAMIDAL CELLS BY HIGH-FREQUENCY, DEPRESSING INHIBITION, IN THE PRESENCE OF INTRACELLULAR NOISE

Stephen A. Kunec

Dr. Amitabha Bose, Dissertation Advisor — Date
Associate Professor of Mathematical Sciences, NJIT

Dr. Denis Blackmore, Committee Member — Date
Professor of Mathematical Sciences, NJIT

Dr. Victoria Booth, Committee Member — Date
Assistant Professor of Mathematical Sciences, NJIT

Dr. Gyorgy Buzsaki, Committee Member — Date
Professor II of the Center for Molecular and Behavioral Neuroscience, Rutgers-Newark

---

Dr. Farzan Nadim, Committee Member — Date
Associate Professor of Mathematical Sciences, NJIT and Associate Professor of Biological Sciences, Rutgers-Newark

BIOGRAPHICAL SKETCH

Author: Stephen A. Kunec

Degree: Doctor of Philosophy

Date: May 2002

Undergraduate and Graduate Education:

- Doctor of Philosophy in Mathematical Sciences,
  New Jersey Institute of Technology and Rutgers-Newark, Newark, NJ, 2002
- Master of Science in Applied Mathematics,
  New Jersey Institute of Technology, Newark, NJ, 1999
- Bachelors of Science in Mathematics,
  Lafayette College, Easton, PA, 1997

Major: Mathematical Sciences

Presentations and Publications:

S. Kunec and A. Bose,
"Role of synaptic delay in organizing the behavior of networks of self-inhibiting neurons,"
Physical Review E, Vol. 63, 0219081-13, 2001.

A. Bose and S. Kunec,
"Synchrony and frequency regulation by synaptic delay in networks of self-inhibiting neurons,"
Neurocomputing, Vol. 38-40, pp.505-513, 2001.

SUCCESS

To laugh often and much;
to win the respect of intelligent people and
the affection of children;
to earn the apprecitation of honest critics and
endure the betrayal of false friends;
to appreciate beauty, to find the best in others;
to leave the world a bit better,
whether by a healthy child,
a garden patch or
a redeemed social condition;
to know even one life has breathed easier
because you have lived.

This is to have succeeded.

– Attributed to Ralph Waldo Emerson

ACKNOWLEDGMENT

I would like to thank my advisor, Dr. Amitabha Bose, for guiding me in the right direction and for being patient with me. I also wish to extend thanks to my dissertation committee, Dr. Farzan Nadim, Dr. Denis Blackmore, Dr. Gyorgy Buzsaki and Dr. Victoria Booth, for taking time out of their busy schedules and spending it with me.

I received funding from the NJIT Department of Mathematical Sciences and from the National Science Foundation, Grant NSF-DMS 9973230. Thank you for the financial support.

Along the way, various people have helped me with the technical side of getting my dissertation completed: Irene Giouvanos deserves thanks for fixing all the little things that I found not working in the computer labs and for getting those problems fixed. Dr. Darrell Henze answered many questions about neuroscience when I could not find a particular reference. An extra special thanks goes to Dr. Bard Ermentrout, who provided me with a way to add tables of data to my XPP program and who wrote the program in the first place. Dr. Adrienne James and Dr. Jerry Chen get thanks for adapting and updating the dissertation LaTeX style file for me and for future generations of NJIT Mathematical Sciences graduate students. I must give thanks to Dr. Gregory Kriegsmann for recruiting me and believing I could succeed here at NJIT and Dr. Arthur Gorman who suggested I apply to NJIT. I also wish to say thank you to Carol Ross, Susan Sutton, Monica Figueroa and Lilana Boland for all the help they gave me, despite all the other work they had to do. And last, but not least, Padma Gulati derserves my thanks for getting me accees to Cullimore on weekends, for helping to get computers fixed, for being understanding, for offering help when I needed it the most and for a bunch of other things it would take too long to mention.

Among those who I consider peers, I wish to say thank you to Hoa Tran for many things, such as helping me with LaTeX, discussing mathematics, and giving me moral support. Said Kas-Danouche also gave me support and is an all-around nice guy. I wish him good luck. Here are some other friends that I give my thanks to: Jennifer White, Lyudmyla Barannyk, Michelle Debonis, Brandy Rapatski, Arnaud Goullet, Eliana Antoniou, Ray Addabbo, Urmi Ghosh-Dastidar, Jyoti Champanerkar and Nick Kintos. I have probably forgotten many more. I hope you are not mad at me.

TABLE OF CONTENTS

TABLE OF CONTENTS
(Continued)

Chapter **Page**

LIST OF FIGURES

LIST OF FIGURES
(Continued)

Figure **Page**

LIST OF FIGURES
(Continued)

Figure **Page**

CHAPTER 1

INTRODUCTION

The brain is one of the last frontiers of modern science. Much time and effort has been put into unlocking the mysteries of the mind and its inner workings, spanning centuries of time. Some theories have endured and some have not. For example, in the eighteenth century, Ramón y Cajal proposed the *neuron doctrine*, the principle that the brain consists of "signaling elements," connected at specialized points. Later on, two opposing theories of brain function were offered. The *aggregate field* view suggested that all parts of the brain could perform the same function and that damage to one part of the brain affected the rest of the brain equally. *Cellular connectionists* believed that particular behaviors are controlled by localized regions in the brain, connected by neural pathways. The latter of these two theories is generally held today. Another, more fashionable yet fallacious theory, as seen in Figure 1.1, was called *phrenology*, which hypothesized that the bumps on a person's skull determined which brain functions were more developed [26].

The brain, together with the spinal cord, constitutes the central nervous system. It controls many aspects of our bodily function, including movement, breathing, heart rate, visual and auditory reflexes and memory storage [26]. Within the central nervous system, two types of specialized cells are found, known as *neurons* and *glial cells*. The brain contains on the order of 10^{11} neurons and about 10 times more glial cells.

Glial cells differ from neurons in that they are probably not involved in processing information. However, glial cells have other important functions. Microglia clean debris produced by neuronal injury or death. Macroglia cells known as *astrocytes* help insulate and separate other neurons, buffer K^+ ion concentrations and remove chemical transmitters released during the use of synapses. Astrocytes may even be involved in providing nutrients to neurons. Macroglia cells known as *oligodendrocytes*

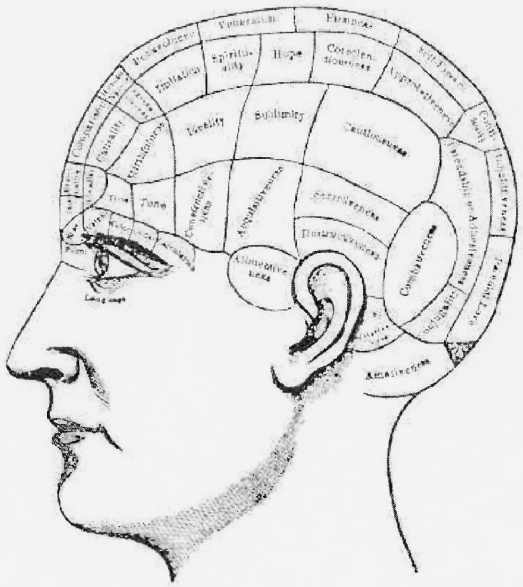

Figure 1.1 The "Science" of Phrenology, which proposed that bumps in particular areas of the skull indicated more development in those brain regions [26].

and *Schwann cells* form myelin, which insulates large axons. Glial cells as provide support and firmness to the brain, as well as guiding neuron migration and directing axon outgrowth [26].

Though there are many types of neurons in the brain, this dissertation will focus on those called *bipolar neurons*, as shown in Figure 1.3. The *soma*, or cell body, contains the nucleus, the "brain" of the neuron. Typically, the *axon* extends from the soma, ready to transmit action potentials to the neighboring neurons. Other processes leading into the soma are called *dendrites*. They receive action potentials sent from other neurons.

Synapses are commonly located at the end of axons. Here, electrical impulses are passed from one neuron to the next across the *synaptic cleft*, a small gap between the presynaptic axon and the dendrites of the postsynaptic cell. Since each neuron makes about 1000 synapses, the brain contains about 10^{14} synapses. Generally, neurons can

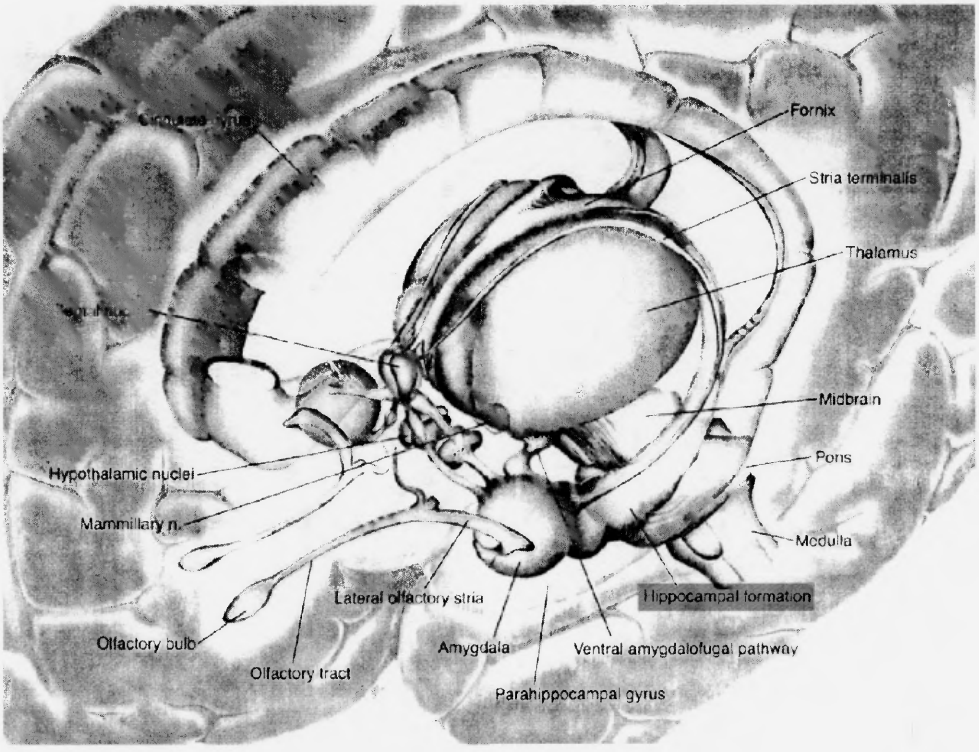

Figure 1.2 The Interior of the brain, showing various structures, including the hippocampus. Taken from http://mbdefault.org/6_memory/

be divided into two types, depending on the type of synapse they make. *Excitatory* synapses increase a cell's probability of firing an action potential. *Inhibitory* synapses cause the opposite effect, decreasing a cell's probability of producing a spike.

This dissertation refers to two groups of neurons. The first type makes excitatory synapses onto other cells and are called *pyramidal cells*. The second type are *interneurons* and they make inhibitory connections onto other cells.

One particular area of brain research revolves around our ability to learn and remember. It is generally thought that the area of the brain directly related to these tasks is the hippocampus. The hippocampus is a part of the limbic system, which is responsible for other processes like generating emotions [26]. Interesting facts have been learned regarding the hippocampus. "Place" cells, found within the hippocampus, are thought to encode information about particular locations in space

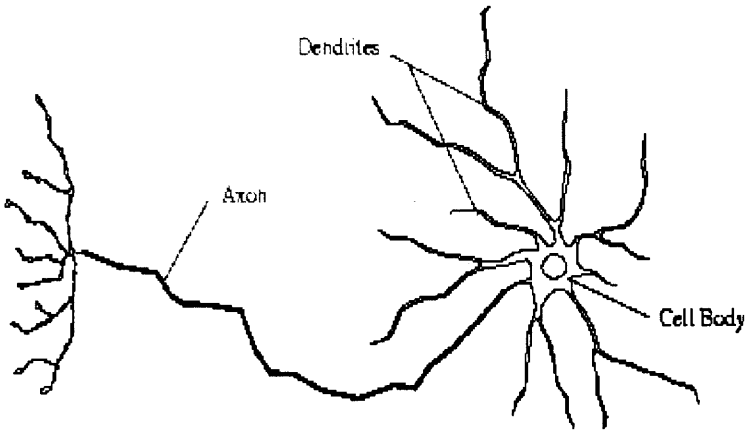

Figure 1.3 Simple Diagram of a Bipolar Neuron. Taken from "Synapse Web" at http://synapses.bu.edu/anatomy/dendrite/dendrite.stm

[36]. Experiments on rats have shown that the hippocampus also plays a role in odor discrimination [11]. In some human cases of hippocampal damage, the subjects had problems forming new episodic memories (those learned through experience) [48]. Lastly, it is thought that the hippocampus also takes a part in memory retrieval processes [44].

Different types of rhythms are experimentally recorded from the hippocampus, such as theta ($4 - 12$ Hz) and gamma ($40 - 100$ Hz) oscillations. The theta rhythm is observed during exploratory behaviors and is believed to be involved in memory storage and long-term potentiation, a form of synaptic plasticity [24]. Gamma oscillations are seen in the hippocampus in conjunction with sensory input [3].

Another intriguing oscillation, which is the motivation behind this research, is the *Sharp Wave-associated Ripple* (SPWR). Figure 1.4 depicts two different SPWRs recorded from a rat hippocampus during slow-wave sleep. The extracellular ripple is a high-frequency oscillation that discharges at a frequency of $140 - 200$ Hz and is typically observed during immobility, sleep, and consummatory behaviors [50]. The SPWR is thought to be brought about by a concentrated, excitatory event initiated in the CA3 region of the hippocampus, which travels across the Schaffer collaterals and

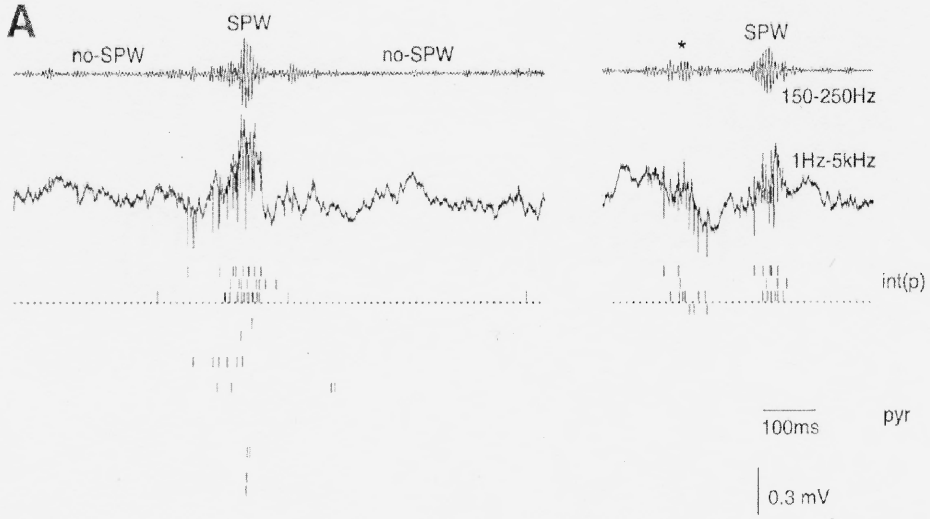

Figure 1.4 Two experimentally recorded ripples from the CA1 region of a mouse during slow-wave sleep. The top recording displays $150 - 250$ Hz frequencies. The middle recording shows a broadband recording, that includes frequencies $1 - 5000$ Hz. Above the dotted line are the action potentials of three different interneurons located in the pyramidal cell layer. Below the dotted line are the action potentials for 15 different pyramidal cells [9].

stimulates the CA1 network [6]. In contrast to the CA3 region, the CA1 region has very sparse connectivity [8]. Figure 1.5 depicts a schematic of the rat hippocampus, showing the relative locations of the CA3 and CA1 regions.

The cycle is initiated by the synchronous discharge of a large number of CA3 pyramidal cells. This is thought to be accomplished through the rich, recurrent collateral system between CA3 pyramidal cells. The concentrated amount of excitation, or sharp wave (SPW), travels along the Schaffer collaterals, then inundates several sites in the CA1 region. As a result, $0 - 40\%$ (on average 10%) of the total population of pyramidal cells fire during a ripple throughout the CA1 region. The probability of an individual pyramidal cell firing during a ripple varies from rarely to 40%. Also, pyramidal cell firing tightly correlates to the negative peak of the local field oscillation being recorded from the pyramidal cell layer, as depicted in Figure 1.6.

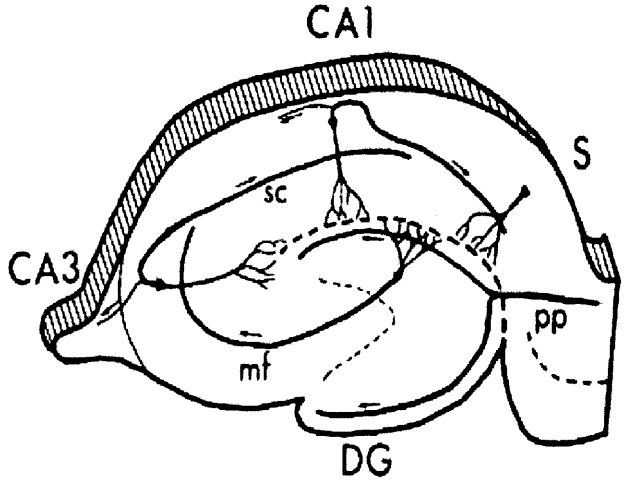

Figure 1.5 Diagram of the rat hippocampus, showing the CA3 and CA1 regions, connected by the Schaffer collaterals (SC). Taken from http://mbdefault.org/6_memory/default.asp

In general, due to SPW excitation, interneurons fire during every ripple event. Some individual interneurons fire during almost every ripple. Those interneurons that discharge during the SPWR maintain an oscillation frequency of $150 - 250$Hz for the entire length of the ripple [50]. Interneurons preferentially fire $0 - 2$ msec after the pyramidal cells, but on average begin to fire earlier than the pyramidal cells at the start of the ripple [9].

Both populations contribute to the recorded extracellular, measurable event during the SPWR. The pyramidal cells synchronize both temporally and spatially across the the CA1 region, firing only several times during the event. Also, interneurons synchronize rapidly during the first few moments of the Sharp Wave excitation [6]. The entire sharp wave, and therefore the ripple, takes about $40 - 120$ msec to complete, while the time between SPWRs is $0.02 - 3$ sec. The SPWR eventually ends, perhaps due to the end of sharp wave input from CA3 and/or through interaction between pyramidal cells and interneurons. The ripple's importance is still debated, though evidence suggests that it helps to coordinate and synchronize

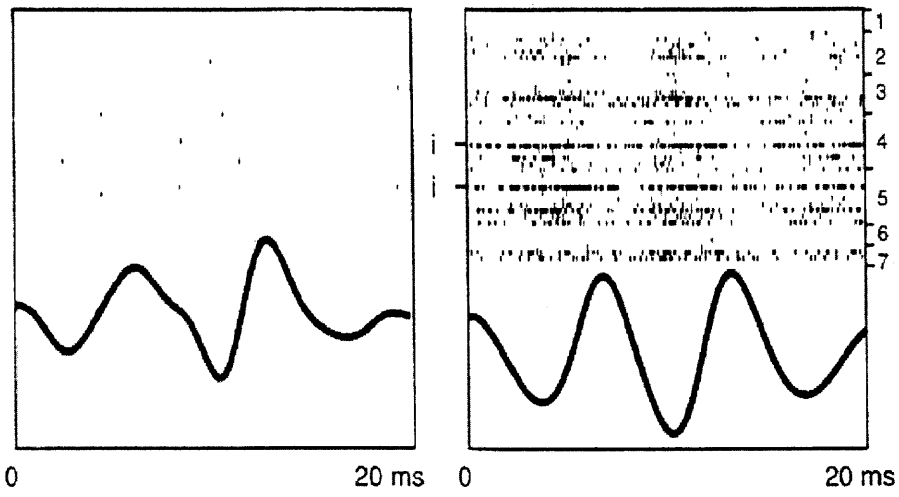

Figure 1.6 Extracellular Field Recording in the Pyramidal Cell Layer. Left figure is a single ripple event. Right figure is an average field event with superimposed spikes from seven different recording sites. 40 simultaneous pyramidal cells and 2 interneurons (labeled i) were recorded [50].

networks of neurons in the hippocampus [4] and may play a role in synaptic plasticity [5, 28].

Despite knowing much about the SPWR, the process whereby the SPWR generates, operates and terminates is being debated by neuroscientists. It is thought to be a network-formed rhythm, not brought about through the interaction of intrinsic membrane currents. One idea is that there are two competing effects during the ripple [50]: dendritic excitation from the CA3 region and somatic inhibition from interneurons excited by CA3 input. The most important of these is the inhibition of the CA1 pyramidal cells. The oscillating interneurons produce fast fluctuation of the membrane potential in CA1 pyramidal cells. This affects the timing of action potentials produced by CA1 pyramidal cells, recruiting them to fire synchronously during the population oscillation. This recruitment is thought to occur as follows: CA3 input causes interneurons to fire at ripple frequency. These interneurons affect the timing of pyramidal cell action potentials, causing some to synchronize. When the synchronized pyramidal cells fire, they reset the phase of their interneuron targets

in time for the next cycle of the ripple. It is important to note that no single site leads these oscillations. However, the timing is a result of pyramidal cell synchronization.

Another theory hypothesizes that ripples arise from the network of pyramidal cells, connected by axo-axonal gap junctions [46]. Between sharp wave events, distal axons are hyperpolarized, suppressing ectopic spikes (spontaneously firing action potentials) in the CA1 network. As the input from CA3 arrives, axon membrane potentials across the CA1 region increase, allowing these ectopic spikes to occur. There, spikes propagate down the axons (and sometimes in reverse up the axon to the soma), causing pyramidal cells to fire, and so on. A wave of activity quickly spreads across the pyramidal cell network, causing the high frequency oscillation observed during the ripple. The rapid spread of activity is achieved through chains of the axon-to-axon gap junctions, which allow the action potentials to directly cross from one axon to another. The interneurons fire at a high rate, some at ripple frequency, due to the excitation from the pyramidal cell network. Interneurons play little to no role in ripple generation in this model.

The main purpose of this dissertation is to understand the neural mechanisms responsible for synchronization and spike timing of pyramidal cells in the CA1 region during the SPWR. As discussed previously, pyramidal cells in CA1 are sparsely connected and receive two different kinds of synaptic input: excitation from the CA3 region and high-frequency inhibition from interneurons in the CA1 region. We will show that excitation alone is not sufficient to synchronize pyramidal cells. Rapid pyramidal cell synchronization during the initial stages of the SPWR can be accomplished through the high-frequency inhibition applied by the interneurons, something low-frequency inhibition may not be able to do over such a small interval of time. The ability to produce action potentials and the timing of the action potentials produced by CA1 pyramidal cells during the ripple is shown to be dependent on the frequency of the inhibition and on depressing synapses from the interneurons to the

pyramidal cells, as well as the timing of the Sharp Wave excitation. These conclusions support the explanation proposed by [50], that interneuron-pyramidal cell interaction produces the ripple.

Action potential timing and synchronization is theorized to be also dependent on intrinsic noise, possibly caused by sodium channel inactivation. While this noise cannot be avoided, certain "biological parameters" may be modulated to increase the precision between pyramidal cells receiving the same inhibition and to improve their chances of firing under these circumstances. Specifically, increasing the amount of synaptic depression is shown to improve the ability of noisy pyramidal cells to produce an action potential during the SPWR.

Geometric, singular perturbation theory is utilized throughout this work. This method takes advantage of a small parameter, say ϵ, present in the mathematical equations and considers the system when ϵ equals zero. In this singular limit, the periodic motion of neurons can be broken down into sequences of "slow" motions (the cell in the silent state and the decay of the inhibitory synapse), and "fast" jumps (while the cell produces action potentials and the rise of synaptic inhibition). While in the "slow" and "fast" regimes, the spiking model reduces from a three-dimensional system to more manageable two-dimensional configurations. The cell's dynamics are then analyzed in various two-dimensional, and sometimes one-dimensional, phase spaces, where issues of spike timing and synchronization can be visualized. It is shown in [32] that the results proven for $\epsilon = 0$ also hold for ϵ near zero. This technique is commonly used in mathematical neuroscience and further examples of its use can be found in such works as [2, 29, 37, 38, 42, 43].

Using this theory, the existence and stability of two types of periodic solution in the sub-network are proven. The synchronous solutions are treated as the limits of a sequence of synaptic strengths along a single phase line. This differs from other sources that use contraction mapping techniques to show stability and uniqueness

[29, 43]. The type of synchronous solution is shown to be primarily dependent on the period of the inhibition applied to the pyramidal cells. Additionally, a mechanism for time compression is introduced and is found to be integral to the synchronization of the pyramidal cells. Probability theory is invoked to numerically compute confidence intervals for the spike timing between two cells, when intracellular noise is present. The amount of compression is quantified and is shown to depend in proportion with the inhibition frequency and number of inhibition, and inversely proportional to the rate of depression.

CHAPTER 2

OVERVIEW

The dissertation is divided into several chapters. The spiking model used to represent neurons mathematically is introduced in Chapter 3. It is a three-dimensional, coupled system of ordinary differential equations, describing a single compartment neuron. Depressing synapses are incorporated into the model, which play an important role in the ability of pyramidal cells to produce an action potential and in the temporal synchronization process. Geometric, singular perturbation theory is utilized to show how a pyramidal cell produces an action potential, with and without a non-depressing synapse. A relation between inhibition frequency and the spike timing properties of a pyramidal cell for non-depressing synapses is derived. How the rate of excitatory input affects spike timing is also discussed. Additionally, in Chapter 3, a subnetwork of the CA1 region is introduced. The Sharp Wave-Associated Ripple is simulated numerically within this subnetwork, from initiation to termination.

In Chapter 4, the existence and stability of two types of periodic orbits within the subnetwork of the CA1 network is proved, with depressing synapses. The type of periodic orbit produced by the subnetwork is shown to depend primarily on the frequency of the inhibition within the subnetwork. One kind of periodic orbit is a stable, sub-threshold orbit. The other kind is stable and produces action potentials, but its frequency depends on the properties of the depressing synapses.

Chapter 5 contains a discussion of how the model operates under the influence of intracellular noise. We show that high-frequency, depressing inhibition can still synchronize spike timing of pyramidal cells in the presence of noise. We relate our results to that of [30], where it is shown that a pyramidal cell displays low reliability over many trials when receiving tonic input. However, if the pyramidal cell receives identical patterns of white noise input, the cell displays high reliability. A particular

source of noise is identified, that of sodium channel inactivation, and is simulated by a finite resources model. Using phase plane analysis, the noise is shown to be responsible for reliability problems among pyramidal cell receiving tonic input. Also, the analysis shows how rapid, random input improves reliability. Also in Chapter 5, a general equation for the spike timing of individual pyramidal cells with intracellular noise is derived. An explicit formula for spike timing for special parameter regimes is given. Furthermore, using probability theory, a method for deriving a distribution for the timing between pyramidal cells is discussed and a particular case is analyzed. Using numerical integration methods, confidence intervals for the timing between cells with noise can be computed. Incorporating the evolution of sodium channel inactivation and synaptic depression, the amount of time compression between the cells as they synchronize is quantitatively realized. The compression factor is shown to depend on several biological parameters.

In Chapter 6, the major findings of this work are reviewed and several options for future work are addressed. For example, in addition to pyramidal cell synchronization during the SPWR, interneurons also synchronize. Several theories have been put forth concerning how this occurs. The primary suspects are *gap junctions*, physical linkings between neurons through which ions can pass directly, causing changes in potential [16]. However, this is not without controversy. Experimental studies, where the genes that express gap junctions have been removed, show that SPWRs still occur despite the lack of electrotonic connections [10, 22]. Another topic left for future work is heterogeneity amongst the cells of the network. In this dissertation, the pyramidal cells were identical and received identical input. Articles such as [34] and [49] both address this issue and have shown that such quantities as firing rates and synaptic decay times have an effect on the ability of heterogeneous networks to oscillate synchronously. Synaptic delay is also a subject not included. Spatial distances in the hippocampus exclude instantaneous transmission of action potentials

between neurons, yet pyramidal cells still manage to synchronize across the CA1 region during SPWRs. In the articles [1, 29], synaptic delays have been shown to affect small networks of self-inhibiting neurons, but larger networks with more realistic architecture need to be analyzed.

CHAPTER 3

THE MODEL

Before the 1950s, mathematicians played little or no role in the field of neuroscience. During the early part of that decade, two visionaries, Alan Lloyd Hodgkin and Andrew Fielding Huxley, opened the way for mathematicians to be able to participate in the arena of neuroscience. They performed a series of voltage-clamp experiments on the giant axon of the squid *Logilo* and determined that the production of an action potential along the squid giant axon was caused by the influx of Na^+ ions followed by an outflux of K^+ ions through the axon's membrane.

Using a parallel conductance circuit model, as in Figure 3.1, Hodgkin and Huxley derived a general equation:

$$\begin{aligned} I_m &= C_m \frac{dv}{dt} + I_K + I_{Na} + I_L \\ &= C_m \frac{dv}{dt} + g_K(v,t)(v - V_K) + g_{Na}(v,t)(v - V_{Na}) + g_L(v - V_L), \end{aligned} \tag{3.1}$$

where the total current across the membrane, I_m, was equal to the sum of the capacitive current $C_m \frac{dv}{dt}$, the potassium current I_K, the sodium current I_{Na} and a leak current I_L.

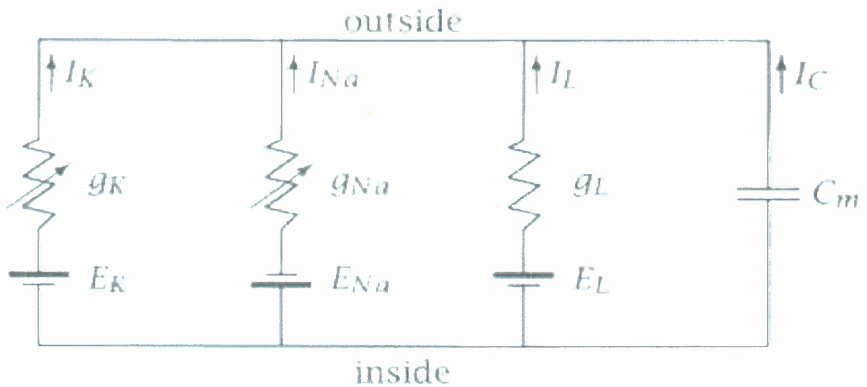

Figure 3.1 Diagram of Hodgkin and Huxley's Parallel Conductance Model [24].

Hodgkin and Huxley proposed a "gating" model, whereby the flow of ions into and out of the axon is controlled by channel protein "gates." These gates are voltage dependent. Experimentally, Hodgkin and Huxley determined that these gates adhere to power rules:

$$g_K = \bar{g}_K n^4 (v - V_K) \tag{3.2}$$

and

$$g_{Na} = \bar{g}_{Na} m^3 h (v - V_{Na}), \tag{3.3}$$

where $\bar{g}_{Na}$ and $\bar{g}_K$ are the maximum conductances of each respective current. The variable n controls how the potassium channels open and close. The variable m determines how the sodium channels open and h determines how they close. The dynamics of these gating variable were also determined by Hodgkin and Huxley, depicted in Figure 3.2.

A final model was proposed.

$$\begin{aligned} I_m &= C_m \frac{dv}{dt} + \bar{g}_K n^4 (v - V_K) + \bar{g}_{Na} m^3 h (v - V_{Na}) + g_L (v - V_L) \\ \frac{dn}{dt} &= \frac{n_\infty(v) - n}{\tau_n(v)} \\ \frac{dm}{dt} &= \frac{m_\infty(v) - m}{\tau_m(v)} \\ \frac{dh}{dt} &= \frac{h_\infty(v) - h}{\tau_h(v)}, \end{aligned} \tag{3.4}$$

where $n_\infty(v)$, $m_\infty(v)$ and $h_\infty(v)$ are steady state functions for the gating variables. The voltage-dependent rate constants at which the gating variables approach the steady state curves are $\tau_n(v)$, $\tau_m(v)$ and $\tau_h(v)$, respectively [18, 19, 20, 21, 24, 45]. Specific examples of the steady state functions and the voltage-dependent rate constants are given in the next section for the model presented in this dissertation.

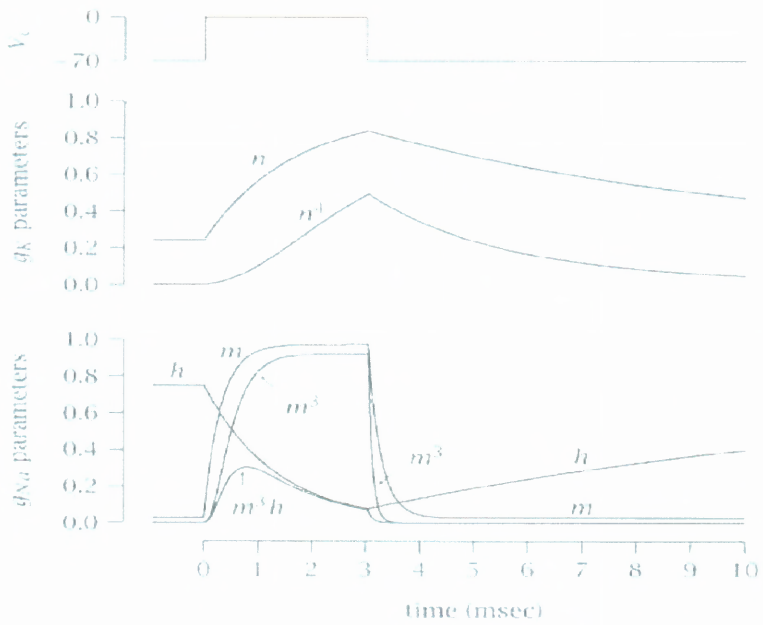

Figure 3.2 The Time Courses of n, n^4, m, m^3, h and m^3h, Following a Depolarizing Voltage Step (from -70 mV to 0 mV for 3 msec [24].

3.1 The Equations for the Spiking Model

The model being used in this research is a reduced Hodgkin-Huxley model for a spiking neuron, presented in [13]. Both interneurons and pyramidal cells are relaxation oscillators, represented by this general set of equations:

$$\begin{aligned} \frac{dv}{dt} &= f(v, w, s) \\ \frac{dw}{dt} &= \epsilon y(v, w), \end{aligned} \tag{3.5}$$

where ϵ is a small parameter. In later simulations, $\epsilon = 0.1$. This value was chosen to preserve the scaling seen in the terms (3.11), (3.14) and (3.15), which are of the same order.

$$f(v, w, s) = \left[I_0 - I_{leak} - I_{K^+} - I_{Na^+} - I_{syn}\right]/C, \tag{3.6}$$

such that the differential equation for voltage, v, includes an input current, I_0, a leak current

$$I_{leak} = g_L(v - V_L), \tag{3.7}$$

a potassium current

$$I_{K+} = g_K w^4 (v - V_K), \tag{3.8}$$

a sodium current

$$I_{Na+} = g_{Na} m^3 h (v - V_{Na}) \tag{3.9}$$

and, if a connection exists, a synaptic current, I_{syn}.

The parameters g_L, g_K and g_{Na} are the conductances of the ion channels, respectively. The reversal potentials of these channels are V_L, V_K and V_{Na}, respectively. The parameter C is the cell's membrane capacitance.

The gating variable for the potassium channels is w.

$$y(v, w) = \frac{w_\infty(v) - w}{\tau_w(v)}, \tag{3.10}$$

where $w_\infty(v) = \frac{a_w(v)}{a_w(v)+b_w(v)}$ and $\tau_w(v) = \frac{1}{a_w(v)+b_w(v)}$.

$$a_w(v) = \frac{0.32(v + 53.75)}{1 - e^{-\frac{v+53.75}{5}}} \tag{3.11}$$

and

$$b_w(v) = 5e^{-\frac{58.75+v}{40}}. \tag{3.12}$$

The steady state curve $w_\infty(v)$ is an increasing function of v. It is also the equation for the w-nullcline, when the differential equation is set to 0. See Figure 3.3 for graphs of these functions.

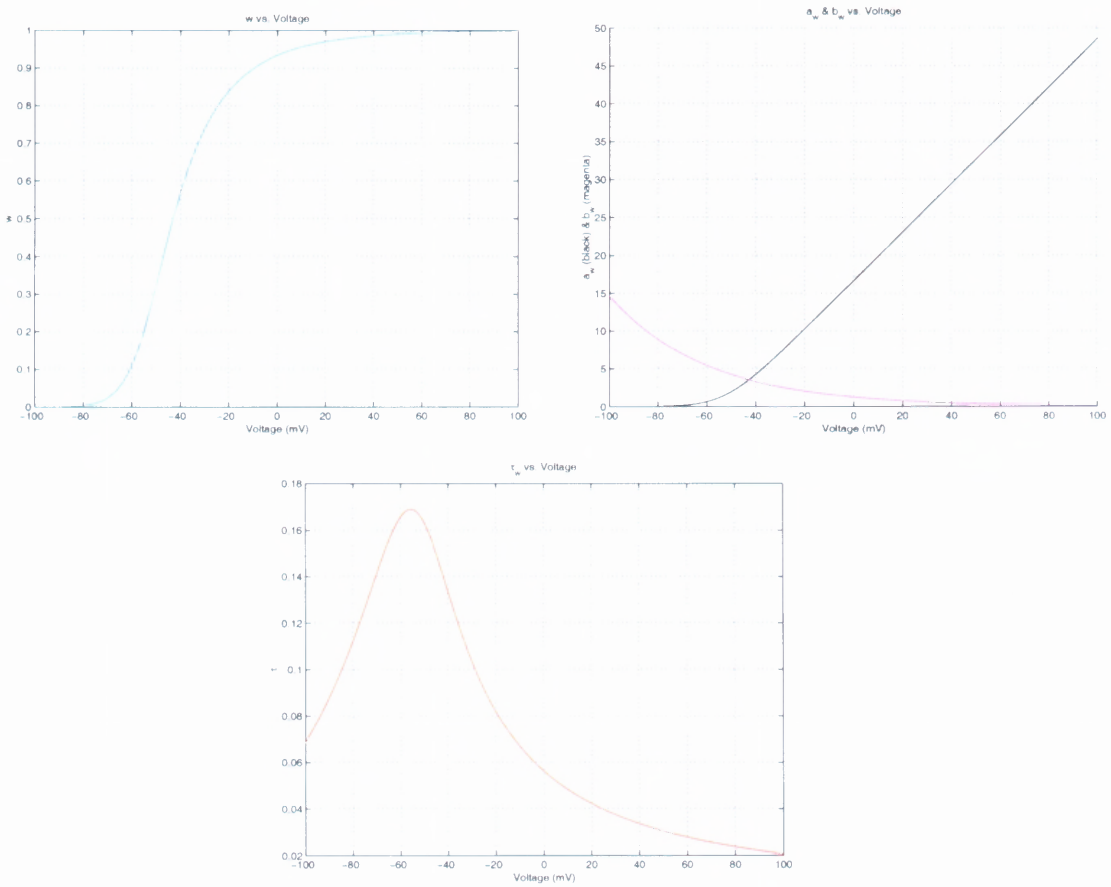

Figure 3.3 Plot of $w_\infty(v)$, $a_w(v)$, $b_w(v)$ and $\tau_w(v)$

The variables m and h are gating variables for sodium ion channels.

$$m \equiv m_\infty(v) = \frac{a_m(v)}{a_m(v) + b_m(v)}, \tag{3.13}$$

where

$$a_m(v) = \frac{0.32(54 + v)}{1 - e^{-\frac{v+54}{4}}} \tag{3.14}$$

and

$$b_m(v) = \frac{0.28(v + 27)}{e^{\frac{v+27}{5}} - 1}. \tag{3.15}$$

The variable m is assumed to evolve sufficiently fast, relative to w and h, so that it quickly approaches steady state, which is solely governed by the cell's potential. All three functions are depicted in Figure 3.4.

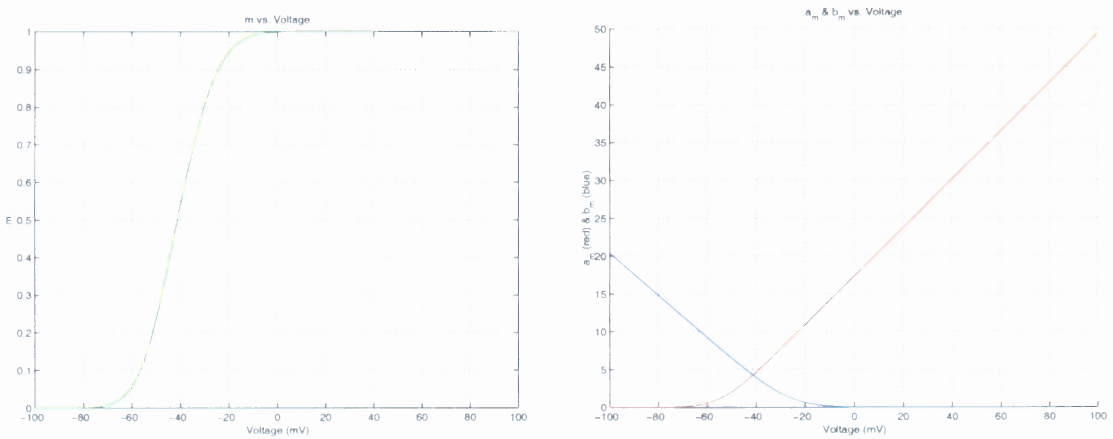

Figure 3.4 Plot of $m_\infty(v)$, $a_m(v)$ and $b_m(v)$

The final gating variable is set to $h = max(1 - 1.25w, 0)$ in order to reduce the model into a two-dimensional system. This assumption about h and w follows from the fact that if the Hodgkin-Huxley system were projected onto the $h - w$ phase plane, the cell's path would be linear. The slope of this line depends on the values of h and w while at the cell's resting potential. Figure 3.5 shows the graph of $h(w)$.

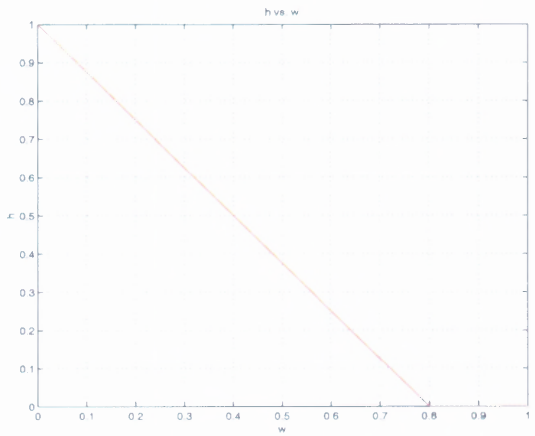

Figure 3.5 Plot of $h(w)$

3.2 Modeling Synapses

For each active synaptic connection present, the following term is added to the postsynaptic cell's voltage equation:

$$I_{syn} = g_{syn} s(t)(v - V_{syn}), \tag{3.16}$$

where the function s is the synapse's effective strength. The variable s evolves according to its own differential equation defined below. The parameter g_{syn} is the maximum synaptic strength and V_{syn} is the synapse's reversal potential. The value of V_{syn} determines whether the synapse is excitatory or inhibitory. For example, in the simulations presented later, $V_{syn} = -80$ mV for inhibitory synapses. When the postsynaptic cell's voltage is greater than -80 mV, the synaptic current term in (3.16) will be positive, so it will be subtracted from the voltage equation in (3.6), lowering the cell's potential towards -80 mV. If this inhibition is strong enough, the cell is prevented from firing. For excitatory synapses, V_{syn} is typically higher than the postsynaptic cell's voltage, so the synaptic current term is negative and is added to (3.6). This will cause the postsynaptic cell's voltage to rise towards V_{syn}. If the voltage reached the action potential threshold, the postsynaptic cell fires.

Depending on the model, s can be modeled in different ways. Typically, s evolves according to the following equation:

$$\frac{ds}{dt} = \frac{(1-s)}{\tau_a} H(v_{pre} - v_{th}) - \frac{s}{\tau_b} H(v_{th} - v_{pre}), \tag{3.17}$$

where H is the Heaviside function. When the presynaptic cell's potential, v_{pre}, is above the synaptic voltage threshold, v_{th}, s approaches 1 with rate $1/\tau_a$. If the presynaptic cell's potential is below its synaptic threshold, s decays to 0 with rate $1/\tau_b$.

The equation (3.17) is a simple and useful model, but some synapses may change strength as they are used. Those synapses whose strength is a function of usage

are called either *depressing* or *facilitating* synapses. If the synaptic strength is a decreasing function of frequency, the synapse is depressing. If the synaptic strength is an increasing function of frequency, it is a facilitating synapse. A different approach is used to represent depressing synapses. This model is attributed to [2]:

$$\begin{aligned} \frac{ds}{dt} &= -\frac{s}{\tau_k}H(v_{th}-v_{pre}) - \frac{s}{\tau_b}H(v_{pre}-v_{th}) \\ \frac{dD}{dt} &= \frac{(1-D)}{\tau_a}H(v_{th}-v_{pre}) - \frac{D}{\tau_b}H(v_{pre}-v_{th}) \\ s(t_{jump}) &= D(t_{jump}), \end{aligned} \tag{3.18}$$

where t_{jump} is the time when the presynaptic cell crosses its synaptic threshold. The variable s still represents the synapse's effective strength. The variable D represents the "resources" of the synapse, such as the amount of neurotransmittors available to the synapse. The parameter τ_k is the time constant governing the decay of the effective strength of the inhibiting synapse while below synaptic threshold and τ_a controls the rate of D's recovery while below synaptic threshold. The parameter τ_b is the time constant in control of the use of these "synaptic resources" while the presynaptic cell is above the synaptic threshold.

As an example, consider a single interneuron that synapses onto a single pyramidal cell. When the interneuron's potential is below synaptic threshold ($v_{pre} < v_{th}$), the variables satisfy the following equations:

$$\begin{aligned} \frac{ds}{dt} &= -\frac{s}{\tau_k} \\ \frac{dD}{dt} &= \frac{1-D}{\tau_a}. \end{aligned} \tag{3.19}$$

The variable s decays to 0 since the effects of the synapse are receding. D is increasing to 1 as the cell recovers its "synaptic resources." For sufficiently small values of τ_a, D will recover fully each time the presynaptic cell goes below its synaptic threshold, i.e. the synapse is not depressing.

When the inhibiting cell fires and its voltage crosses the synaptic threshold ($v_{pre} \geq v_{th}$), s is set equal to D, representing the fact that the strength of the synapse can only be as great as the available recovered "resources." This occurs instantaneously, mimicking synapses with very fast rise times, such as GABAergic synapses [24]. While above threshold, the synapse follows these equations:

$$\begin{aligned} \frac{ds}{dt} &= -\frac{s}{\tau_b} \\ \frac{dD}{dt} &= -\frac{D}{\tau_b}. \end{aligned} \tag{3.20}$$

Both variables decrease at the same rate, $\frac{1}{\tau_b}$, as "synaptic resources" are being used and, simultaneously, the strength of the synapse decreases. Figure 3.6 illustrates qualitatively how s and D evolve, along with the rate constants involved.

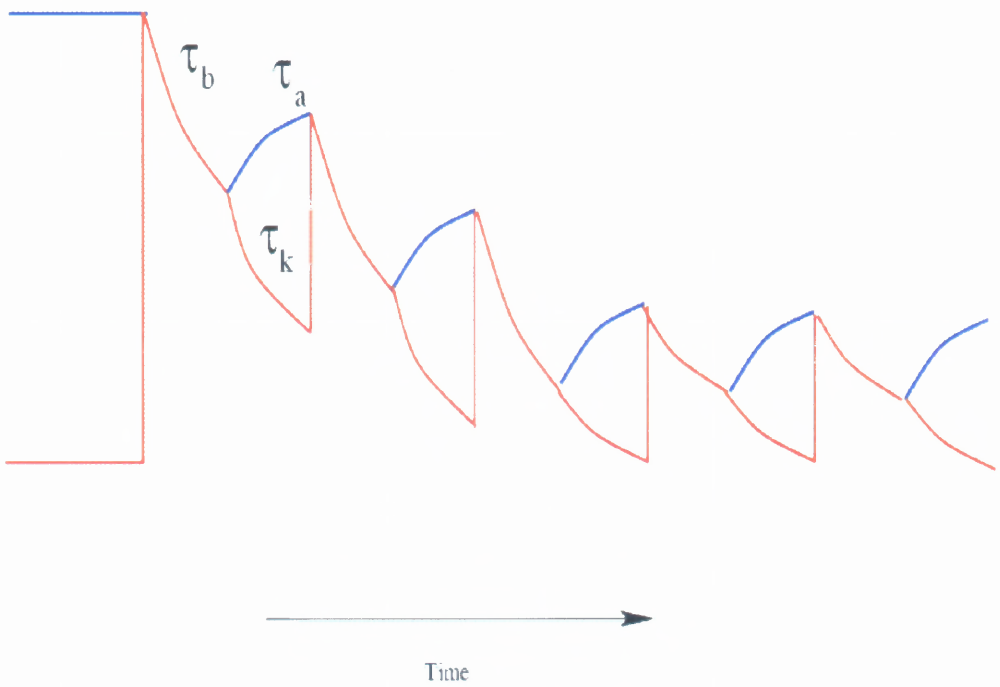

Figure 3.6 Diagram of How s and D Evolve with Time

For the remainder of this dissertation, the depressing synapse model will be used. However, in certain cases, the synapse will be considered as non-depressing, meaning D recovers fully between uses of the synapse.

Typical parameter values for this research are $\epsilon = 0.1$, $C = 1\ \mu\text{F/cm}^2$, $g_{Na} = 100$ mS/cm^2, $g_K = 80$ mS/cm^2, $g_L = 0.05$ mS/cm^2, $V_{Na} = 50$ mV, $V_K = -100$mV, $V_L = -63.8$ mV (for inhibitory neurons) and $V_L = -66.65$ mV (for excitatory neurons). $V_{syn} = -80$ mV (for inhibitory synapses), $V_{syn} = 0$ mV (for excitatory synapses), and $g_{syn} = 0.04$ mS/cm^2. In the simulations, $\tau_k = 100$ msec, $\tau_b = 5$ msec, and $\tau_a = 100$ msec.

When the equations for a single cell (without synaptic connections) are integrated using XPP [12], the cell displays oscillatory behavior. The cell spends little time in the active phase, producing sharp, narrow action potentials. By injecting "negative" current into the cell, it can be trapped in a lower voltage level. When the current is removed, the cell resumes its oscillation.

A source of heterogeneity may come from varying I_0, the input current. This parameter affects the intrinsic frequency of the cell. Figure 3.7 illustrates how input affects the oscillation frequency of cells modeled by (3.5). Experimental evidence suggests that a typical CA1 pyramidal cell fires at a mean frequency of 1.4 ± 0.01 Hz, while interneurons fire at a mean frequency of 14.1 ± 1.43 Hz if located in the pyramidal cell layer, and 13.0 ± 1.62 Hz in the st. oriens/alveus layer (another area of the CA1 region) [9].

3.3 How a Pyramidal Cell Fires in the $v - w$ Phase Plane

Neurons modeled by (3.5) have very narrow action potentials, characterized by a rapid rise and fall of the voltage potential. Between spikes, the cell slowly recovers, preparing to produce another action potential. Also, in this model, synaptic strengths

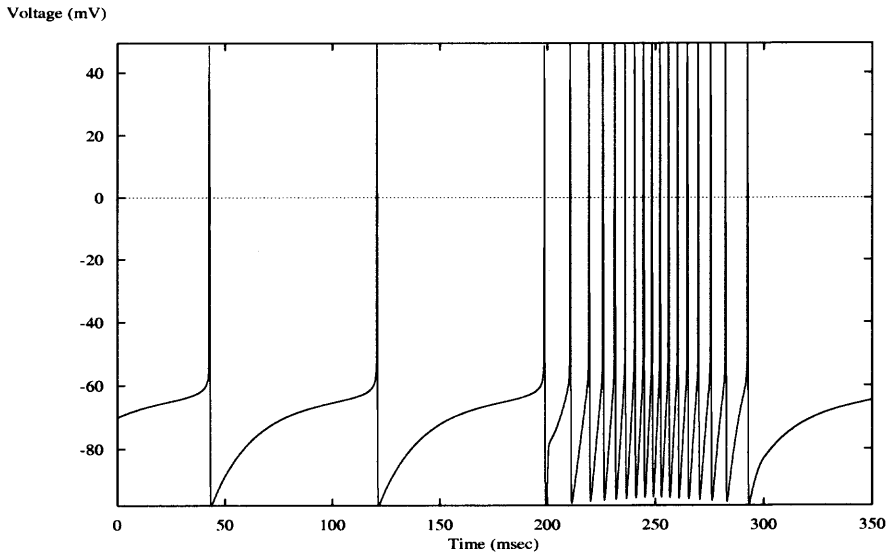

Figure 3.7 Typical Voltage Trace of a Modeled Spiking Neuron. Sharp wave input comes between 200msec and 300msec, causing the oscillation to reach ripple frequency ($\sim$ 200Hz).

will rise instantaneously, but decay slowly. These differing speeds of evolution are characterized by the equations themselves.

Consider a pyramidal cell being synapsed upon by a single interneuron. The equations for the pyramidal cell, as they originally appear in (3.5), combined with an equation for the effective synaptic strength of a depressing synapse (3.18) are:

$$\begin{aligned} \frac{dv}{dt} &= f(v,w,s) \\ \frac{dw}{dt} &= \epsilon y(v,w) \\ \frac{ds}{dt} &= \begin{cases} -\frac{\epsilon s}{\tau_b} & , v_{pre} \geq v_{th} \\ -\frac{\epsilon s}{\tau_k} & , v_{pre} < v_{th} \end{cases} \end{aligned} \tag{3.21}$$

The presence of the small parameter ϵ can be used to our advantage when analyzing these equations. The system can be considered in two different time scales, a "fast" and "slow" time scale. Refer to (3.21) as the "fast" time system.

By setting $\tau = \epsilon t$, (3.21) can be re-scaled into "slow" time:

$$\begin{aligned} \epsilon\frac{dv}{d\tau} &= f(v,w,s) \\ \epsilon\frac{dw}{d\tau} &= \epsilon y(v,w) \\ \epsilon\frac{ds}{d\tau} &= \begin{cases} -\frac{\epsilon s}{\tau_b} & , v_{pre} \geq v_{th} \\ \\ -\frac{\epsilon s}{\tau_k} & , v_{pre} < v_{th} \end{cases} \end{aligned} \tag{3.22}$$

Since the pyramidal cell produces narrow action potentials, it spends little time in the active phase. The following geometric, singular perturbation analysis will therefore focus on the pyramidal cell when it is below threshold, when the cell is in its silent phase. In terms of the simulation, the pre-defined synaptic threshold, $v_{th} = 0$. The analysis is performed in the singular case, $\epsilon \to 0$. The results proven in the singular case also hold for $\epsilon \ll 1$ [32].

Consider the "fast" equations as $\epsilon \to 0$:

$$\begin{aligned} \frac{dv}{dt} &= f(v,w,s) \\ \frac{dw}{dt} &= 0 \\ \frac{ds}{dt} &= 0 \end{aligned} \tag{3.23}$$

The variable v evolves the fastest of the variables, such that w and s are considered constant while v evolves. When the pyramidal cell fires, the action potential is produced in "fast" time, accounting for the thinness of the spike. Figure 3.8 shows how the vector field in the $v - w$ phase plane, as v evolves in "fast" time.

The singular, "slow" equations are

$$\begin{aligned} 0 &= f(v,w,s) \\ \frac{dw}{d\tau} &= -b_w(v)w \\ \frac{ds}{d\tau} &= -\frac{s}{\tau_k}. \end{aligned} \tag{3.24}$$

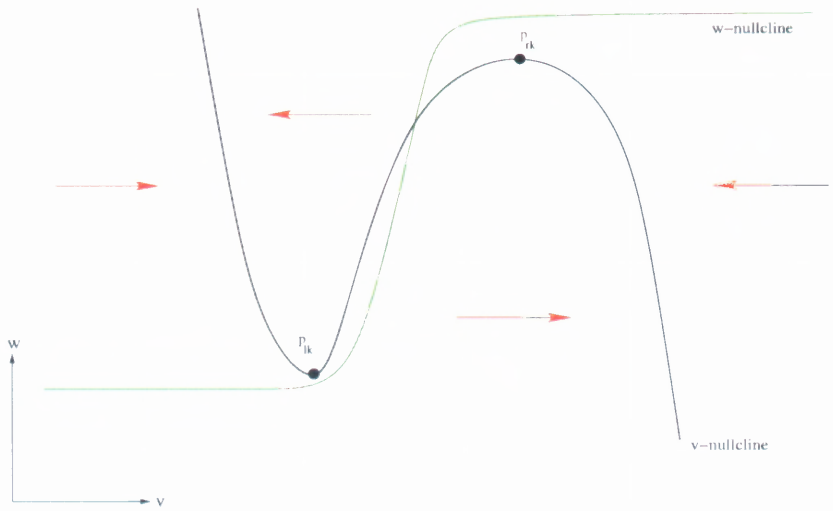

Figure 3.8 The variable v evolves in "fast" time in the $v-w$ phase plane. Generally, below the v-nullcline, v moves to the right and above the v-nullcline, v moves left.

According to "slow" time, the cell is constrained to satisfy the algebraic equation derived from the voltage equation, while w decays to 0 during the cell's recovery phase (below threshold). Figure 3.9 illustrates w's movement in the $v-w$ phase plane, along the v-nullcline, while s is constant. Note that while the pyramidal cell is below threshold, $a_w(v) \approx 0$. Also during this time, the effective strength of a presynaptic cell's synapse, s, decays to 0.

Combining both time scales, one can consider the cell's movement in the $v-w$ phase plane. The cell is constrained to move along its v-nullcline in "slow" time, making "fast" jumps between the branches of the nullcline only when the cell reaches a local extrema of the v-nullcline (also known as the "knees" of the nullcline), where the vector field bifurcates, as in Figure 3.10. Let the lower-left knee be denoted by the point $p_{lk} \equiv (v_{lk}, w_{lk})$ and the upper-right knee as $p_{rk} \equiv (v_{rk}, w_{rk})$. (In later sections, p_{lk} and p_{rk} may depend on s, as the nullcline shifts up or down, according to the

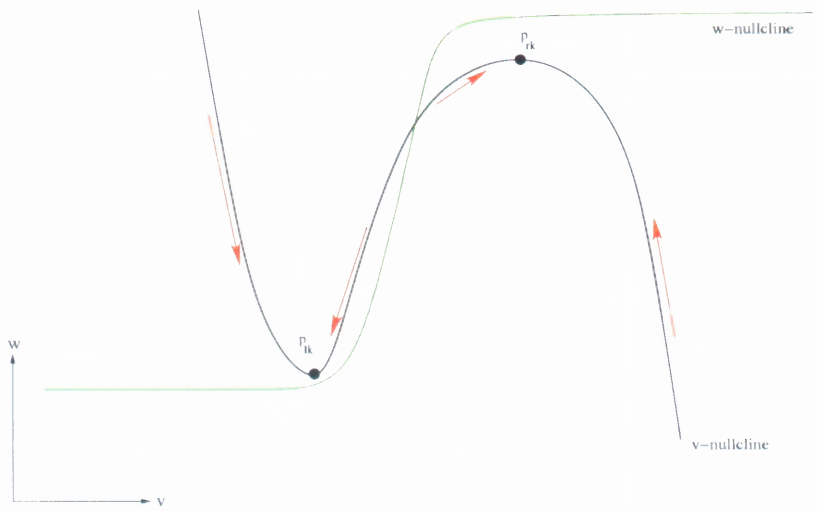

Figure 3.9 The variable w evolves in "slow" time in the $v - w$ phase plane, constrained to the v-nullcline. Generally, on the left branch of the v-nullcline, w moves down and on the right branch of the v-nullcline, w moves up. Along the middle branch, the cell moves away from the unstable, intersecting critical point. This diagram assumes s is constant.

amount of synaptic input.) Figure 3.11 shows the simulated movement of the cell in the $v - w$ phase plane.

In this dissertation, the case when the nullclines intersect in only one point will be considered, though, in general, the nullclines may intersect in multiple places. When the cell oscillates, the critical point is unstable and is located on the middle branch of the v-nullcline, as in Figure 3.10. When the critical point is located on either the right or left branches of the v-nullcline, it is stable and the cell will become trapped there, as in Figure 3.12.

If there is inhibition present, each time the interneuron fires, s is set to D instantaneously, causing the v-nullcline to lower in the phase plane instantaneously, due to the term (3.16) in the pyramidal cell's voltage equation, (3.6). Activation of

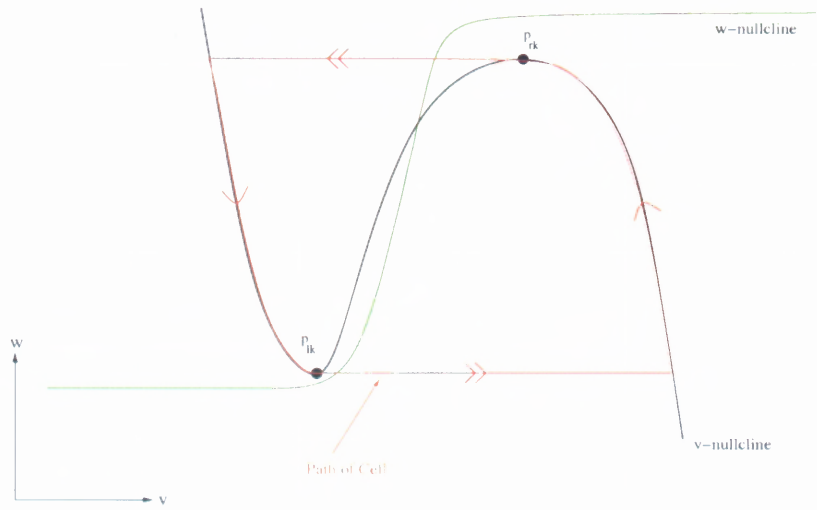

Figure 3.10 Movement of the cell in the $v - w$ Phase Plane ("Fast" and "Slow" Time Scales). Double arrows represent "fast" time and single arrows represent "slow" time.

this term introduces a negative amount, which causes the move to a lower position. This movement shifts the intersecting critical point. If D is large enough, the intersecting critical point shifts from the v-nullcline's middle branch to the left branch, and its stability changes from unstable to stable. So, as w approaches 0, the cell becomes trapped at the intersection of the w and v-nullclines. This remains the case as s decays to 0 in "slow" time. Once s becomes sufficiently small ($s = s^*$), the nullcline rises enough in the phase plane so that the nullclines no longer intersect on the left branch of the v-nullcline and the cell "has access" to $p_{lk}(s^*)$, from which it can jump, as seen in Figure 3.13.

In summary, the pyramidal cell fires normally without inhibition. With a constant level or no input, its firing frequency depends chiefly on how w decays while in the silent phase (or how the cell recovers). If the pyramidal cell receives inhibition, whether it fires depends on the decay rate of the inhibition, the strength

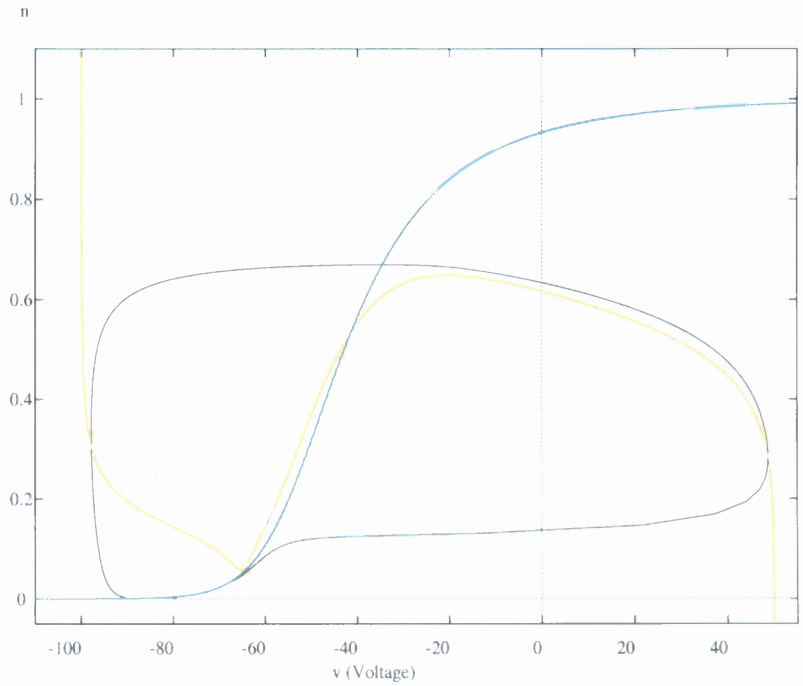

Figure 3.11 Orbit of a P_2 in the Phase Plane, depicting both nullclines. The pyramidal cell spends most of the orbit between -80 to -60 mV and 0 to 0.15 w units. This is typical for the other two pyramidal cells, as well as the interneurons. However, interneurons spend less time in the region just mentioned since they have a higher oscillation frequency.

of inhibition, the usage of "synaptic resources" D, and the frequency of the inhibiting cell. For a fixed rate of synaptic decay, if the inhibition frequency is small enough, the cell will have enough time to reach a knee and fire before more inhibition is applied. If the frequency is too high, the cell will not be able to reach the knee before the interneuron inhibits the pyramidal cell again. This will happen every cycle and the pyramidal cell will never fire. This will be discussed mathematically in Section 3.5.

However, with depressing synapses, the value of D may become smaller each time the inhibiting neuron fires (if D cannot recover fully between uses of the synapse). As a consequence, s is reset to a smaller D-value each time, and it takes less time for the inhibition to decay to a value where the cell has access to a knee. Therefore,

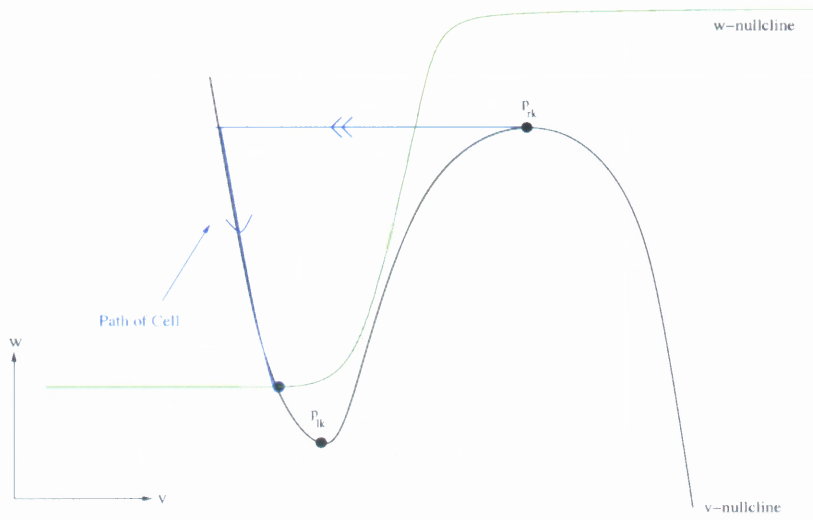

Figure 3.12 A Cell's Excitable Trajectory in the $v - w$ Phase Plane. The intersecting critical point is stable and the cell becomes trapped.

while during one cycle of inhibition the cell may not fire, due to a decrease in D, it may fire during the next cycle. This will be discussed in detail in Section 4.1.

3.4 The $g - w$ Phase Plane and the g Phase Line

In general, (3.5) constitutes a three dimensional system, (v, w, s). As stated before, neurons in these simulations spend the majority of their cycles in the silent state, where "slow" time governs and the cell is constrained to move along the v-nullcline. Consider the "slow" time system, defined as in Section 3.3:

$$\begin{aligned} 0 &= f(v, w, s) \\ \frac{dw}{d\tau} &= -b_w(v)w \\ \frac{ds}{d\tau} &= -\frac{s}{\tau_k}. \end{aligned}$$

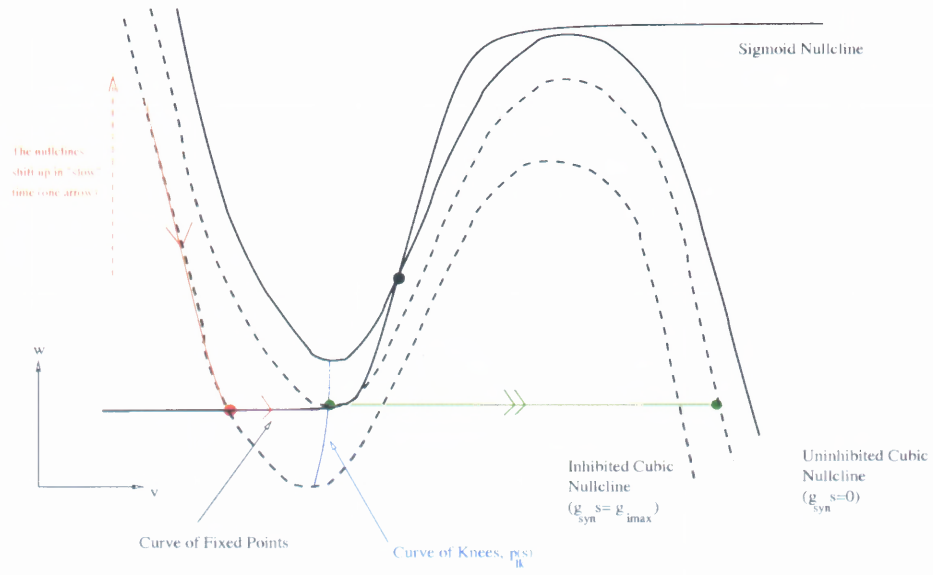

Figure 3.13 Movement in the $v-w$ Phase Plane (The Effects of "Slow" Inhibitory Decay). After receiving inhibition, the nullcline shifts up in "slow" time, as s decays. When the cell gains access to a knee, it fires.

(Recall that these equations are defined in the left portion of the $v-w$ phase plane, when the cell is below its action potential threshold.)

Using the Implicit Function Theorem and the first equation $f = 0$, an equation for v can be found as a function of the other two variables, $v = F(w, s)$, except at points where $\frac{\partial f}{\partial v}(v, w, s) = 0$, i.e. at p_{lk} and p_{rk}. The expression for v can be substituted into the equations for w and s, reducing the system by one dimension:

$$\begin{aligned} \frac{dw}{d\tau} &= -b_w(F(w,s))w \\ \frac{ds}{d\tau} &= -\frac{s}{\tau_k}. \end{aligned} \tag{3.25}$$

This creates, in general, a two-dimensional, $s-w$ phase plane, or $g-w$ phase plane if the effective synaptic strength is multiplied by the maximum strength factor, $g_{syn}s$. This is shown in Figure 3.14. It is worth noting that (3.25) is also valid at p_{lk} and p_{rk}.

Even though the Implicit Function Theorem does not guarantee $F(w, s)$ is defined at these points, $F(w, s)$ can defined at p_{lk} and p_{rk} by continuity of flow, i.e. a cell can approach and jump from them.

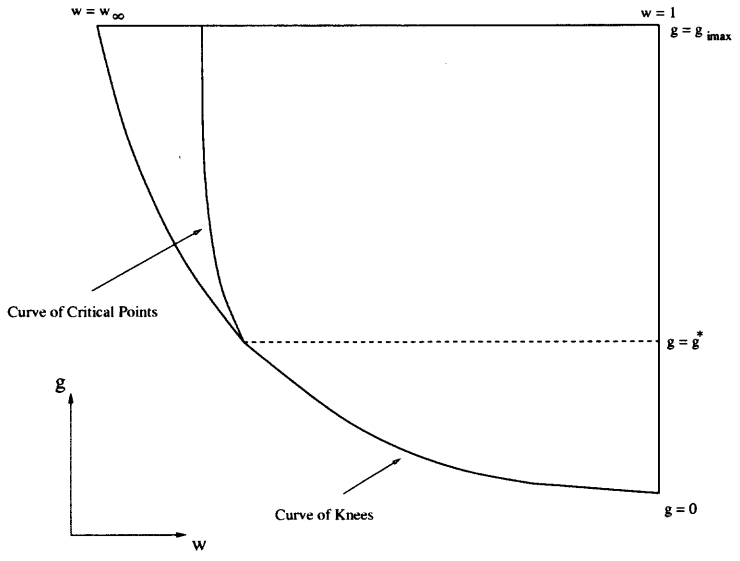

Figure 3.14 The $g - w$ Phase Plane

Suppose a pyramidal cell has fired and has become silent when it receives inhibition. The cell's position in the $g - w$ phase plane is in the upper right-hand corner, where $w = 1$ and $g \equiv g_{syn}s = g_{imax}$, where g_{imax} is the maximum strength of the inhibition. By considering the relative values of the synaptic decay rate and the rate at which the cell recovers, one of three cases can arise in this reduced two-dimensional system:

1. $\frac{1}{\tau_k} \gg b_w(F(w, s))$.

2. $\frac{1}{\tau_k} \sim b_w(F(w, s))$.

3. $\frac{1}{\tau_k} \ll b_w(F(w, s))$.

In the first case, the decay of the synaptic strength is rapid when compared to the recovery of the cell. The synaptic effects wear off before the cell leaves its recovery phase (while the cell is on the left branch of the v-nullcline). When the cell recovers, it can reach the *curve of knees* where the intersecting critical point undergoes a *saddle-node bifurcation*, changing from stable to unstable and the cell has access to a knee. Once the cell reaches this curve, the cell fires, as in Figure 3.13. The inhibition has little or no affect on the timing of the pyramidal cell in this case. An example of the cell's trajectory is given in Figure 3.15.

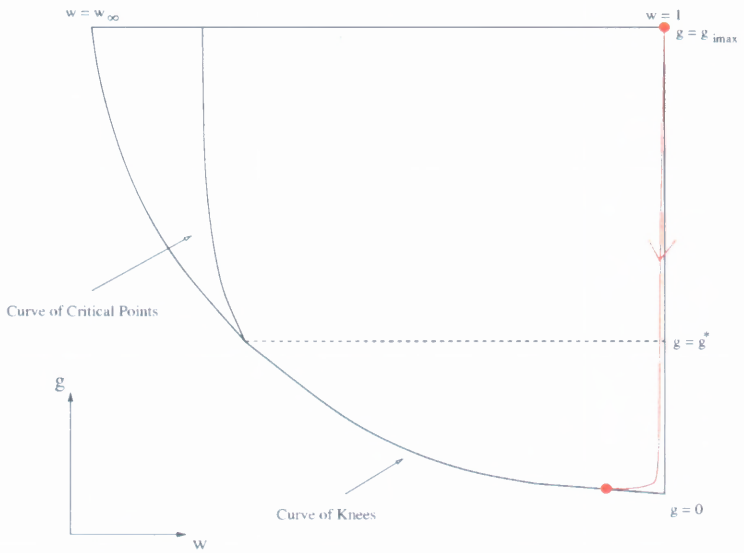

Figure 3.15 A Typical Trajectory in thee $g - w$ Phase Plane when $\frac{1}{\tau_k} \gg b_w(F(w,s))$. The synaptic strength decays rapidly and the cell can access a knee and fire.

In the second case, the synaptic decay and the cell's recovery progress at approximately the same rate. Two types of trajectories can be observed in this case, shown in Figure 3.16. For one type of trajectory, in cases when the cell's recovery is slightly faster than the decay of the synapse, the cell first reaches the curve defined by the continuum of intersections of the two nullclines while the critical

point is stable, or the *curve of critical points* (seen before in Figure 3.13), and must wait for the synaptic strength to decay enough before it can fire. For the second type of trajectory, when the synapse decays slightly faster than the cell's recovery, the synaptic strength has already decayed sufficiently, so the cell can fire when it has finished recovering. Analysis related to this second case is performed in [43] for mutually coupled slow inhibitory neurons.

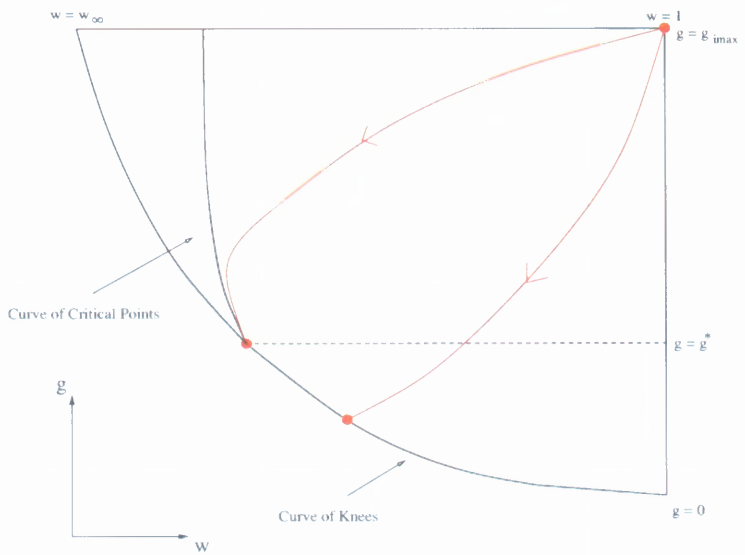

Figure 3.16 Typical Trajectories in the $g - w$ Phase Plane when $\frac{1}{\tau_k} \sim b_w(F(w, s))$. The synaptic strength and the cell's recovery occur at the same rate. Two different types of trajectories can be observed.

For the third case, w evolves much faster than the decay of g, i.e. the cell recovers much faster than the decay of the synapse. Assuming the inhibition is strong enough, the cell becomes trapped at the *curve of critical points*. Now g decays towards 0, and the cell travels along the *curve of critical points* until the cell reaches the curve of knees and the cell fires, as in Figure 3.13. Figure 3.17 illustrates this in the $g - w$ phase plane. The third case will hold for the rest of this paper.

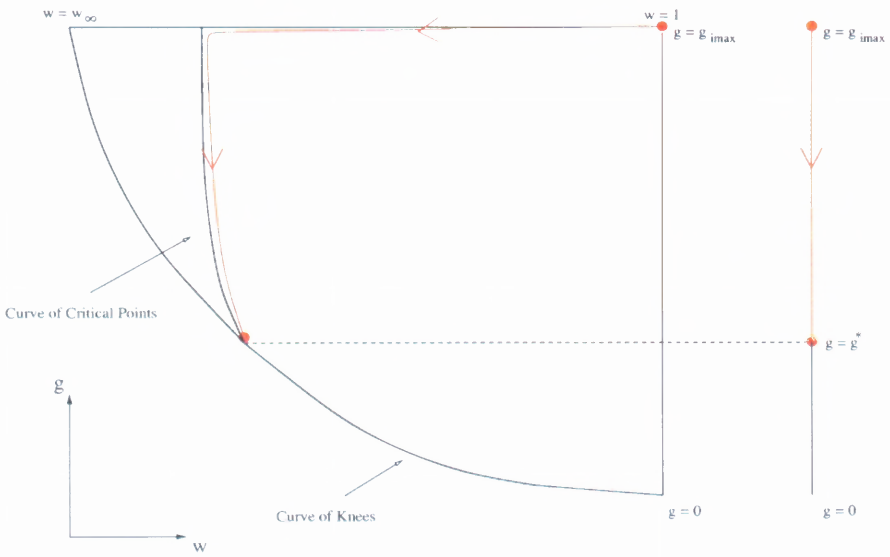

Figure 3.17 A Typical Trajectory in the $g - w$ Phase Plane and on the g Phase Line, when $\frac{1}{\tau_k} \ll b_w(F(w, s))$. The pyramidal cell travels down the left branch of the v-nullcline rapidly and becomes trapped by the *curve of critical points*. It must wait until g decays sufficiently before it can fire. This case can be reduced to a one-dimensional phase line.

Further simplification can be made to the phase space. Since each value of g while $w = 1$ can be mapped uniquely onto a matching value of g while $w = w_\infty$. The $g - w$ phase plane can be collapsed into a g phase line, as seen in Figure 3.17. It assumes that w has already decayed to 0 and a cell fires if the cell can move from g_{imax} to g^* before more inhibition is applied, where g^* represents the amount of inhibition when the intersecting critical point bifurcates from stable to unstable and the cell can fire from a knee.

If tonic current is injected into the cell, the cell's starting position in the $g - w$ phase plane is different. The cell no longer starts at $w = 1$ and $g = g_{imax}$. Instead, the cell starts at a g-value lower than $g = g_{imax}$. The cell will then travel along that particular stable manifold and reach the *curve of critical points* (if $g > g^*$) or

reach the curve of knees (if $g \leq g^*$), and fire instantaneously. See Figure 3.18 for an illustration of this.

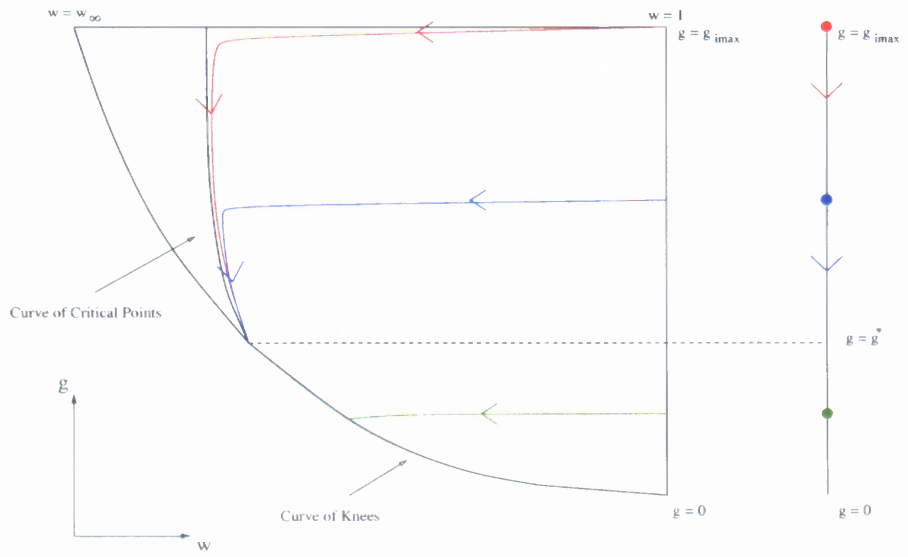

Figure 3.18 The $g - w$ Phase Plane and the g Phase Line when excitatory input is applied to the simulated cell. The *red* path indicates no input. The *blue* path indicates low input, and the cell still has to wait until it has access to a knee to fire, though less time than no input. The *green* path indicates high input, and the cell has access to a knee and fires.

3.5 A Relation Between Synaptic Decay and Inhibition Frequency for Non-Depressing Synapses

A relation between synaptic decay and inhibition frequency can be derived in the case without depressing synapses using (3.17). Solving the s-equation, for $s(0) = 1$ (i.e. the presynaptic, inhibitory neuron has just fired):

$$s(\tau) = e^{-\frac{\tau}{\tau_k}}. \tag{3.26}$$

In terms of $g_{syn}s$,

$$g(\tau) = g_{syn}s(\tau) = g_{imax}e^{-\frac{\tau}{\tau_k}} \tag{3.27}$$

since, after the synapse fires, the synapse starts at maximum strength. It takes

$$\tau^* = \tau_k \ln\left(\frac{g_{imax}}{g^*}\right) \tag{3.28}$$

time to reach g^*. In terms of "fast" or normal time,

$$t^* = \frac{\tau_k}{\epsilon} \ln\left(\frac{g_{imax}}{g^*}\right). \tag{3.29}$$

The action potentials of an interneuron are very narrow. The interneuron's period, $T_{in} = \Delta t_s + \Delta t_f$ (where Δt_s is its time spent in the silent phase and Δt_f is its time spent in the active phase), can be approximated as $T_{in} \approx \Delta t_s$, since $\Delta t_f \sim \mathcal{O}(\epsilon^2)$. So, g can reach g^* and the cell fires if

$$T_{in} \approx \Delta t_s \geq \frac{\tau_k}{\epsilon^2} \ln\left(\frac{g_{imax}}{g^*}\right). \tag{3.30}$$

This corresponds to a frequency

$$\nu \leq \frac{\epsilon^2}{\tau_k \ln\left(\frac{g_{imax}}{g^*}\right)}.$$

Figure 3.19 depicts how a change in inhibition frequency can either prevent or allow a pyramidal cell to fire. Note that from this point on, all calculations will be using the approximation that the interneuron's frequency equals the time it spends in the silent phase, T_{in}.

3.6 The PIP Mini-Network and the Simulated Ripple

Often, the best course of action when studying a complex problem is to consider simpler cases and build upon the results found for the simple system. Following this

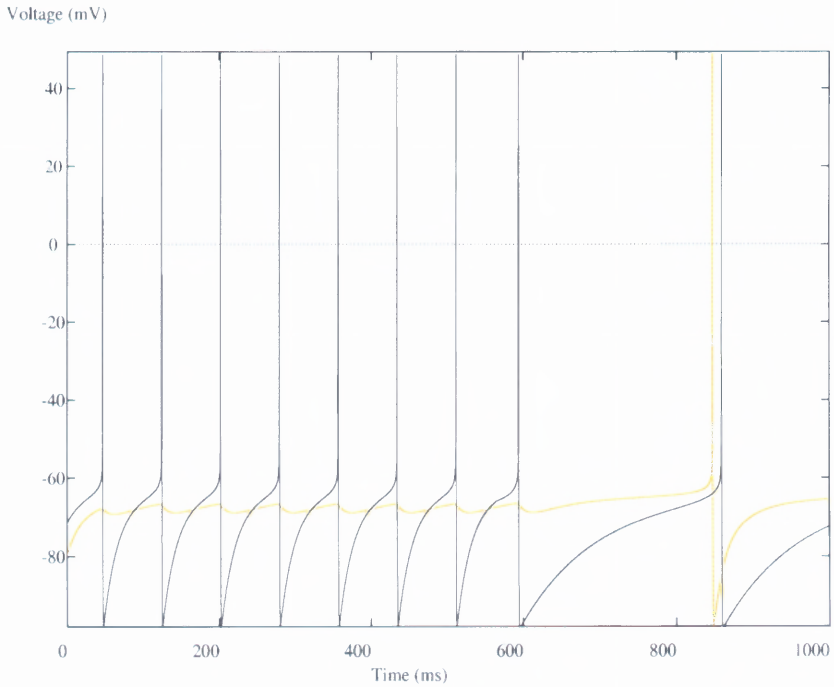

Figure 3.19 How Inhibition Frequency Affects the Firing Properties of a Pyramidal Cell. The inhibiting cell begins with a frequency of $\sim$ 15 Hz and it prevents the Pyramidal Cell from firing. At $t = 600$ msec, the inhibition frequency is reduced to $\sim$ 5 Hz. The Pyramidal Cell is now able to reach g^* on the $g_{syn}s$ Phase Line and it can fire. Synaptic strength is $g_{syn} = 0.05$.

line of reasoning, the PIP Mini-Network, shown on Figure 3.20, is a representative sub-network of the CA1 network.

A single interneuron synapses onto two pyramidal cells. For most of the analysis, the inhibitory synaptic connections are depressing and the pyramidal cells are identical. One may notice the lack of connections between pyramidal cells in the network. The CA1 region has been revealed to have sparse synaptic connectivity between pyramidal cells, as opposed to the dense recurrent collaterals in the CA3 region [8]. This is reflected in the PIP model. This fact is thought to reinforce the need for interneuron-pyramidal cell cooperation within the CA1 region during the sharp wave-associated ripple.

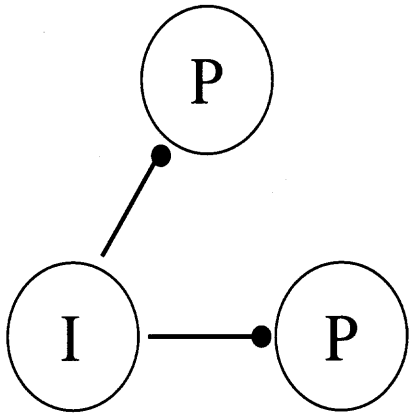

Figure 3.20 The PIP Mini-Network

Figure 3.21 shows simulated output of the PIP network as it receives Sharp Wave input. The goal of the simulations was to reproduce several key characteristics of the SPWR. In the experimentally recorded ripple, Buzsaki and collaborators observed several things. Interneurons generally start to fire before pyramidal cells. Interneurons fire at ripple frequency during the sharp wave. It is thought that high frequency oscillations of CA1 interneurons during ripples are caused by intrinsic properties [50]. Individual pyramidal cells fire once or twice during the ripple and they discharge together in a small window of time, anywhere from $5 - 100$ msec [9].

The sequence of the simulation occurs as follows:

1. The interneuron and pyramidal cells begin by oscillating at their intrinsic frequency: $\sim 13 - 14$ Hz for the interneuron and ~ 1 Hz for the pyramidal cells. The pyramidal cells are oscillating at some initial phase not equal to 0.

2. The CA3 Sharp Wave excites the interneuron first, before the pyramidal cells. Realistically, this may be true is some cases, depending on, among other things,

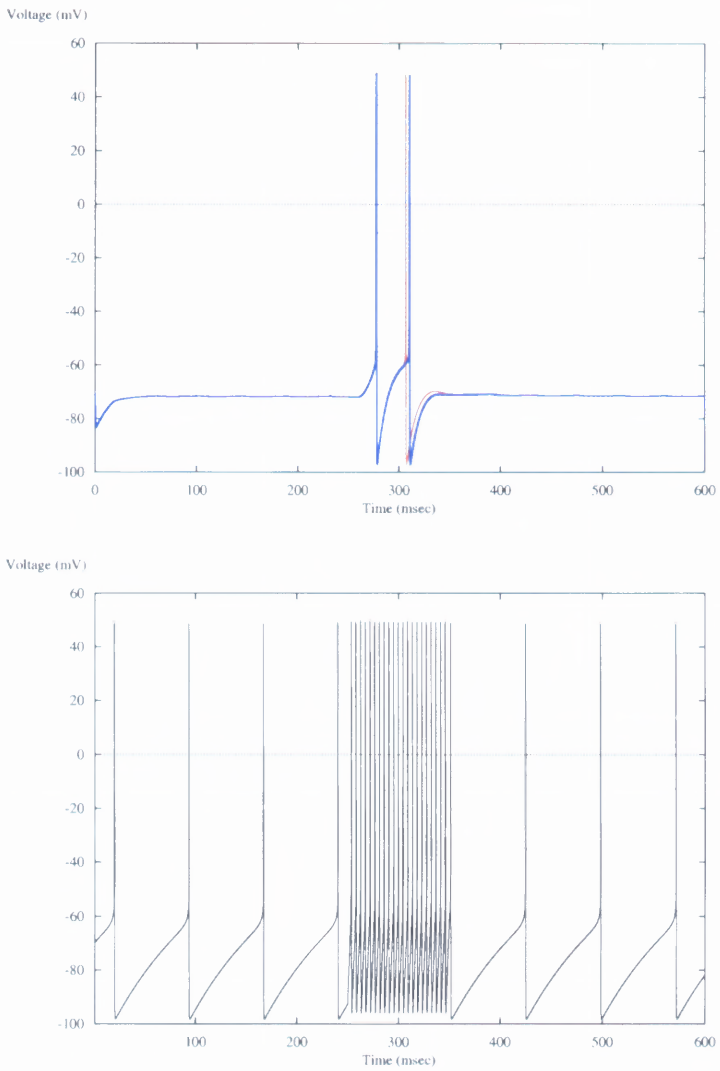

Figure 3.21 Simulated Output of the PIP Network. In the left figure, both simulated pyramidal cells fire twice during the Sharp Wave ripple, while receiving high-frequency inhibition from a single interneuron depicted in the right figure. The Sharp Wave excitation arrives at $t = 250$ msec and ends 100 msec later. As seen experimentally, the interneuron fires before the pyramidal cells and maintains a frequency of $\sim$ 200 Hz. The pyramidal cells fire only twice. Each pyramidal cell also has an element of intracellular noise, which will be discussed in Chapter 5. This noise prevented the pyramidal cells from synchronizing in the figure above. The parameters for this simulation are listed in Section 3.2.

where in the CA3 region the input comes from and the length of the Schaffer collaterals between CA3 and CA1. The Sharp Wave input to the interneuron is modeled as a flat pulse that lasts for a period of 100 msec, as seen in Figure 3.22. As shown previously, input to the neurons increase their firing frequency (as in Figure 3.7). The pulse's height was chosen to make the interneuron oscillate at ripple frequency.

3. A short time after the SPW excites the interneuron, the pyramidals cells are excited. The SPW input is modeled by a piece-wise linear, ramp function, as seen in Figure 3.22. The timing of the first spike produced by the pyramidal cell's during the simulation coincides with the rise of the ramp function.

4. As the pyramidal cell SPW excitation decays, they produce another action potential. Even though the excitation is decreasing, the pyramidal cells are able to fire again because the synaptic strength has depressed due to the high-frequency of inhibition.

5. The SPW excitation leaves the pyramidal cells. They fire no more during the SPWR due to a combination of the loss of excitation and the high-frequency, depressed inhibition.

6. The SPW excitation leaves the interneuron. It returns to its intrinsic frequency.

They arrival of the SPW excitation to the pyramidal cells causes them to fire for the first time during the SPWR. This is a consequence of the steep slope of the excitation's rise. Consider a single action potential produced by a pyramidal cell. If a source of repeated, non-depressing inhibition is applied to the pyramidal cell, then the action potential will only have a chance to fire between inhibitions, if the cell is allowed to fire at all. Suppose the pyramidal cell receives Sharp Wave excitation, while being repeatedly inhibited by an interneuron, such as what occurs during the SPWR.

Let T_{in} be the time between inhibitions and let $g_n^{T_{in}} = g(T_{in}) = g_n e^{-\frac{T_{in}}{\tau_k}}$ be the maximum distance traveled by the cell in the g-direction between the n^{th} and $(n+1)^{st}$ inhibitions, where g_n is the sequence of synaptic strengths when the pyramidal cell receives the n^{th} dose of inhibition. Also, let τ^* be the time it takes the cell to reach g^*. In Section 3.5, the time to fire was shown to be $\tau^* = \frac{1}{\beta}\ln\left(\frac{g_n}{g^*}\right) = \tau_k \ln\left(\frac{g_n}{g^*}\right)$ and that if $\tau^* < T_{in}$, then the cell fires. Or, in other words, if $g^* > g_n^{T_{in}}$, the cell fires.

As the excitation from the sharp wave increases, g_n will lower on the g phase line, since the excitation raises the v-nullcline and it cannot shift as low when it receives inhibition.

If the rate of increase of the excitation is less than the decay rate of the synapse, then the time to fire is $(n-1)T_{in}+\tau_n^*$, where $n-1$ is the number of times the inhibitory cell applies inhibition before the pyramidal cell fires and τ_n^* is the time to reach g^* from the g_n (the g-level associated with the nth inhibition).

If the rate of increase of excitation is greater than the synaptic decay, the cell will fire at $t = (n-1)T_{in} + (\tau_e - (n-1)T_{in}) = \tau_e$, where τ_e is the time when the excitation is great enough to allow g_n to become less than g^*, as measured from $\tau = 0$. The cell will then fire during this time between inhibitions. The quantity $(\tau_e - (n-1)T_{in})$ is the time from the most recent inhibition to when the cell fires.

In the numerical simulations, the pyramidal cells' sharp wave excitation was represented by

$$I_{sw}(t) = 2\left[\frac{1}{15}H(t-260) - \left(\frac{1}{15}+\frac{1}{65}\right)H(t-275) + \frac{1}{65}H(t-340)\right], \qquad (3.31)$$

a piece-wise, linear, ramp function, as in Figure 3.22. The excitation starts at $t = 260$, peaks at $t = 275$ and ends at $t = 340$. The function H is the Heaviside function. The rate of change of the excitation for the initial portion of the Sharp Wave is $\frac{2}{15} \approx 0.133$, which is the an order of magnitude greater than the rate of the synaptic

decay ($\tau_k = 20$). So, the simulation falls into the second case discussed above and the timing of the initial spike is determined by the arrival of the Sharp Wave.

Both cells were highly synchronized while producing the first action potential during the SPWR. The mechanism for synchronizing the pyramidal cells will be discussed in Chapter 4 and is dependent on the inhibition applied to the pyramidal cells. The second spike displayed less synchrony between the pyramidal cells. This is a consequence of intracellular noise added to the pyramidal cells whenever they produce an action potential. The first spike produced during the SPWR cause the noise to appear. This noise will be discussed in Chapter 5. The noise did not affect the first action potential because the intracellular noise decays on the order of 1 sec. Before the SPW arrives, the pyramidal cells oscillate at approximately 1 Hz, so the randomness dies out between action potentials.

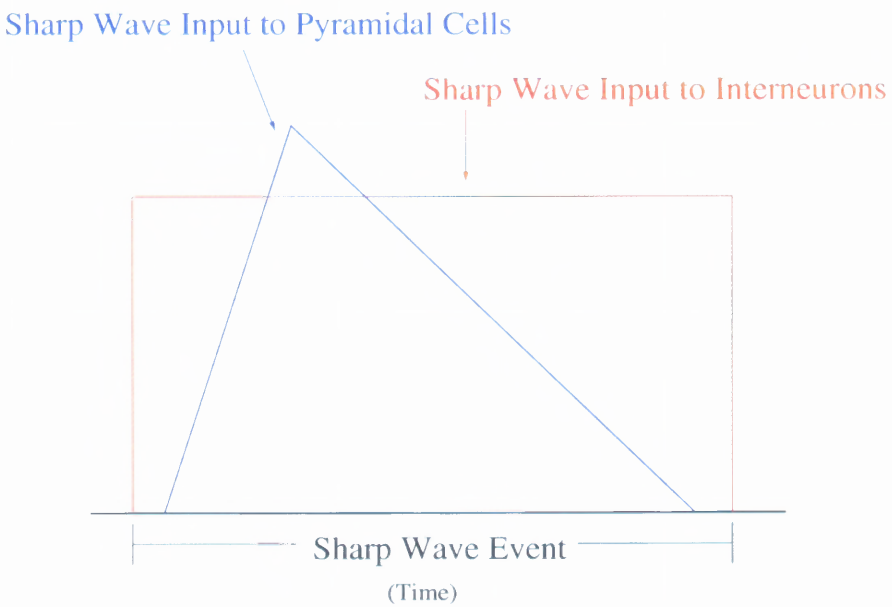

Figure 3.22 Sharp Wave Input Shapes. The first firing of pyramidal cells occurs when the excitation first exceeds the inhibition (i.e. the sharp wave input arrives). The pyramidal cells fire again when the excitation again dominates the inhibition, later on in the ripple.

As seen above, the rapid rise of the SPW excitation affected the timing of the pyramidal cells. Consequently, the shape of the sharp wave could be important during the ripple event. Other shapes may produce other types of firing patterns. For example, suppose the Sharp Wave had a slow rise and a rapid decline. Figure 3.23 shows a simulation of this case. Due to the slow rise, the first spike is delayed until after the midpoint of the Sharp Wave, when the excitation is sufficient to exceed the inhibition.

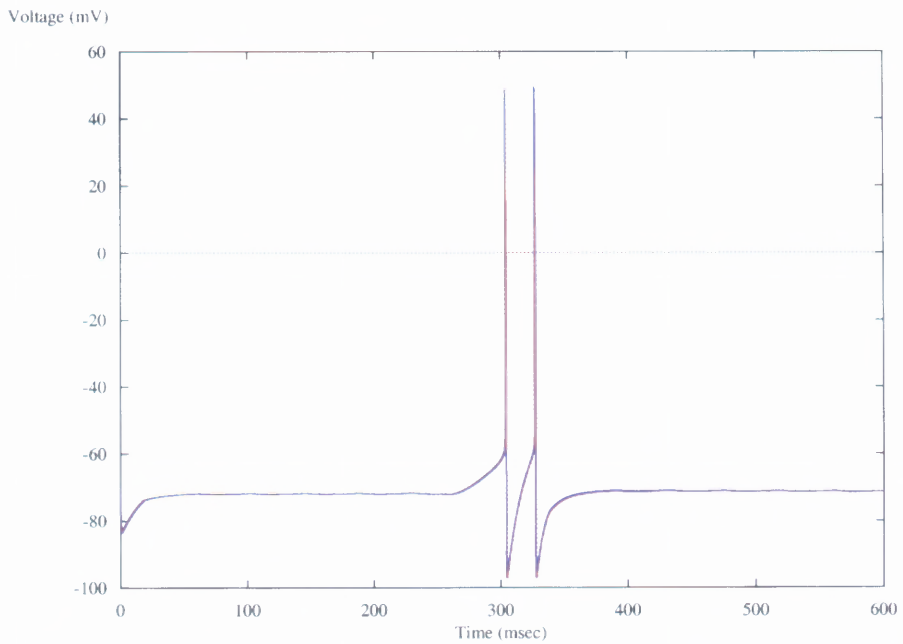

Figure 3.23 Simulation Results for a Sharp Wave Input to the Pyramidal Cells With a Slow Rise. Since the excitation slowly builds, the first action potential is delayed until after the midpoint of the Sharp Wave event. The pyramidal cells receive Sharp Wave input from $t = 260$ until $t = 340$.

CHAPTER 4

EXISTENCE AND STABILITY OF PERIODIC SOLUTIONS

In this chapter, it is proven that stable, periodic solutions exist within the PIP network. Action potential timing of single and paired pyramidal cells is discussed.

4.1 Existence of Periodic Solutions in the PIP Mini-Network, with Depressing Synapses

In this section, a proof is given of the existence of synchronous, periodic solutions between two, uncoupled pyramidal cells, both receiving inhibition from a single interneuron, as depicted in Figure 3.20. The PIP mini-network is used to demonstrate how pyramidal cells are synchronized rapidly during the SPWR, which lasts for only a short period of time, approximately 100 msec. Requirements for existence will be given. The stability of these solutions will be discussed in the Section 4.2.

In the Section 3.4, the process whereby a pyramidal cell fires was explained, and the mechanism was illustrated by the $g - w$ phase plane and the g phase line. Recall that a pyramidal cell fires if the cell can move from g_{imax} to g^* before more inhibition is applied. In Appendix A, two sequences, $\{g_n\}$, given by (A.4), and $\{g_n^{T_{in}}\}$, given by (A.7), are derived, describing how the synaptic strength evolves while the synapse is being used. The value g_n represents the amount of inhibition applied to the pyramidal cell each time the interneuron fires. The value $g_n^{T_{in}}$ equals the level of synaptic strength g_n decays to between inhibitions, right before receiving another inhibitory dose. If the synapse is depressing and repeated high-frequency inhibition is applied to the pyramidal cells (such as during the SPWR), g_n and $g_n^{T_{in}}$ will decrease, meaning the synapse cannot recover fully between uses. It was also shown that regardless of initial conditions, the sequences g_n and $g_n^{T_{in}}$ will approach the same respective steady state, given by g_∞ and $g_\infty^{T_{in}}$, whose equations are (A.5) and (A.8). Figure 4.1 shows a voltage trace of how a pyramidal cell can fire if depression is present.

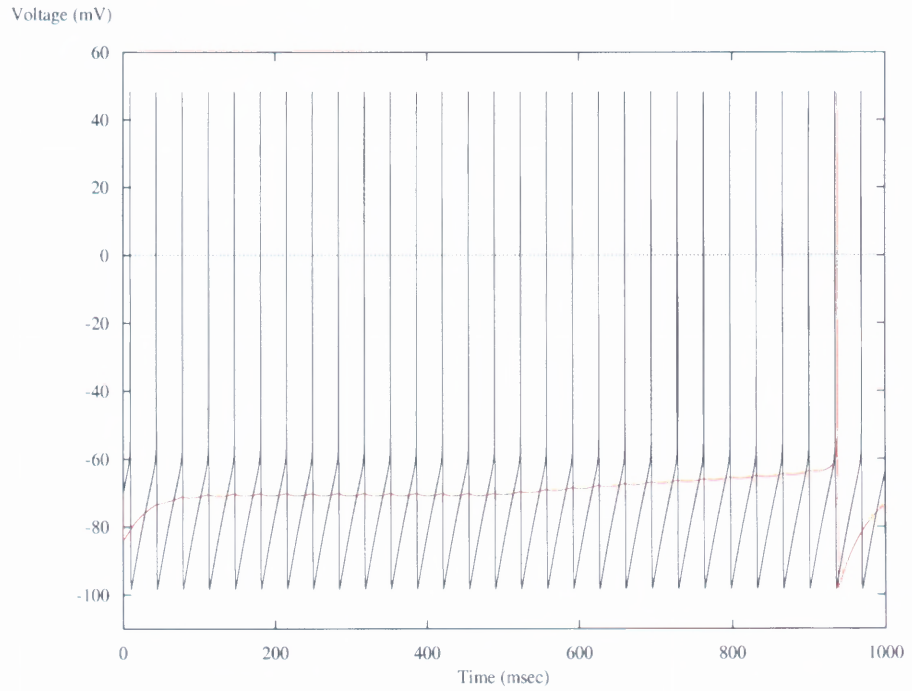

Figure 4.1 A Pyramidal Cell Fires if Depression is Present. At $t = 0$, a pyramidal cell (red) begins its approach to fire, but an interneuron begins to apply inhibition at a frequency $\sim$ 30 Hz. Each time the pyramidal cell receives inhibition, it is prevented from firing. The value of τ_a was chosen to be very small, allowing the synapse to recover between dose of inhibition. At $t = 400$ msec, τ_a is set to 500, causing depression to occur. Eventually, the strength of the synapse is low enough that the pyramidal cell can fire. Note here that because the interneuron is oscillating at such a low frequency, τ_a needed to be large in order for there to be enough depression. Even at this large value, it still took a long time for the pyramidal cell to overcome the inhibition and fire.

Figure 4.2 illustrates how a pyramidal cell may fire while receiving depressing, inhibition. The sequences $\{g_n\}$ and $\{g_n^{T_{in}}\}$ decrease because the synapse cannot fully recover between uses, so eventually g crosses g^* and the pyramidal cell can fire. Using this as the condition for a cell to fire and (A.8), the number of cycles needed for the cell to fire can be derived from

$$\begin{aligned} g^* &\geq g_n^{T_{in}} \\ &\geq g_{syn} e^{-K} \left[1 - \left(e^B - 1 \right) \left(\frac{1 - e^{-(n+1)(A+B)}}{1 - e^{-(A+B)}} - 1 \right) \right], \end{aligned} \tag{4.1}$$

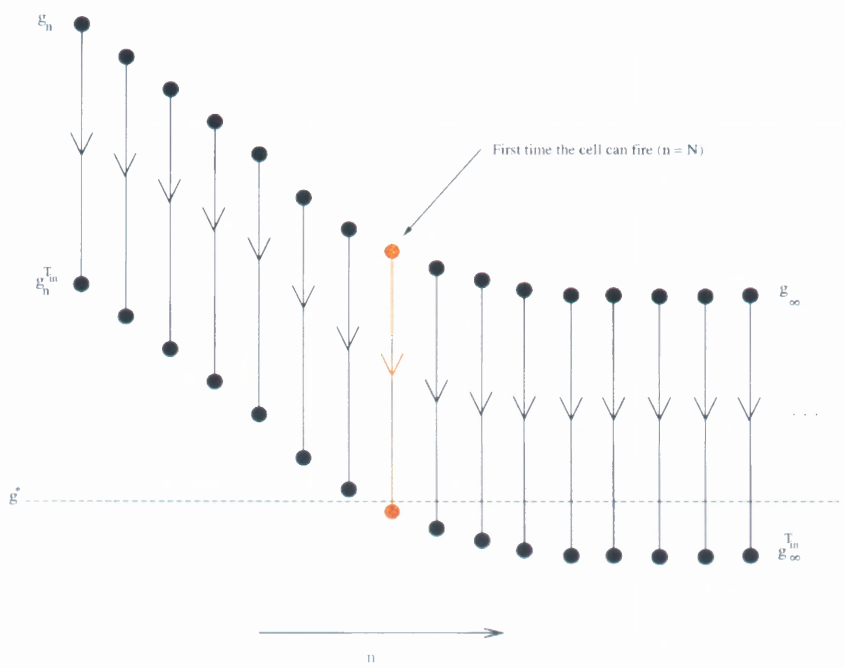

Figure 4.2 An illustration of how g_n and $g_n^{T_{in}}$ evolve with time.

where $A = \frac{T_{in}}{\tau_a}$, $B = \frac{\Delta t_f}{\tau_b}$ and $K = \frac{T_{in}}{\tau_k}$. For any n greater than some N, (4.1) will be satisfied. By solving (4.1) for n, the number of cycles of inhibition needed to allow the pyramidal cell to fire is

$$N = \frac{1}{A+B} \ln \left[\frac{e^{-A}(1-e^{-B})}{\left(\frac{g^*}{g_{syn}}\right) e^{K}(1-e^{-(A+B)}) + e^{-A} - 1} \right] \tag{4.2}$$

rounded up to the nearest integer.

Now, consider how certain parameters affect the sequence $\{g_n^{T_{in}}\}$. Recall that as τ_a increases, A decreases. From (A.2), we see that D_n decreases more quickly if τ_a increases, since the terms being subtracted are larger. Thus, $\{g_n^{T_{in}}\}$ will decrease more quickly. In the case of very slow recovery of D, τ_a is so large that A is effectively 0. Thus,

$$g_n^{T_{in}} = g_{syn} e^{-K} \left[1 - \left(e^{B} - 1\right) \left(\frac{1 - e^{-(n+1)B}}{1 - e^{-B}} - 1 \right) \right] \tag{4.3}$$

$$= g_{syn} e^{-(K+Bn)}. \tag{4.4}$$

And, as $n \to \infty$, $g_{\infty}^{T_{in}} \to 0$.

The value for n that allows the cell to fire is

$$N = \frac{1}{B} \ln \left[\frac{g_{syn} e^{-K}}{g^*} \right]. \tag{4.5}$$

In the case of very high frequency inhibition, where T_{in} is very small, and therefore $A = K = 0$:

$$g_n^{T_{in}} = g_{syn} e^{-Bn}. \tag{4.6}$$

As $n \to \infty$, $g_{\infty}^{T_{in}} \to 0$. And the value for n that allows the cell to fire is

$$N = \frac{1}{B} \ln \left[\frac{g_{syn}}{g^*} \right]. \tag{4.7}$$

While slowly recovering, depressing synapses and very high-frequency inhibition produce the same qualitative result: slow synaptic recovery allows the cell to fire in a shorter amount of time than very high-frequency inhibition, since the number of inhibitions needed for the pyramidal cell to fire in (4.7) is less than that for slow synaptic recovery in (4.5), as $n \to \infty$. This is because for very high-frequency inhibition, the synapse does not get a chance to decay between inhibition, while for lower frequencies with slow recovery, the added decay of the synapse allows g to approach g^* more quickly.

The frequency of the inhibition affects $\{g_n^{T_{in}}\}$ in a peculiar way. As T_{in} increases, so do A and K. From (A.2) and (A.7), we see that D_n decreases more slowly, but $g_n^{T_{in}}$ achieves lower values since the synaptic strength is able to decay longer for larger periods between inhibitions. This interplay between frequency of inhibition and synaptic recovery leads to the two different regimes where the cell has access to a knee, $T_{in} \geq T^*$ or $T_{in} \leq T_*$, where $T_* < T^*$. For $T_{in} \geq T^*$, the inhibition period is long enough so the cell can reach the knee, despite the fact that D_n decreases more

slowly. For $T_{in} \leq T_*$, D_n decreases rapidly, allowing access to the knee, despite the fact that $g_n^{T_{in}}$ does not reach lower values.

These intervals can be visualized. If

$$g_\infty^{T_{in}} - g^* > 0, \tag{4.8}$$

the cell will never fire. The inhibition period, T_{in} is implicit on the left-hand side of (4.8). By plotting the left-hand side in Figure 4.3 and determining which portions of the function are less than or equal to 0 , it becomes evident that if $T_{in} \geq T^*$ or $T_{in} \leq T_*$, the cell can fire eventually. If $T_* < T_{in} < T^*$, the cell will not fire.

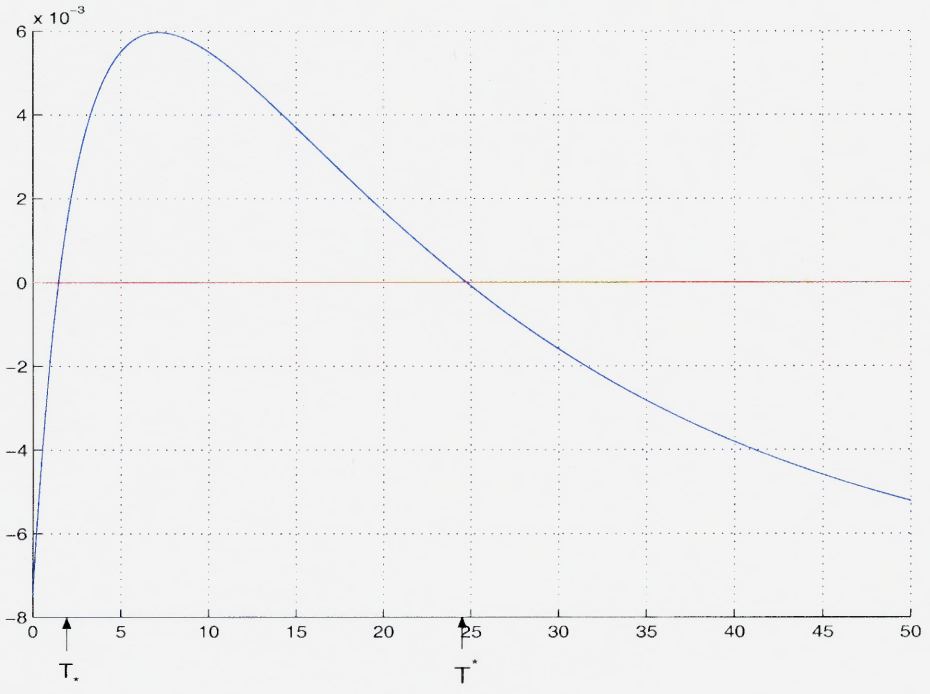

Figure 4.3 The Pyramidal Cell will never fire for $T_{in} \in (T_*, T^*)$s. The independent variable is T_{in} (msec). The dependent variable is $g_\infty^{T_{in}} - g^*$. The parameter values are $g_{syn} = 0.03$, $\tau_k = 20$, $\tau_a = 2000$, $\tau_b = 5$, $g^* = 0.075$ and $\Delta t_f = 0.01$. The value of τ_a was inflated in order to make the interval from 0 to T_* more pronounced.

A theorem for existence can now be stated, using the previous reasoning:

Theorem 1 (Existence). *For a fixed rate of recovery (τ_a), synaptic resource usage (τ_b), synaptic decay (τ_k), synaptic strength (g_{syn}), and period of inhibition (T_{in}), there*

exists a synchronous, periodic solution in the PIP Network, based upon the system of equations (3.5) with depressing synapses defined by (3.18). The type of synchronous, periodic solution depends on T_{in}. Furthermore, there exist $T_* < T^*$ such that

1. *if $T_* < T_{in} < T^*$, there exists a sub-threshold, synchronous periodic solution.*
2. *if $T_{in} \leq T_*$ or $T_{in} \geq T^*$, there exists a synchronous, periodic solution that produces action potentials, which could be one of two types:*
   (i) An orbit that oscillates at the cell's intrinsic frequency.
   (ii) An orbit that oscillates with a frequency that is $\mathcal{O}(\frac{1}{\tau_k})$.

The existence of these three intervals for T_{in} can be proven by showing that left-hand side of (4.8) has a single maximum that's greater than zero and that, on either side of the maximum, the function decreases to a negative number. This proof is given in Appendix B.

If excitatory input is applied to the cell, as discussed in Section 3.4, the sequence $\{D_n\}$ and, therefore, $\{g_n\}$, will shift down in the $g-w$ phase plane. The new condition for never firing will now be

$$g_\infty^{T_{in}} - g_{excite} - g^* > 0, \tag{4.9}$$

where g_{excite} is the g-value corresponding to the input current. The curve in Figure 4.3 will lower accordingly, reducing the range of T_{in} for which the cell cannot fire. Recall, however, that too much excitation will trap the cell in the active state. The amount of excitation must be kept below that value.

Both types of synchronous solutions will now be identified by construction. Along a synchronous solution, the cells behave identically, so the activity of only one cell will be examined.

4.1.1 Existence of the Synchronous Solution for $T_* < T_{in} < T^*$

Consider the case when $T_* < T_{in} < T^*$. See Figure 4.4. Assume the inhibition strength has reached a steady state, as in (A.8). On the g phase line, the cell starts at $g = g_\infty$. At $g = g_\infty$, the cell has just received a dose of inhibition, w has decayed and the cell has become trapped by the intersecting critical point along the *curve of critical points*. The variable g decays and travels down the g phase line, as the inhibition decays. However, when $g = g_\infty^{T_{in}}$, the cell receives another dose of inhibition. Since (4.8) is satisfied ($g_\infty^{T_{in}} > g^*$), the cell has not fired. The inhibition sets $g = g_\infty$ and the process repeats. The cell oscillates at the intrinsic frequency between doses of inhibition.

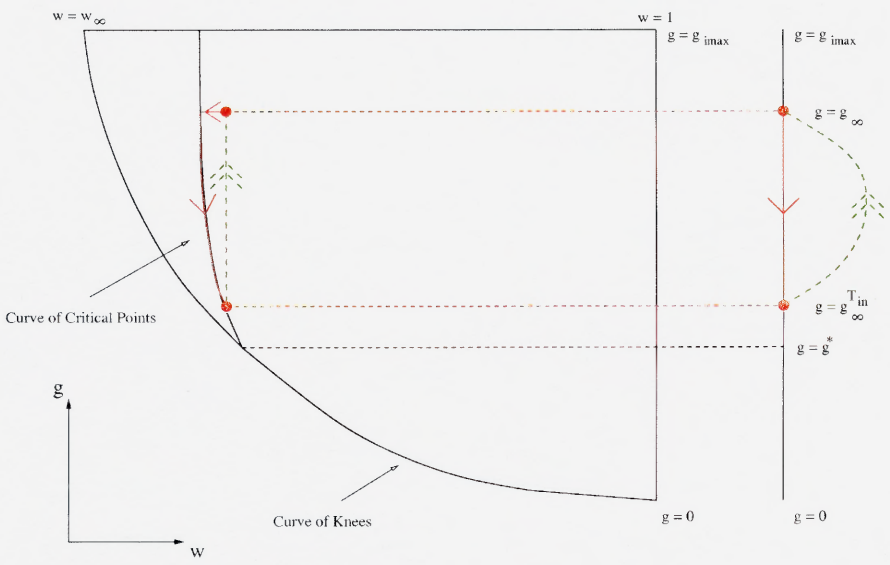

Figure 4.4 The Synchronous Solution for $T_* < T_{in} < T^*$. The orbit depicted represents the synchronous orbit as $g_n \to g_\infty$. The cell travels down the *curve of critical points* until it receives more inhibition. Then, the cell jumps in "fast" time to a different w-value and decreases until it is trapped by the *curve of critical points*. The process repeats.

4.1.2 Existence of the Synchronous Solution for $T_{in} \geq T^*$ or $T_{in} \leq T_*$

Consider the case for $T_{in} \geq T^*$ or $T_{in} \leq T_*$. The cell will eventually fire for some $n \geq N$, as determined in (4.2). On the g phase line, the two types of action potential-producing, periodic orbit can be visualized. See Figure 4.5. Assume that the required number of inhibition cycles has been reached ($n > N$, where $N < \infty$). As before, assume that the inhibition has reached a steady state, as in (A.8). The $g = g_\infty^{T_{in}}$ is less than that for Section 4.1.1, since for these ranges of T_{in}, $g_\infty^{T_{in}}$ is less than g^*.

Let the synchronized cells start at $g = g_\infty$ and a particular w-value on the two-dimensional, "slow" manifold. If $g_\infty \leq g*$, the cell travels along a trajectory on the "slow" manifold, accesses a knee and fires. It is mapped to the same g-value, since the jump happens instantaneously in "fast" time, but it is mapped to a w-value away from the *curve of knees*. Again, the cell travels down a trajectory on the "slow" manifold and approaches the *curve of knees* in "slow" time. However, g decays as well. The cell will again reach the *curve of knees* and fire. The cell will produce a number of action potentials that depends on its intrinsic frequency and the time between inhibitions. For a high intrinsic frequency and a long inter-inhibition period, the cell may produce multiple spikes. For a low intrinsic frequency and a short inter-inhibition period (as during the experimentally observed SPWR), the cell may only produce one action potential. As the pyramidal cell fires, $g \to g_\infty^{T_{in}}$. Then, it receives more inhibition and is mapped back to $g = g_\infty$ and the original w-value, where it continues the same process. This orbit is pictured in Figure 4.5. The frequency of this orbit is $\mathcal{O}(\tau_k)$, since τ_k is the rate constant that determines the time it takes the cell to reach the curve of knees and produce its action potentials.

If $g_\infty > g^*$, the cell travels along the "slow" manifold, but cannot immediately access a knee. It has to wait until $g = g_\infty$ decays to $g = g^*$. At which point, the cell fires and, as described above for the other type of action potential-producing orbit, begins to oscillate at its intrinsic frequency. The variable $g = g_\infty$ continues to decay

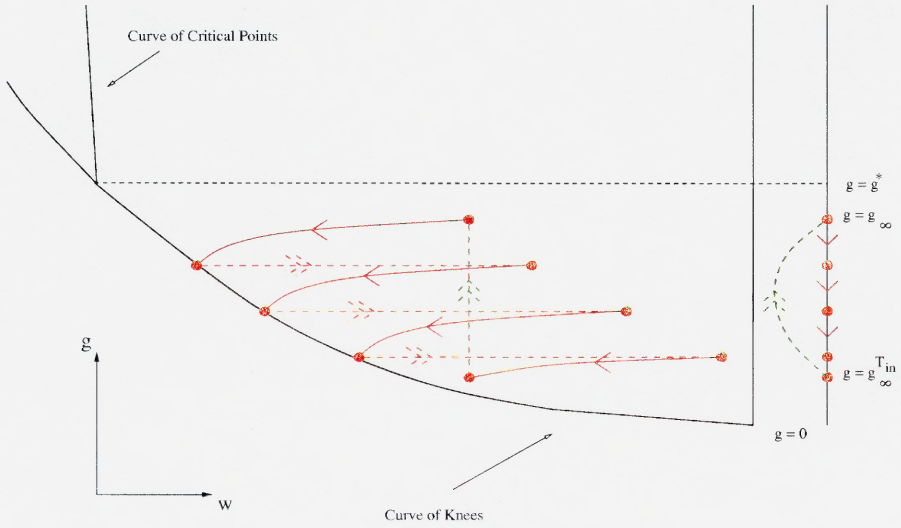

Figure 4.5 The First Type of Synchronous Solution for $T_{in} \geq T^*$ or $T_{in} \leq T_*$. In this case, $g_\infty \leq g^*$, so the cell can access a knee and fire at intrinsic frequency as g decays. When $g = g_\infty^{T_{in}}$, the cell receives more inhibition at some position while w is decaying, defined by $g_\infty^{T_{in}}$, and the cell is mapped onto a new stable manifold defined by g_∞, represented by the dotted, green line. This process repeats. The dotted, double-arrow line represents the fact that the cell is firing action potentials in "fast" time as g decays, but this movement in the v-direction is not pictured on the $g - w$ phase plane. Again, this orbit can also be visualized on the g phase line. For illustrative purposes, the frequency of the pyramidal cell is much higher than that of the interneuron.

to $g = g_\infty^{T_{in}}$. When it receives more inhibition, the cell is mapped to $g_\infty > g^*$ again, where it must wait to fire as g decays. The sequence continues. In this case, the periodic orbit has two modes of oscillation. One is the intrinsic frequency when the cell can reach a knee. The other frequency depends on the time it takes the cell to decay from g_∞ to g^*. This orbit is shown in Figure 4.6.

These synchronous orbits may be more readily visualized as voltage traces. Figure 4.7 shows examples of each type of synchronous solution.

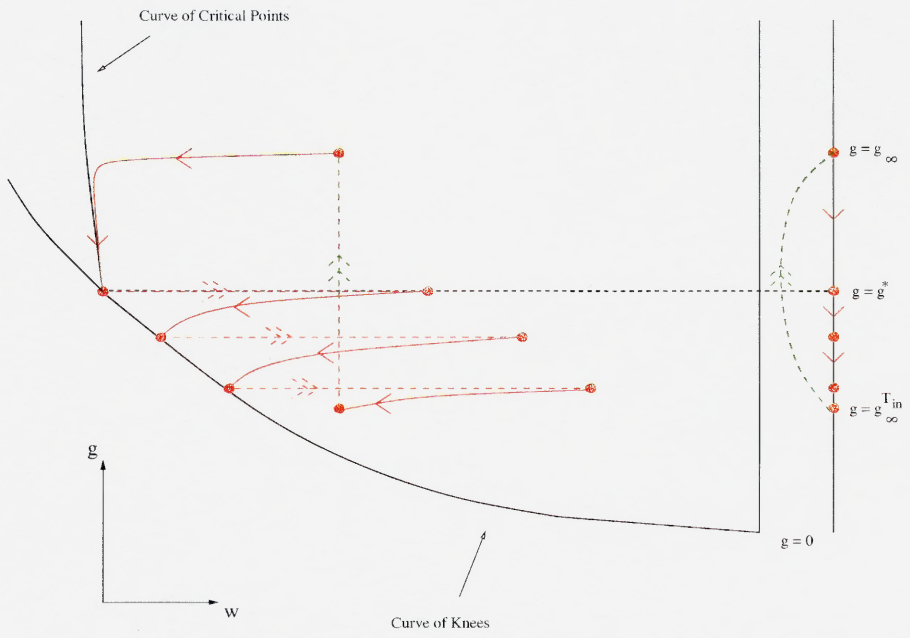

Figure 4.6 The Second Type of Synchronous Solution for $T_{in} \geq T^*$ or $T_{in} \leq T_*$. In this case, $g_\infty > g^*$, so the cell cannot access a knee and must wait. When a knee is available, the cell fires at its intrinsic frequency as g decays. When $g = g_\infty^{T_{in}}$, the cell receives more inhibition at some position on the w-manifold defined by $g_\infty^{T_{in}}$ and the cell is mapped onto the w-manifold defined by g_∞. This process repeats. The dotted, double-arrow line represents the fact that the cell is firing action potentials in "fast" time as g decays, but this movement in the v-direction is not pictured on the $g - w$ phase plane. Again, this orbit can also be visualized on the g phase line. For illustrative purposes, the frequency of the pyramidal cell is much higher than that of the interneuron.

4.2 Stability of the Synchronous Solutions

In the previous section, it was shown that a synchronous solution exists for different inhibition frequencies. Now, the question of stability is addressed.

Theorem 2 (Stability). *For fixed rates of synaptic recovery (τ_a), synaptic resource usage (τ_b), synaptic decay (τ_k), synaptic strength (g_{syn}), and period of inhibition (T_{in}):*

1. *The sub-threshold, synchronous, periodic solutions defined in Theorem 1 is stable and unique.*

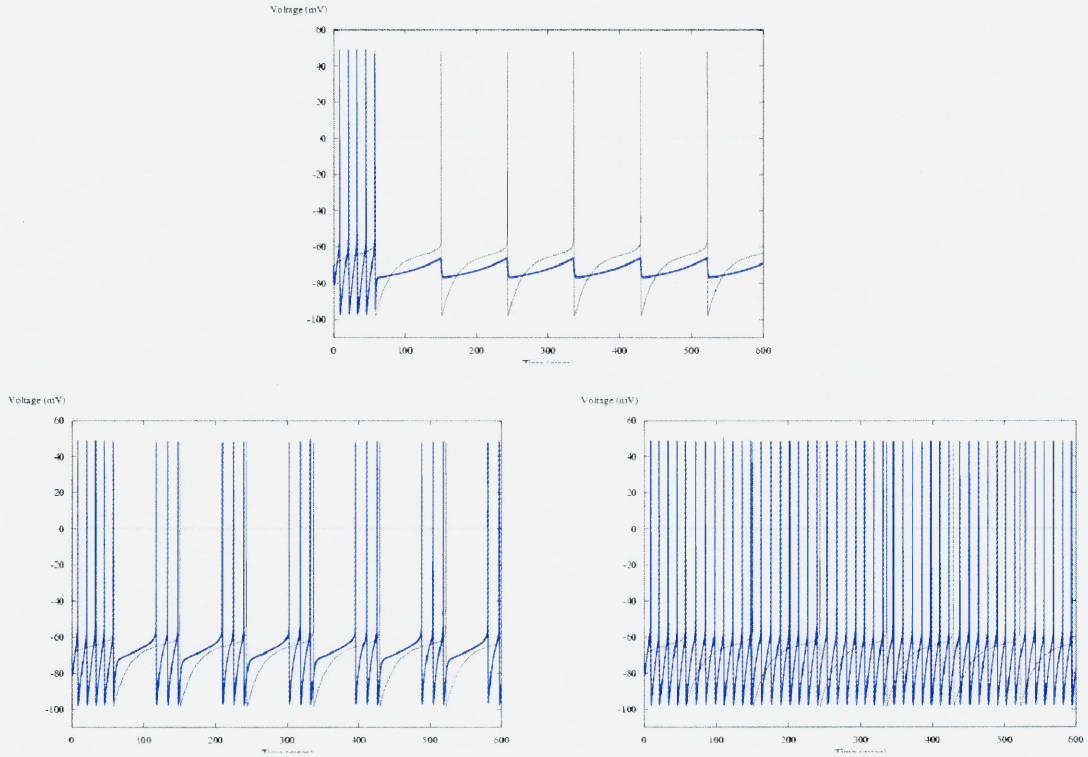

Figure 4.7 Voltage Traces of the Three Types of Synchronous, Periodic Orbits of the PIP Sub-Network. The upper trace shows the sub-threshold, synchronous orbit. The lower left trace shows the action potential-producing, synchronous orbit that oscillates with a frequency on the order of the synaptic decay rate. The lower right trace depicts the synchronous orbit that produces action potentials, oscillating at the cells' intrinsic frequencies.

2. *The action potential-producing, synchronous periodic orbit, that oscillates at its intrinsic frequency, as defined in Theorem 1, is stable and unique.*

3. *The action potential-producing, synchronous periodic orbit, that oscillates with a combination of the cell's intrinsic frequency and the time it takes for the cell to reach threshold, as defined in Theorem 1, is stable and unique.*

Proof. This proof of stability and uniqueness uses the work done in Appendix A. Recall that the type of synchronous solution was determined from the following two

sequences:

$$g_n = g_{syn}\left(\frac{1-e^{-A}+e^{-n(A+B)}\left[D_0(1-e^{-(A+B)})+e^{-A}-1\right]}{1-e^{-(A+B)}}\right) \quad (4.10)$$

and

$$g_n^{T_{in}} = g_{syn}e^{-K}\left(\frac{1-e^{-A}+e^{-n(A+B)}\left[D_0(1-e^{-(A+B)})+e^{-A}-1\right]}{1-e^{-(A+B)}}\right), \quad (4.11)$$

which describes, respectively, the level of synaptic strength after the n^{th} dose of inhibition and prior to the $(n+1)^{st}$ dose of inhibition after having decayed for T_{in} time.

As $n \to \infty$, these two sequences define all the steady state, synchronous, periodic solutions constructed in Section 4.1. Consider these sequences to be mappings of the pyramidal cell on the g phase line. The steady state, synchronous, periodic solutions correspond to the fixed points of these mappings. If it can be shown that these fixed points are stable and unique, then the periodic orbits will also be stable and unique.

Since both mappings are equivalent, one being a scalar multiple of the other, consider only the mapping defined by $g_n^{T_{in}}$. Let a single cell be located on the steady state, synchronous, periodic solution defined by $g_\infty^{T_{in}}$. Another cell is perturbed away from the cell along the g phase line at $g = g_\Delta$. From (4.10), $g_n^{T_{in}}$ depends on the initial amount of synaptic resources, D. So, for the second cell, let the amount $D = D_\Delta$. The perturbation D_Δ has a range of $[0,1]$ and for $g_\infty^{T_{in}}$, the corresponding synaptic resources $D_\infty^{T_{in}} \in (0,1)$.

As time starts, the first cell will remain at the steady state solution. If the second cell starts at g_Δ corresponding to $D_\Delta = 1 > D_\infty^{T_{in}}$, as $n \to \infty$, the sequence $g_n^{T_{in}}$ will decrease to $g_\infty^{T_{in}}$, as defined by (A.8). If the second cell starts at g_Δ corresponding to $D_\Delta = 0 < D_\infty^{T_{in}}$, as $n \to \infty$, the sequence $g_n^{T_{in}}$ will increase to $g_\infty^{T_{in}}$. Thus, the steady state, periodic, synchronous solutions are stable and unique. □

4.2.1 Approach to Synchrony for $T_* < T_{in} < T^*$

While each synchronous orbit has been shown to be stable and unique, each solution is approached in different ways. For the case of $T_* < T_{in} < T^*$ and the sub-threshold synchronous orbit, consider two, identical pyramidal cells, c_1 and c_2, as illustrated in Figure 4.8. The cells have just received a first dose of inhibition by the interneuron. The cell c_1 has already jumped down onto the left branch of the inhibited v-nullcline and is at $g = g_0$. The cell c_2 has just jumped down onto the same stable manifold, but is behind c_1 in time. The time distance between the two cells is measured from the leading cell and to the trailing cell, though c_1 may not always be the leading cell.

At time $t = 0$, the cells travel along the same trajectory on the "slow" manifold, and become trapped by the *curve of critical points* at $w = w_\infty$, defined by (3.10). Here, as time evolves, the cells continually move closer together spatially, but not temporally, since each cell approaches the critical point at the same rate. They remain t_0 time apart.

The g-values for both cells decay towards 0 and the cells move down the *curve of critical points*, but remain on the same trajectory as g changes. At some point, the cells receive another dose of inhibition, before they can access the *curve of knees*. The "fast" inhibition maps the cells onto a different trajectory on the "slow" manifold, but to higher g values, since D recovers while the inhibiting cell is silent. However, assuming D does not recover fully, the new g-values associated with the cells are less than when they originally jumped down, as expressed mathematically by the decreasing sequence $\{D_n\}$ in (A.2). Since the inhibition occurs in "fast" time, the cells map instantaneously to their new position, remaining the same spatial distance apart. However, the cell's are farther away from the $w = w_\infty$ and, therefore, their velocity in the w-direction has increased. This is a reasonable assumption, since inhibition would cause faster recovery. As a consequence, the cells will have moved closer together in time, such that their new time distance is $t_1 < t_0$. Note that the cells' position have

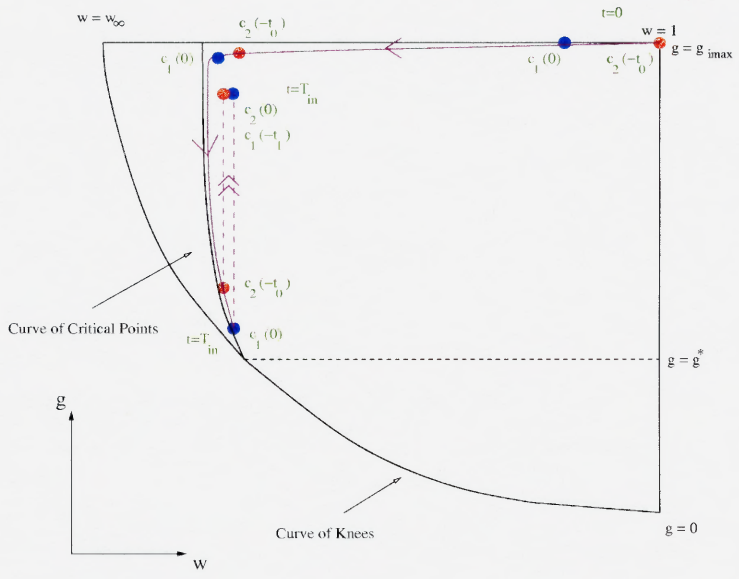

Figure 4.8 An illustration of how two cells compress temporally after the first dose of inhibition. At $t = 0$, the cell have just jumped down from the active state and travel down the stable manifold, where they are trapped by the critical point. They are still time t_0 apart (each cell's distance from the leading cell is recorded, i.e. cell 1 is the trailing cell so it is assigned $c_1(0)$ and cell 2 is t_0 behind c_1 so it is assigned $c_2(-t_0)$). The cells are being compressed spatially due to the presence of the fixed point. Then, the cells follow the *curve of critical points* as g decays. At $t = T_{in}$, the cells receive inhibition and they jump instantaneously to a new stable manifold. Since they increased their velocities, but instantaneously increased their speed in the w-direction while keeping the same spatial distance apart, time has compressed between the cells. The new time distance $t_1 < t_0$. Also, the leading and trailing cells have interchanged, since the leading cell had a larger w-value along the *curve of critical points* when both cells received inhibition. When the cells arrive on the new stable manifold, the higher w-value places the leading cell behind the previously trailing cell.

interchanged. The leading cell had a larger w-value when it received inhibition, thus, when it instantaneously jumped to a new stable manifold, it became the trailing cell. This analysis is similar to work presented in [42]. However, in [42], the cells fired simultaneously, compressing in time as they crossed the action potential threshold and were mapped to a different "slow" manifold. Here, the cells compress in time below threshold and they are mapped onto the same "slow" manifold.

Note that the above reasoning uses an assumption that $g_{n+1} > g_n^{T_{in}}$. In order for $g_n^{T_{in}}$ to be less than g_{n+1}, the following inequality, obtained using, using (A.4) and (A.7), must hold:

$$g_{syn}e^{-K}\left[\frac{1-e^{-A}+e^{-A}\left(1-e^{-B}\right)e^{-n(A+B)}}{\left(1-e^{-(A+B)}\right)}\right] < g_{syn}\left[\frac{1-e^{-A}+e^{-A}\left(1-e^{-B}\right)e^{-(n+1)(A+B)}}{\left(1-e^{-(A+B)}\right)}\right]. \tag{4.12}$$

Through algebraic manipulation, the condition becomes

$$\rho = \frac{\left[e^{-A}\left(1-e^{-B}\right)e^{-n(A+B)}\right]\left[e^{-K}-e^{-(A+B)}\right]}{\left(1-e^{-K}\right)\left(1-e^{-A}\right)} < 1. \tag{4.13}$$

If $\rho > 1$, D recovers so slowly that when g_n is set equal to $g_{syn}D_n$, the cells jump down in the g-direction, causing expansion in the time between cells.

Continuing with the approach to synchrony, the cells will again travel down a stable manifold and become trapped. This time, their g-values will reach a lower value than before, and the cells will move further to the right as they follow the *curve of critical points.* When the cells receive inhibition again, they will be mapped again to a new g-value, again switching positions. There will be time compression when they receive the inhibition, such that the new time distance $t_2 < t_1$. This process will now repeat. Figure 4.9 illustrates this process.

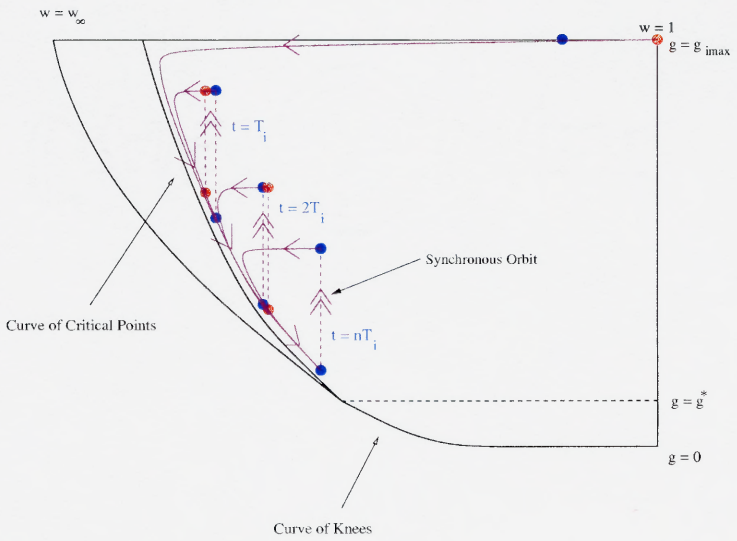

Figure 4.9 An illustration of how two cells repeatedly compress in time, due to inhibition. As g decreases in value, the orbits approach the limiting, synchronous orbit defined in Section 4.1.1. In this picture, the *curve of critical points* is exaggerated in order to better visualize the cells' movements.

Since $T_* < T_{in} < T^*$, the cells will never reach a knee, and they will approach the sub-threshold, synchronous solution discussed in Section 4.1. Each time the cells receive "fast" inhibition, time compresses between the cells and $t_n \to 0$.

4.2.2 Approach to Synchrony for $T_{in} \geq T^*$ or $T_{in} \leq T_*$

Recall that there can be two different, synchronous orbits for these ranges of T_{in}. The same arguments about time compression below threshold, used in the previous section, hold in this case for cycles of inhibition $n < N$. Now, consider the cycle $n = N$. From the previous inhibition, the cells are on a trajectory on the "slow" manifold, t_N time apart. The cells have been compressed in time for N cycles. Note that the amount of compression depends on the value of N, which depends on the various parameters.

As g decays, the cells will access the *curve of knees* when their g-value equals g^*. Since either cell may be leading at this time, without loss of generality, let c_1 jump first, followed by c_2. The variable g evolves on the "slow" time manifold, decaying while each cell oscillates at the same rate, staying the same time distance apart. This will continue until they receive more inhibition. The cells produce an action potential in "fast" time. Since "fast" time happens instantaneously relative to "slow" time, the cells can receive inhibition only when they are on the "slow" manifold. When this happens, the same time compression occurs as described in previous sections, as the cells jump to a new, stable manifold that has w-values farther away from w_∞. The cells are now time distance $t_{N+1} < t_N$ apart. Note that in this case, the cells do not switch positions. See Figure 4.10.

If, while on this new trajectory, $g > g^*$, the cells must again wait until they can access a knee before firing and repeating the process above. If $g \leq g^*$, the cells will continue to oscillate, each time receiving inhibition while on the "slow" manifold and compressing in time each time they receive inhibition. This process will continue as g decays to its steady state, which defines the synchronous solutions constructed in the previous section. Again, the cells will not switch positions. See Figure 4.11.

4.3 Synchronous Solutions Within the Simulated Ripple

Now that various synchronous solutions have been identified and shown to be stable within the PIP sub-network, the simulated results seen in Section 3.6 can be explained. Recall that before the SPW arrives, the pyramidal cells are oscillating out of phase with a frequency of $\sim$ 1 Hz. The SPW excitation reaches the interneurons first, causing them to oscillate at ripple frequency, $\sim$ 200 Hz. The high frequency inhibition applied to the pyramidal cells has a period $T_{in} \in (T_*, T^*)$ and the pyramidal cells are prevented from firing. However, the cells compress together in time below threshold as they receive repeated inhibition.

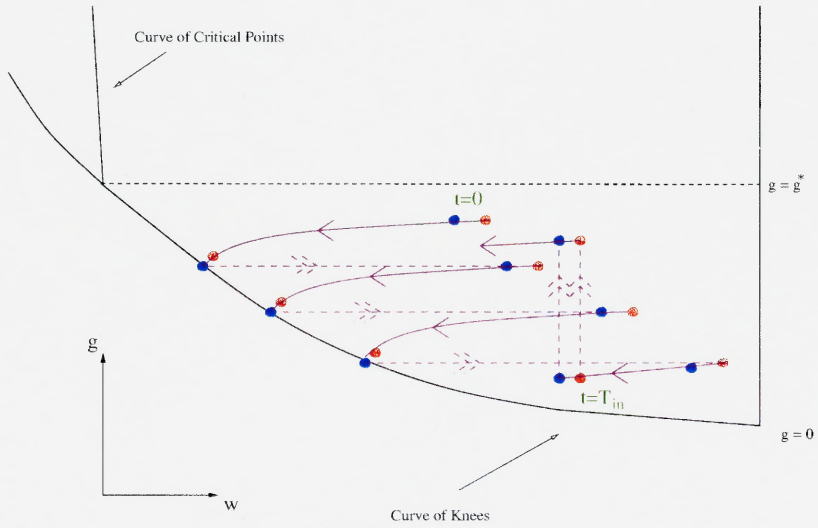

Figure 4.10 An illustration of how two cells compress temporally after a dose of inhibition, for the First Type of Synchronous Orbit. At $t = 0$, the cells travels down a trajectory on the "slow" manifold. The cells reach the *curve of knees* and fire, staying the same time distance apart. They continue to fire as g decays. At $t = T_{in}$, the cells receive inhibition, causing them to instantaneously jump to a different trajectory. Since their velocities have increased and they remain the same spatial distance apart, the time between them has decreased. Note that for this case, $g < g^*$ when they receive inhibition.

When the SPW excites the pyramidal cells, the curve shown in Figure 4.3 will lower, as discussed at the end of Section 4.1, and the interval (T_*, T^*) will decrease and may disappear all together, if the excitation is strong enough. Since the interneuron maintains the same period of inhibition, T_{in} will now be in the interval $(0, T_*]$, for which the pyramidal cells can fire. This concept is illustrated in Figure 4.12. Due to the sub-threshold time compression, they fire synchronously.

After the initial action potential, while the pyramidal cells recover, the curve in Figure 4.3 raises as the SPW begins to leave the PIP sub-network. However, due to the high frequency inhibition, the synaptic strength has decreased over the course of the SPWR, preventing the curve in Figure 4.3 from raising sufficiently so that T_{in}

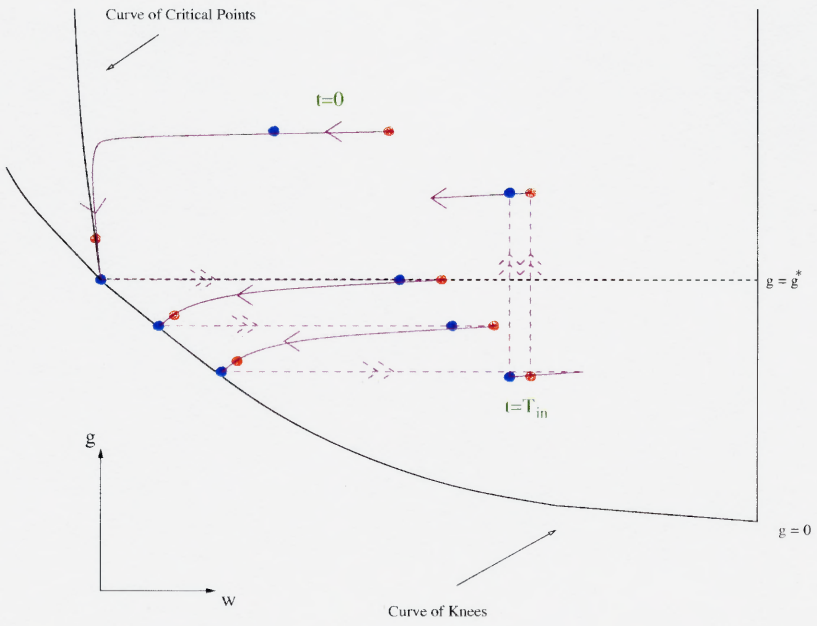

Figure 4.11 The cells approach the Second Type of Synchronous Orbit. At $t = 0$, the cells are on a trajectory on the "slow" manifold and become trapped by the *curve of critical points*, compressing in space. When the cells reach g^*, they begin to oscillate. When the cells receive inhibition and are instantaneously mapped to another trajectory, where they continue this process. As described in previous arguments, there is time compression. The cells do not switch position.

is again in the range (T_*, T^*). This allows the pyramidal cells to fire a second time before the SPW leaves the region completely and the sub-network returns to normal. It is also possible that if the SPW excitation leaves the pyramidal cells rapidly that T_{in} may enter the interval (T_*, T^*) for a brief period of time before the synaptic depression causes it to leave again, allowing the pyramidal cells to fire the second time.

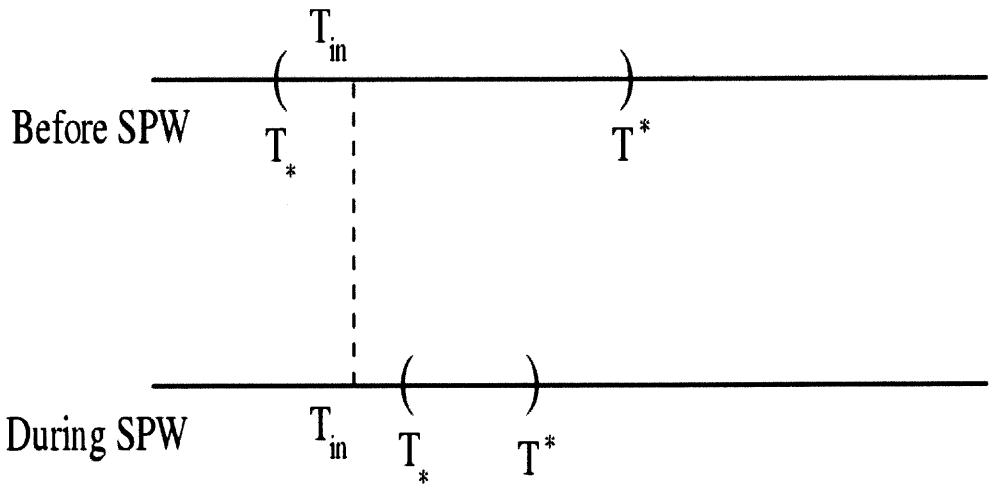

Figure 4.12 Sharp Wave Excitation Decreases the Interval of Inhibition Periods for which the Pyramidal Cells Cannot Fire. The curve in Figure 4.3 shifts down when the pyramidal cells are excited, decreasing the portion of the curve greater than 0. For the same inhibition period, T_{in}, the cells that before the SPW could not fire are able to fire during the SPW. This phenomenon is equivalent to the decrease of synaptic strength during depression.

CHAPTER 5

INTRACELLULAR NOISE

Neurons rarely display ideal output as described by the Hodgkin-Huxley system. One may ask what causes the observed discrepancies between a model and the actual neuron output. It could be that some process yet to be quantified is affecting how the neuron produces action potentials. This component may display seemingly random properties and could be modeled by adding noise to the original, deterministic system.

In this chapter, a particular type of intracellular noise produced by sodium channel inactivation is introduced. The model is extended to include this intrinsic randomness and it is used to explain experimental results about pyramidal cell reliability. Also, pyramidal cell timing and synchronization are addressed in the presence of this intrinsic noise. Finally, a question is answered: Can high frequency inhibition, with tonic excitation and no noisy external input, as seen during the SPWR, produce synchronization amongst identical pyramidal cells, despite intracellular noise?

5.1 Sodium Channel Inactivation

In an article by Henze and Buzsaki [17], they discuss how the threshold voltage of action potentials vary for CA1 pyramidal cells in vivo, and how this may contribute to the timing of action potentials. They conclude that one of the factors that cause this variability of threshold was the inactivation of sodium ion channels. Other papers have investigated this phenomenon [31], and have linked it to the activity-dependent attenuation of back-propagating action potentials [25].

This dissertation proposes that sodium channel inactivation (or a similar process) accounts for the low reliability for tonic input, as seen in [30] and discussed in Section 5.6.

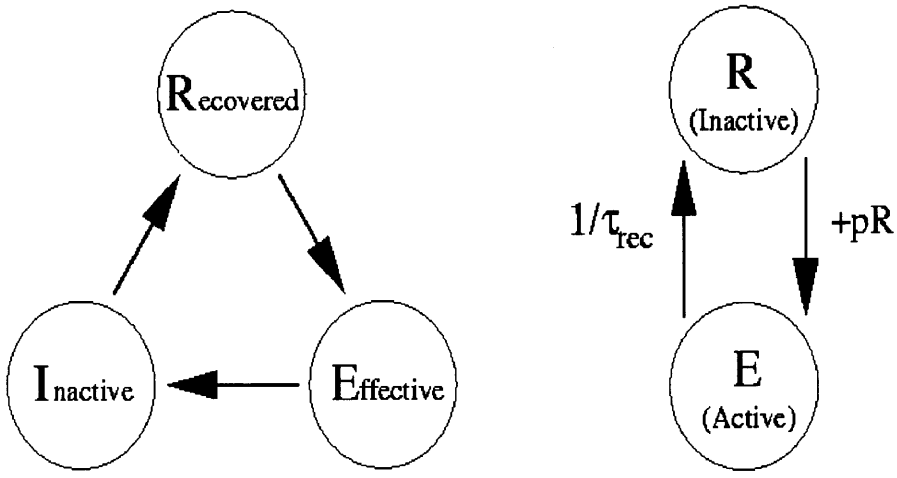

Figure 5.1 The Three States of Sodium Ion Channels and the Reduction to Two States.

Sodium channels can be in one of three different states [26], summarized as: effective, inactive, and recovered. Effective channels are open and allow sodium ions to flow in and out. Inactive channels are closed, but are not available to be opened. Recovered ion channels are closed but are ready to open. The left diagram in Figure 5.1 illustrates these three states.

Modeling the opening and closing of sodium channels is potentially a complex task. For simplification, the sodium ion channels in the current study are modeled as follows:

$$\begin{aligned} \frac{dR}{dt} &= \frac{E}{\tau_{rec}} - pR\delta(t - t_j) \\ \frac{dE}{dt} &= -\frac{E}{\tau_{rec}} + pR\delta(t - t_j), \end{aligned} \tag{5.1}$$

where E is the proportion of active (effective) channels and R is the number of non-active (inactivated and recovered) channels. The function $\delta(t)$ is the Dirac Delta function. The inactivated and the recovered channels were combined into one group because qualitatively, both groups are closed. For the purposes of this model, that was the essential characteristic (see the right side of Figure 5.1). This model for

sodium channel inactivation is based upon the work proposed in [47], which modeled neurotransmitter release.

Since the total number of sodium channels are conserved, $E + R = 1$. Each time an action potential is generated (at times t_j), a random portion, p, of the non-active channels becomes active, adding to those already open. From there, the active channels close (become non-active) with a rate $\frac{1}{\tau_{rec}}$. In simulations, the value of $\frac{1}{\tau_{rec}} = 0.01 \sim \mathcal{O}(\epsilon^2)$ causing E and R to evolve on the "slow" time scale (Recall that $\epsilon = 0.1$, as defined in Section 3.1). Determining the proportion of channels that become active during each action potential is discussed in Section 5.7.1.

Assuming the proportion of active sodium channels affects the conductance of the sodium ion current, the v-nullcline for various values of g_{Na} was plotted in Figure 5.2. As g_{Na} decreased, the equation for the v-nullcline changed and the v-nullcline deformed in such a way that the left knee, p_{lk} moved to the right. If g_{Na} decreased sufficiently, the intersecting critical point became stable, preventing the cell from firing. A possible way to incorporate E into the sodium current term follows: $-g_{Na}(1 - E)m^3h(v - V_{Na})$.

As E increases, p_{lk} moves to the right, eventually intersecting the w-nullcline, producing a stable critical point, and preventing the pyramidal cell from firing. However, quantifying the deformation of the v-nullcline is potentially a difficult task. To emulate this shifting of the knee due to nullcline deformation, E was introduced into the pyramidal cell voltage equation in the following manner:

$$\frac{dv}{dt} = f(v - E, w, g) = f(v, w, g, E). \tag{5.2}$$

Therefore, an increase in E (as with each action potential) will shift the entire v-nullcline to the right in the $v - w$ phase plane. As the sodium channels become non-active, the nullcline returns to its intrinsic position, when no sodium channels are open.

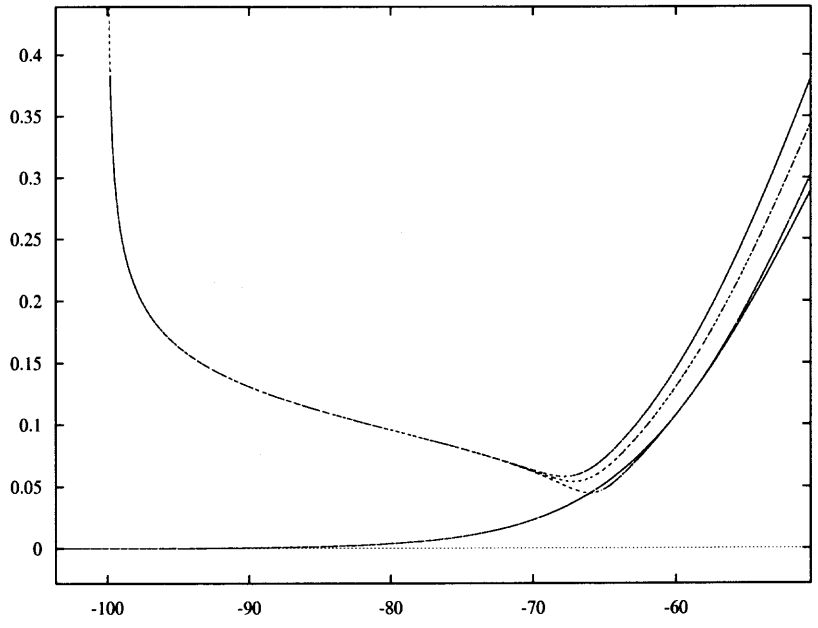

Figure 5.2 Deformation of the v-nullcline (dotted curves) by varying g_{Na}. Keeping E constant, g_{Na} was varied from 150 (top), 100(middle), and 50(bottom). The v-nullcline deformed and p_{lk} (the local minimum on the left branch of the v-nullcline) shifted right. For $g_{Na} = 100, 150$, the critical point is unstable, but for $g_{Na} = 50$, the critical point becomes stable.

The shifting of the nullcline simulates the change in threshold voltage observed in [17], since pyramidal cells enter the active phase by jumping from p_{lk} on the v-nullcline.

5.2 The $g - E$ Phase Plane

Shifting to the right can be combined with the previous idea that the v-nullcline can shift up or down in the phase plane, in response to synaptic inhibition. We know that if the v-nullcline is shifted down sufficiently, the intersecting critical point moves to the left branch of the cubic nullcline, becoming stable. The cell will only be able to fire when the nullcline moves up enough for the cell to reach a knee to jump from (corresponding to g^*). A similar concept governs when the cubic nullcline shifts left

or right. If the nullcline moves sufficiently to the right, the critical point will move to the left branch and become stable, as in Figure 5.3.

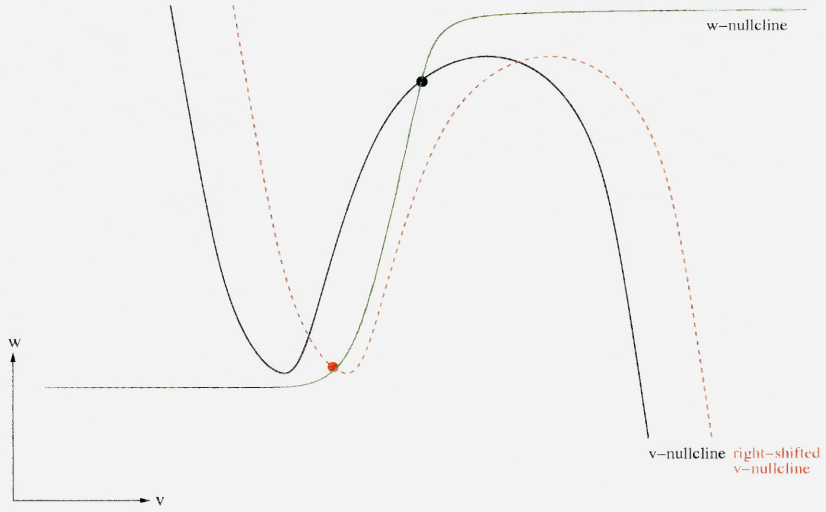

Figure 5.3 With the intrinsic noise, the v-nullcline can now shift to the right. The intersecting critical point can change as well, becoming stable, if shifted far enough to the right.

As before, the dynamics of the shifting v-nullcline can be expressed in a phase plane. However, the addition of E has increased the size of the phase plane from a one-dimensional g phase line to a two-dimensional $g - E$ phase plane. See Figure 5.4.

Previously, the cell moved in the g-direction, along the g phase line. Each time the pyramidal cell was inhibited, g was reset to g_n, as discussed previously, assuming no excitatory input. Now, in addition, each time the pyramidal cell fires, a new E is defined, according to the amount of sodium channels activated. Depending on the value of E, the cell may or may not be prevented from firing.

When no E is involved in this process, the pyramidal cell fires when $g \leq g_0^*$. If E is included, this value of g^* changes, defining the *jump curve*, $g^*(E)$, in the $g - E$

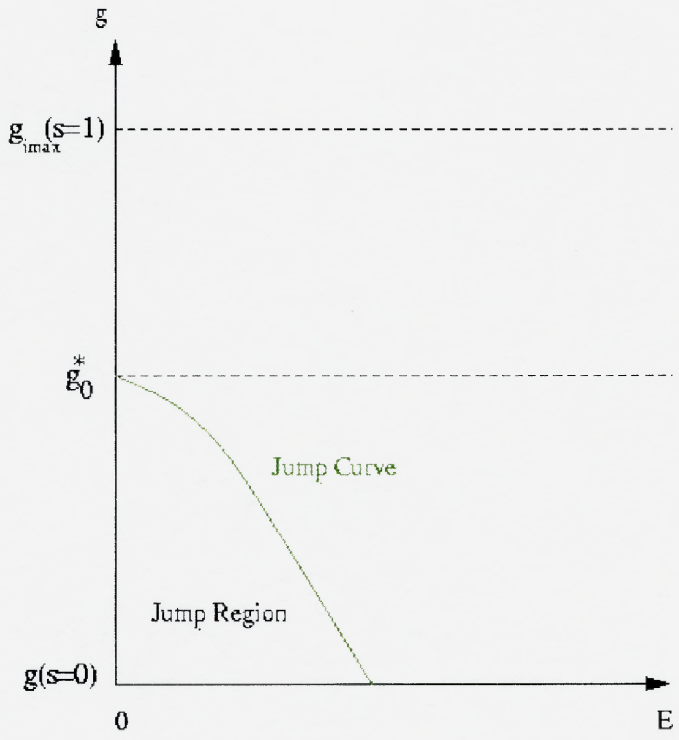

Figure 5.4 The $g - E$ Phase Plane. g_0^* represents the minimum level of inhibition needed for the cell to access a knee when there is no intrinsic noise due to sodium channel inactivation, i.e. all the channels are non-active ($E = 0$).

phase plane. Any time a pyramidal cell crosses this curve into the *jump region*, the cell fires.

The equation for the jump curve can be theoretically derived. The cell's nullclines are defined by the following equations:

$$\begin{aligned} f(v, w, g, E) &= 0 \\ y(v, w) &= 0. \end{aligned} \tag{5.3}$$

By solving these equations simultaneously, the intersecting critical point can be found. However, the critical point can change as g and E vary. Let these intersecting critical points that changes as g and E vary be called $v_0(g, E)$ and $w_0(g, E)$.

Using the Implicit Function Theorem and the y-equation, an equation for $v = Y(w)$ can be defined everywhere, except at points where $\frac{\partial y}{\partial v}(v, w) = 0$. However, there are no points in the considered domain where this happens. The formula for v can be substituted into the f-equation from (5.3),

$$f(Y(w), w, g, E) = 0. \tag{5.4}$$

The function G By substituting in the expression for the critical points, the equation

$$f(Y(w_0(g, E)), w_0(g, E), g, E) = 0 \tag{5.5}$$

defines a two-dimensional space of critical points, some stable, some unstable.

For a given E, the v-nullcline is able to shift up or down, and there is a particular value of g for which the critical point bifurcates between stable and unstable types. All of these values of g for different values of E form the one-dimensional *jump curve*, $g^*(E)$. A linear approximation of $g^*(E)$ is reasonable. The intersecting critical point when $E > 0$ is mainly located on the middle portion of the w-nullcline, which has a chiefly linear characteristic, except at its ends. Therefore, the *jump curve* in the $g - E$ phase plane will be approximated by the equation:

$$g^*(R) = -mE + g_0^*, \tag{5.6}$$

where $m > 0$ and $g_0^* > 0$ is the value of g needed to fire when $E = 0$ (which was originally called just g^*). Note that m and g_0^* depend on the activation of potassium channels, since the shape of the w-nullcline is a representation of this.

5.3 Pyramidal Cell Firing in the $g - E$ Phase Plane

In the Section 3.5, a formula for $g_n(\tau)$ was derived, namely $g_n(\tau) = g_n e^{-\frac{\tau}{\tau_k}}$. A decreasing sequence $\{g_n\}$ was also determined, based upon depressing synapses. In the last Sections 5.1 and 5.2, an equation for the evolution of E and an equation for

the *jump curve* were found. It was noted that as E varies, $g^*(E)$ varies. Specifically, as E increases, $g^*(E)$ decreases, and vice versa, as dictated by (5.6). Combining these facts, a condition for a pyramidal cell to fire can be produced. Recall that if the synaptic strength g_n becomes less than $g^*(E)$, then the cell can fire. Therefore, if for a particular time τ^*,

$$g_n(\tau^*) - g^*(E(\tau^*)) \leq 0, \tag{5.7}$$

then the cell fires. By substituting (5.6) into (5.7) and an expression for $g_n(\tau^*)$, the condition becomes

$$G(\tau^*; E_i) = g_n e^{-\frac{\tau^*}{\tau_k}} + mE_i e^{-\frac{\tau^*}{\tau_{rec}}} - g_0^* \leq 0, \tag{5.8}$$

where $\{E_i\}$ is the sequence of proportions of active sodium channels for each time the pyramidal cell fires.

Given sufficient time, a τ^* can always be found, since both $g_n e^{-\frac{\tau}{\tau_k}}$ and $mE_i e^{-\frac{\tau}{\tau_{rec}}} \to 0$ as time evolves (i.e. $G(\tau; E_i)$ is a decreasing function of time for a particular g_n and E_i), but as previously observed, τ^* needs to be less than T_{in}, the time until the next dose of inhibition, if the pyramidal cell is to fire.

The movement in the $g-E$ phase plane leading to a pyramidal cell firing can be visualized in two ways. For a single cell, it is easier to envision a single g phase line. The function $g^*(E)$ will increase as E decays, as evident by (5.6), while g decreases as the synaptic inhibition decays. When $g \leq g^*(E)$, the cell fires. Figure 5.5 shows this.

For two or more cells in the $g-E$ phase plane, collapsing the cells onto a single line becomes confusing. Figure 5.6 shows the trajectories of two cells in the $g-E$ phase plane.

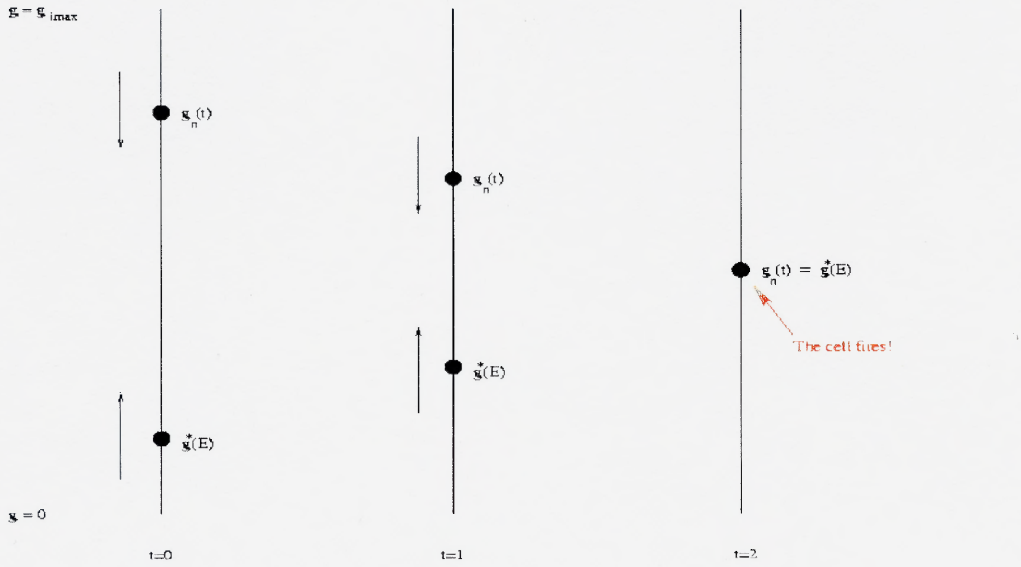

Figure 5.5 Visualizing How a Pyramidal Cell Fires on the g Phase Line for One Cell. At $t = 0$, the cell has just received inhibition and the cell has some level of active sodium channels, corresponding to a certain value on the *jump curve*. At $t = 1$, both the synaptic inhibition and the number of active sodium channels are approaching 0. At $t = 2$, the synaptic strength has decayed to a level such that the cell can fire, equaling $g^*(E)$, which depends on the number of active sodium channels.

5.4 A Reliability Experiment

The results in [30] makes reference to the fact that "neurons transmit information by transforming continuously varying input signals into trains of discrete action potentials." However, it notes, this transformation is yet to be understood. The goal of the article was to determine the reliability with which a single pyramidal cell can take a continuous signal and return spike trains.

By making somatic whole-cell recordings in a current-clamp configuration from a prepared rat cortical slice, they repeatedly injected the same stimulus into the cell and determined the reliability of the produced action potential trains.

The first experiment injected flat current pulses into the cell, from 0 to 250 pA for 0.9 sec. The number of spikes remained roughly the same between runs. However, small changes in interspike intervals decreased the synchronization between trials.

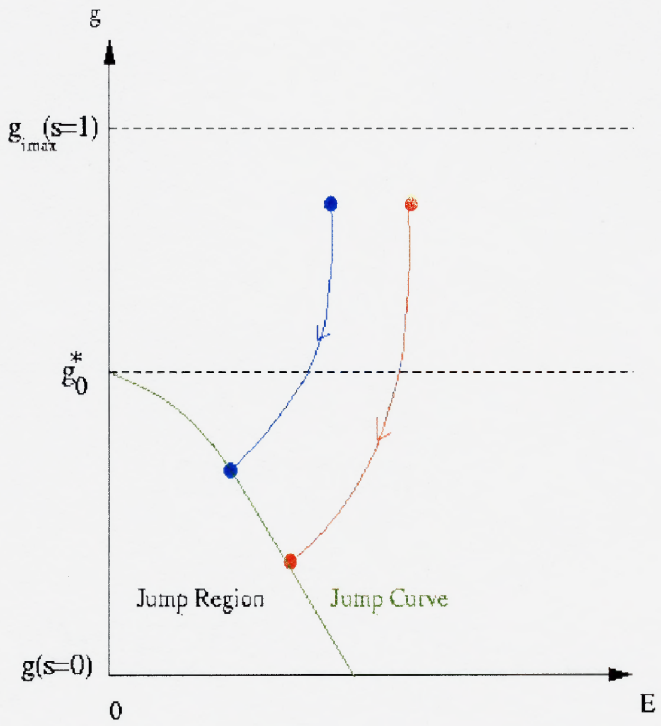

Figure 5.6 Visualizing How a Pyramidal Cell Fires in the $g - E$ Phase Plane for Two Cells. Both pyramidal cells (one blue and one red) start with some level of inhibition. Both g and E decay, as evidenced by the curving of the trajectories. At some time less than T_{in}, the cells encounter the *jump curve* and fire.

The first action potential was locked to the onset of the pulse, but the timing of the last spike was "highly variable." See the left portion of Figure 5.7.

Next, to mimic the summation of synaptic inputs, both excitatory and inhibitory sequences of filtered Gaussian white noise were combined with a constant depolarization. Again, spike count variability was small. However, if the same randomly fluctuating waveform was repeatedly injected into the cell, the experimenters observed high reliability between trials. Occasionally there were misfires, when spikes disappeared, reappeared, or shifted in time, as on the right side of Figure 5.7.

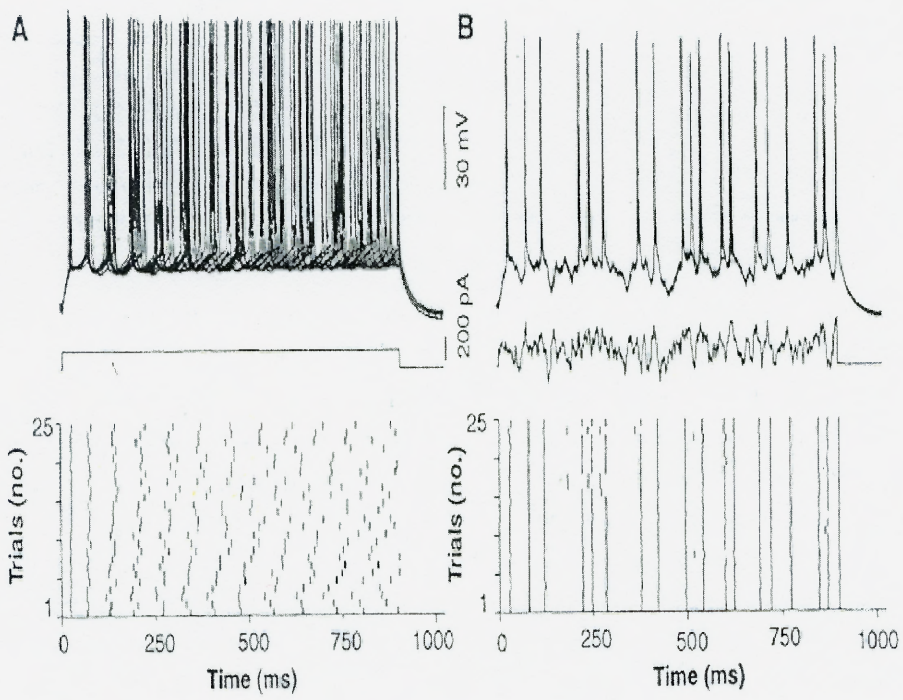

Figure 5.7 Experimental Results from the Mainen/Sejnowski Paper [30]. The top left figure displays the low reliability of a single pyramidal cell between 25 trials where injected flat current pulses of 0 to 250 pA for 0.9 sec were injected into the cell. The lower left figure is the raster plot of the experiment, showing the individual action potentials for each trial. The upper right figure shows high reliability between 25 trials, where the same pyramidal cell received the same sequence of filtered Gaussian white noise with a constant depolarization. The lower right figure is the raster plot of the experiment.

Mainen and Sejnowski propose that the reproducible spike patterns were a result of particular depolarizations and hyperpolarizations in the current. Reverse correlation revealed that spikes tended to be proceeded by a depolarizing transient. At greater mean input currents, the depolarization was weakened and the spikes tended to be proceeded by a hyperpolarizing transient. Also, a maximum stimulus slope of 5 to 10 nA/sec preceded spikes (corresponding to about 10 excitatory post-synaptic currents of 5 to 10 pA within 10 ms).

In this dissertation, it is hypothesized that the low reliability issues found by Mainen and Sejnowski can be modeled by including a source of intracellular noise into the equations for the pyramidal cell. Continuous, tonic input is shown not to affect this intrinsic randomness. However, intermittent, rapid depolarizations of an injected current, such as the Gaussian, white noise injected into the pyramidal cell by Mainen and Sejnowski, dominate the intracellular noise, causing high reliability. Furthermore, the rapid, high-frequency inhibition applied to the pyramidal cells during the SPWR is similar to the rapidly changing, injected white noise seen in the Mainen/Sejnowski experiments. Therefore, the reliability of a single, pyramidal cell receiving the same random input pattern across several trials is equivalent to the synchronization of a group of identical pyramidal cells, containing intrinsic noise and receiving the inhibition from the same interneuron.

5.5 Addressing Questions about Experimental Reliability

By considering this new phase plane, we can answer some questions raised by [30]. First, tonic input without inhibition produces low reliability. Tonic input, in this model, is represented as in Figure 5.8. The cell resides on a line corresponding to a constant value of $g = g_{tonic}$, and moves horizontally according to the value of E. If the value of E repeatedly moves the cell to the left of the "jump curve," the cell oscillates because each time the cell has access to a knee. If the cell moves to the right of the

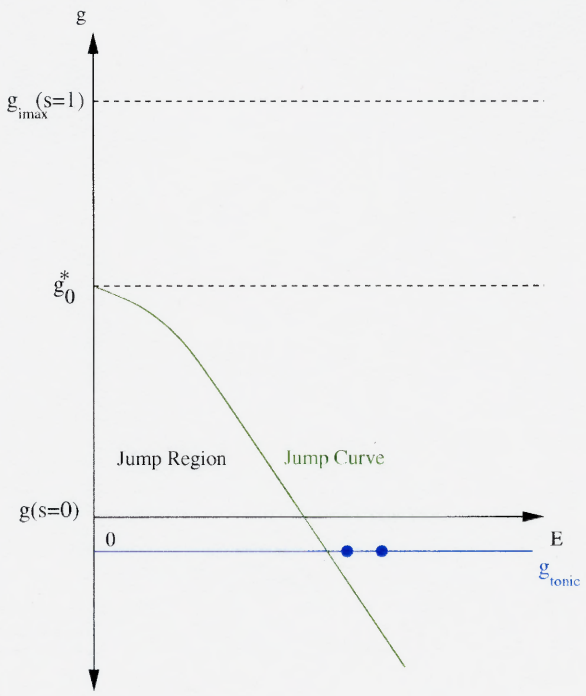

Figure 5.8 Tonic Input Represented in the $g - E$ Phase Plane, without inhibition but with sodium channel inactivation. The cell moves along line defined by g_{tonic}, as E changes.

"jump curve," the cell must wait until E decays enough to cross the "jump line" before the cell fires. This delays the firing of the cell and produces low reliability after many trials, since the value of E is random. Note that more excitation will increase the intersections of the line defined by g_{tonic} and the jump region, increasing the chances that a pyramidal cell will fire, and thus improving reliability. However, too much excitation will cause the pyramidal cell to become trapped in a high voltage state, as the intersecting critical point moves from the middle branch to the right branch of the v-nullcline. Therefore, there is an upper limit to the amount of excitation that will improve reliability and still allow the cell to fire.

In this model, noisy input moves the cell in the $g - E$ phase plane randomly in the vertical g-direction. If, during this movement, the cell enters the "jump region,"

the cell fires, as in Figure 5.9. Therefore, the cell tends to fire on peaks in the noisy input, as seen in [30], since they are more likely to move the cell down into the "jump region." However, this is not always the case. The same peak that caused a cell to fire, while the cell has a sufficiently small value of E, may not produce an action potential if the E value is too large. This mimics the small discrepancies seen in [30] that prevented perfect reliability. To summarize, the high reliability comes from the fact that the cell receives the same noisy input and, if E remains below a certain positive value, the cell fires on the same peaks each time. Figure 5.9 illustrates this phenomenon and Figure 5.10 shows a numerical reproduction of the results.

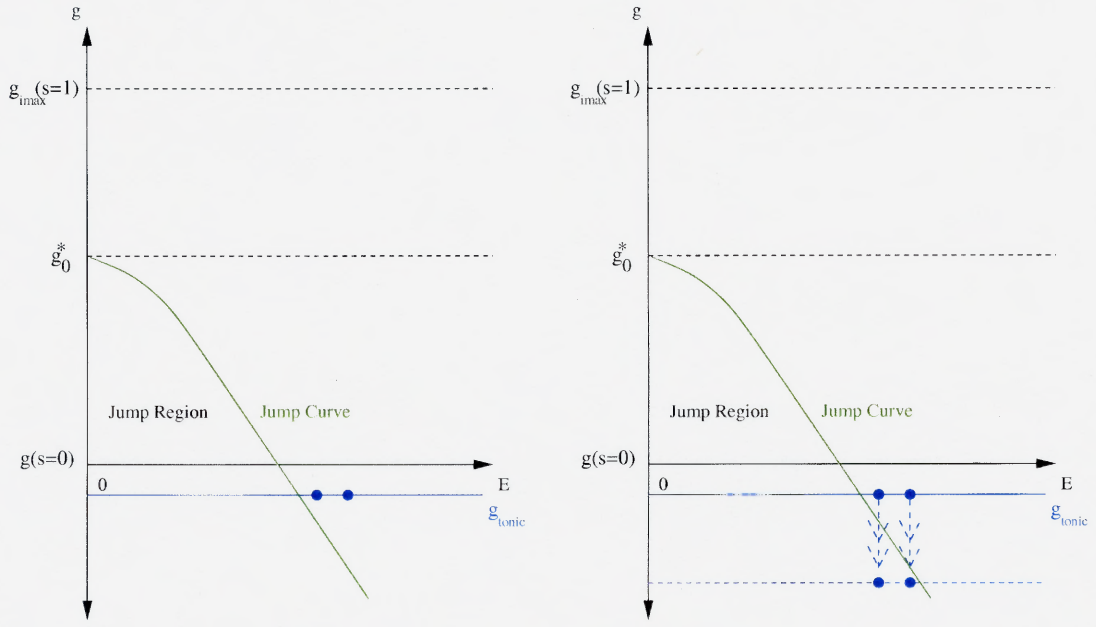

Figure 5.9 On the left, tonic input produces low reliability as the cell fires at an earlier time in the first trial, while in the second trial, the cell must allow extra time for E to decay before it can fire. On the right, rapid noisy input forces the cell in both trials to enter the "jump region," despite differing values of E.

This new model of intrinsic noise has reproduced some of the results presented in [30]. The question now is whether this model will be useful in explaining the SPWR. During the SPWR, an interneuron can oscillate at ripple frequency ($\sim$ 200

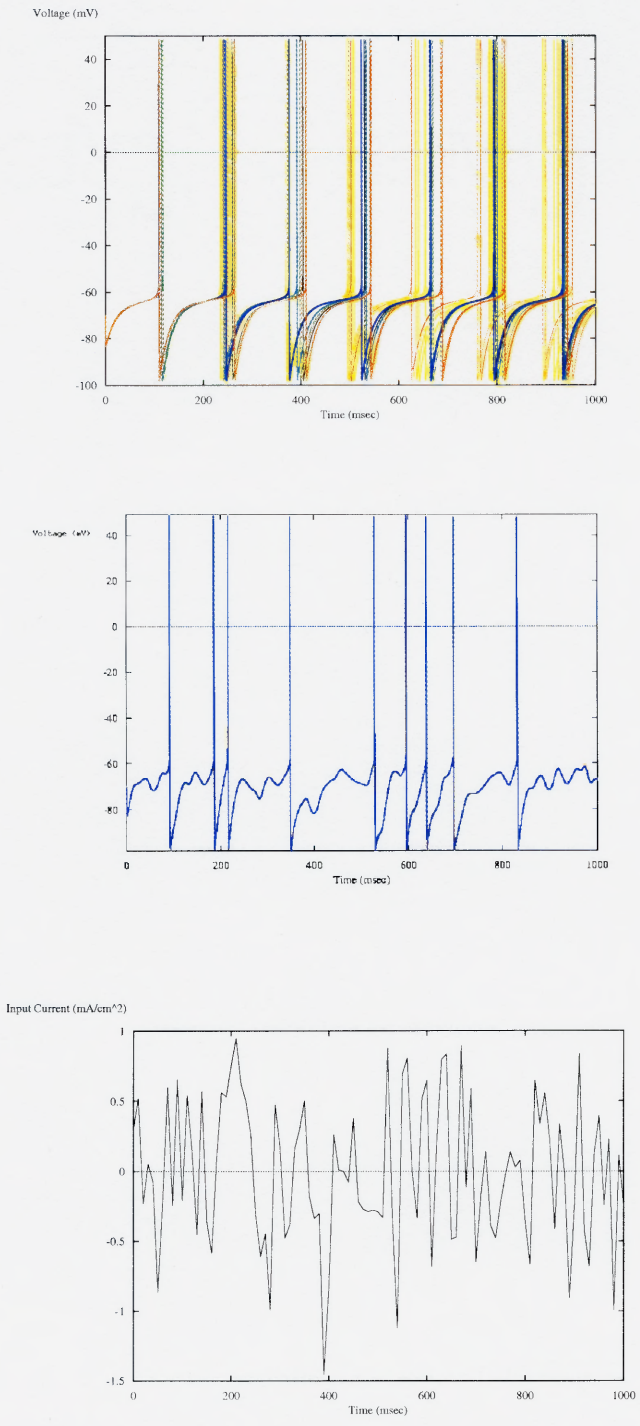

Figure 5.10 Simulation Reproducing Results from the Mainen/Sejnowski Article. On top, 10 trials are shown of a intracellularly noisy pyramidal cell receiving a tonic input of 0.1 mA/cm^2. As in [30], the pyramidal cell exhibits low reliability. The middle picture shows the results when a random current is injected into the same cell 10 times. As in [30], the pyramidal cell now exhibits high reliability. The bottom picture displays the Gaussian, random input ($\mu = 0$, $\sigma^2 = 0.5$).

Hz), repeatedly inhibiting pyramidal cells. Pyramidal cells also receive excitation during the sharp wave. Can high frequency inhibition, with tonic excitation and no noisy external input, produce synchronization amongst identical pyramidal cells, despite intracellular noise?

5.6 Action Potential Timing of a Single Pyramidal Cell with Intracellular Noise

Before answering the question posed in the last section, first consider the firing time of a single, intrinsically noisy, pyramidal cell receiving inhibition.

When $G(\tau; E_i) = 0$, from (5.8), the pyramidal cell fires. In general, however, finding an expression for the time τ^* is impossible. Consider the special case when $\tau_k = \tau_{rec} = \frac{1}{\gamma}$. The condition becomes

$$(g_n + mE_i)\, e^{-\gamma\tau} - g_0^* \leq 0. \tag{5.9}$$

Therefore, the time until firing can be found:

$$\tau^* \geq \frac{1}{\gamma} \ln\left(\frac{g_n + mE_i}{g_0^*}\right). \tag{5.10}$$

Consider another special case if $\frac{1}{2}\tau_k = \tau_{rec} = \gamma_1$ or if $\tau_k = \frac{1}{2}\tau_{rec} = \gamma_2$. The condition becomes

$$\tau^* \geq \frac{1}{\gamma_1} \ln\left(\frac{2g_n}{\sqrt{m^2E_i^2 + 4g_n g_0^*} - mE_i}\right) \tag{5.11}$$

or

$$\tau^* \geq \frac{1}{\gamma_2} \ln\left(\frac{2mE_i}{\sqrt{g_n^2 + 4mE_i g_0^*} - g_n}\right), \tag{5.12}$$

respectively.

Recall from Section 4.1 that g_n is determined by several factors, most importantly by the rate of recovery of synaptic resources (τ_a) and the frequency of

inhibition (T_{in}). E_i is mainly determined by a random process, though τ_{rec} determines how E decays. If the proportion of active sodium channels is too large, τ^* will be greater than T_{in} and the pyramidal cell will not be able to fire between inhibitions.

The discussion now turns to how improve a pyramidal cell's chances of firing between inhibitions, despite large proportions of active sodium channels. To do this, let us determine the effect various parameters have on $G(\tau; E_i)$, as seen in Section 5.3. First, consider τ_a, the rate of recovery of synaptic resources. In (5.20), τ_a is a part of g_n, such that if τ_a increases, g_n decreases faster and can achieve lower values before the next dose of inhibition. As g_n decreases, the cell's chances of firing improves, as evident by the following equation:

$$0 < E_i < \frac{1}{m} e^{\frac{T_{in}}{\tau_{rec}}} \left[g_0^* - g_n e^{-\frac{T_{in}}{\tau_k}} \right], \tag{5.13}$$

derived by evolving (5.8) by T_{in} (the period of the inhibition), and solving for E_i. Thus, an interval for the values of E_i for which a cell can fire before the next dose of inhibition can be found. As g_n decreases, the interval in (5.13) increases. Therefore, a larger τ_a increases the interval of E_i faster and pyramidal cells have a better chance of firing between inhibitions. Plus, since the synapse depresses faster for larger values of τ_a, the cells can fire earlier. Figure 5.11 illustrates these phenomena.

The inhibition period can also have an effect a pyramidal cell's chances of firing. Note the similarity between the right-hand side of (5.13) and (4.8). The quantity inside the bracket in (5.13) is the negative quantity of the left-hand side of (4.8). If the right-hand side of (5.13) is plotted versus T_{in}, as in Figure 5.12 (the green curve), one can discern several things.

First, only those values of the curve greater than 0 are meaningful, since the right-hand side of (5.13) must be non-negative. Second, those values of the curve greater than 0 correspond to the same value for which the cell can fire, without sodium channel inactivation, as seen in Figure 4.3. Third, if $T_{in} \leq T_*$, the lower T_{in}

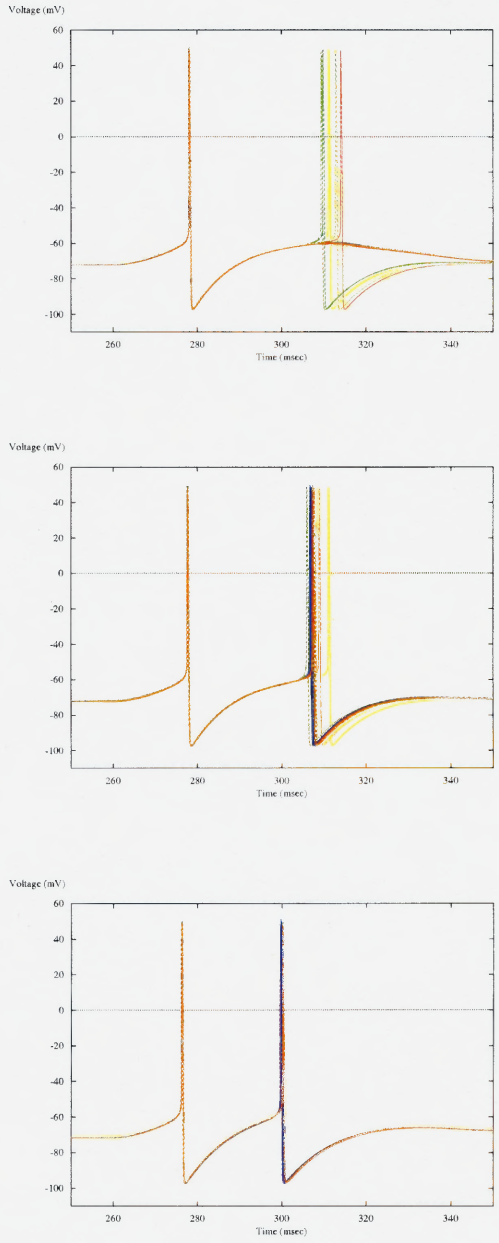

Figure 5.11 How τ_a Affects the Chances of a Pyramidal Cell to Produce Action Potentials. As τ_a increases, the pyramidal cell can access more of the *jump region* as the synapse depresses more. Depicted in each figure are 10 trials with a noisy, simulated neuron. In the top picture, $\tau_a = 0.01$. In the middle picture, $\tau_a = 10$. In the bottom picture, $\tau_a = 100$. The Sharp Wave starts at $t = 250$ msec and ends 100 msec later. The parameters τ_k and τ_{rec} were both chosen to equal 400, sufficiently large so the sodium channel inactivation was more pronounced and the effect of τ_a was more pronounced. Note that it seems that the synchronization of the pyramidal cells has improved. This is not the case. Since the cells fire earlier due to the synaptic depression, the cell are receiving more SPW excitation at this time, causing them to fire faster. However, the cells still maintain their relative phase.

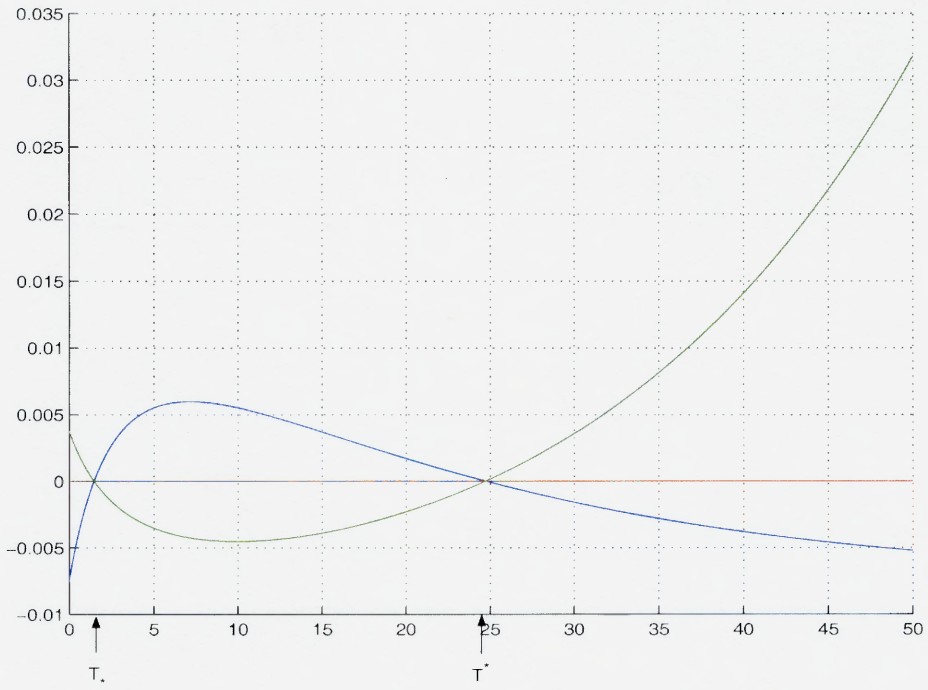

Figure 5.12 The Values of T_{in} for which the Pyramidal Cells Can and Cannot Fire, with Intrinsic Noise. The upper blue curve (this is the same curve shown in Figure 4.3) shows that the Pyramidal Cell will never fire for $T_{in} \in (T_*, T^*)$s. The lower green curve plots the right-hand side of (5.13). If $T_{in} \leq T_*$, the lower T_{in} becomes, reliability improves. If $T_{in} \geq T^*$, the higher T_{in} becomes, reliability improves. The independent variable is T_{in} (msec). The dependent variables are $g_\infty^{T_{in}} - g^*$ (upper blue curve) and $\frac{1}{m} e^{\frac{T_{in}}{\tau_{rec}}} \left[g_0^* - g_n e^{-\frac{T_{in}}{\tau_k}} \right]$ (lower green curve). The parameter values are $g_{syn} = 0.03$, $\tau_k = 20$, $\tau_a = 2000$, $\tau_b = 5$, $g^* = 0.075$, $m = 2$, $\tau_{rec} = 20$ and $\Delta t_f = 0.01$. The value of τ_a was inflated in order to make the interval from 0 to T_* more pronounced.

becomes and the cell has a better chance of firing. This is because high-frequency inhibition causes the sequence g_n to depress rapidly, making more of the *jump region* available between inhibitions. Fourth, if $T_{in} \geq T^*$, the higher T_{in} becomes, the chance of producing an action potential improves. This occurs because more time between inhibitions allows E to decay more, allowing it to reach the *jump curve* before the pyramidal cell is inhibited again.

5.7 Action Potential Timing Between Pyramidal Cells

In this section, the possibility of synchronization between two pyramidal cells with common inhibition and sodium channel inactivation is discussed. The main question is how does the model accommodate intrinsic randomness of the sodium channel usage. Are the previous results proven for pyramidal cells without sodium channel inactivation affected by the noise?

Recall, for inhibitions with periods $T_{in} \in (T_*, T^*)$, without sodium channel inactivation, there exists a stable, sub-threshold synchronous orbit, as shown in Chapter 4. This section shows that the same holds true if sodium channel inactivation is included. If the cells can never reach a threshold to fire, no more sodium channels are used and E decays to 0, as the channels become non-active (recovered). The system reduces to the previous case, where the cells synchronize below threshold.

For cases that the pyramidal cells can reach a threshold to fire, measuring synchrony is more difficult. In this model, each time a pyramidal cell fires, a random portion of sodium channels becomes active. In terms of the $v - w$ phase plane, each time a cell fires, it jumps down onto a random v-nullcline that is shifted to the right. Furthermore, each cell jumps down onto a different v-nullcline. The randomness obscures much of the analysis performed previously. In this section, using basic probability theory, the precision between two noisy pyramidal cells is calculated. Also, the amount of time compression experienced between two pyramidal cells while receiving high-frequency inhibition in the presence of intracellular noise is quantified.

5.7.1 Precision

Let the *degree of precision*, P, equal $\frac{1}{t_{max}}$, where t_{max} is the maximum time distance between two action potentials of different cells. This definition can be applied to groups of pyramidal cells of two or more where the degree of precision within this group is measured by the action potentials that are the farthest time distance apart.

For two cells that are synchronous, they have an infinite degree of precision, or they are *perfectly precise.*

To further investigate the *precision* of pyramidal cells with an inherent randomness due to sodium channel inactivation, the subject of how sodium channels are used must be discussed. It is not known precisely how sodium channels are used, so the process will be represented by a distribution. Later on, a specific distribution for sodium channel usage is chosen, but for now, let this distribution be known as $f_s(x)$, where x is the random variable describing the fraction of sodium channels used each time a pyramidal cell fires. The variable $x \in [0, R]$. Note that $f_s(x) = 0$ for $x \notin [0, R]$. Recall that R is the proportion of recovered sodium channels available to be used in producing action potentials, where $R + E = 1$.

Using $f_s(x)$, a distribution of firing times can be found for a particular g_n, by transforming the independent variable x, using (5.10). The new distribution is

$$\bar{f}_s(\tau) = \begin{cases} \frac{\gamma g_0^*}{m} f\left(\frac{g_0^* e^{\gamma\tau} - g_n}{m}\right) & \text{if } \tau \in \left[\frac{1}{\gamma}\ln\left(\frac{g_n}{g_0^*}\right), \frac{1}{\gamma}\ln\left(\frac{g_n+mR}{g_0^*}\right)\right] \\ 0 & \text{otherwise} \end{cases}, \tag{5.14}$$

Note that g_n changes each time the cell receives inhibition, so a new distribution will hold for the new g-value.

Since the pyramidal cells are identical and they are uncoupled, their times to fire are independent, so a joint distribution for time to fire can be derived by taking the product of their individual density functions.

$$\hat{f}_s(\tau_1, \tau_2) = \begin{cases} \left(\frac{\gamma g_0^*}{m}\right)^2 f\left(\frac{g_0^* e^{\gamma\tau_1} - g_n}{m}\right) f\left(\frac{g_0^* e^{\gamma\tau_2} - g_n}{m}\right) & \text{if } \tau_1 \in \left[\frac{1}{\gamma}\ln\left(\frac{g_n}{g_0^*}\right), \frac{1}{\gamma}\ln\left(\frac{g_n+mR_1}{g_0^*}\right)\right] \\ & \tau_2 \in \left[\frac{1}{\gamma}\ln\left(\frac{g_n}{g_0^*}\right), \frac{1}{\gamma}\ln\left(\frac{g_n+mR_2}{g_0^*}\right)\right] \\ 0 & \text{otherwise} \end{cases}. \tag{5.15}$$

We are interested in the time distance between the cells, not the individual times to fire. This can be computed using the following transformation:

$$u = \tau_1 - \tau_2$$

$$v = \tau_2$$

Now, the variable of focus is u. Applying this transformation, the joint probability density function for the time distance between the cell is

$$\mathcal{F}_s(u,v) = \begin{cases} \left(\frac{\gamma g_0^*}{m}\right)^2 f\left(\frac{g_0^* e^{\gamma(u+v)} - g_n}{m}\right) f\left(\frac{g_0^* e^{\gamma v} - g_n}{m}\right) & \text{if } u \in \left[\frac{1}{\gamma}\ln\left(\frac{g_n}{g_0^*}\right) - v, \frac{1}{\gamma}\ln\left(\frac{g_n+mR_1}{g_0^*}\right) - v\right] \\ & v \in \left[\frac{1}{\gamma}\ln\left(\frac{g_n}{g_0^*}\right), \frac{1}{\gamma}\ln\left(\frac{g_n+mR_2}{g_0^*}\right)\right] \\ 0 & \text{otherwise} \end{cases} \tag{5.16}$$

This joint distribution represents the probability that two pyramidal cells fire within a certain time distance *and* that the second cell has a certain firing time. We only need to know the former. This is accomplished by integrating the joint distribution (5.16) over all values of v, finding the marginal density for u. Once the marginal density is found, the probability that the two cells fire within time distance δ can be found by integrating the marginal density from $-\delta$ to δ. Or, this can be expressed by the double integral

$$\int_{-\delta}^{\delta}\int_{v_1}^{v_2} \mathcal{F}_s(u,v)\, dv\, du, \tag{5.17}$$

where $v_1 = \frac{1}{\gamma}\ln\left(\frac{g_n}{g_0^*}\right)$ and $v_2 = \frac{1}{\gamma}\ln\left(\frac{g_n+mR_2}{g_0^*}\right)$. Using the earlier definition, the probability that the precision $P = \frac{1}{\delta}$, equals (5.17).

A sample distribution, based on (5.13) below, for the usage of sodium channels are presented in Figure 5.13 for two differing values of R. This distribution is used for the remainder of this paper. When a cell fires, the proportion of sodium channels used is determined by the following probability density function:

$$f_s(x) = \begin{cases} \frac{6x}{R^3}(R-x) & \text{if } x \in [0,R] \\ 0 & \text{otherwise} \end{cases} \tag{5.18}$$

The maximum probability is centered around $R/2$, meaning each time a pyramidal cell fires, it is assumed that half of the available channels are most likely to be used.

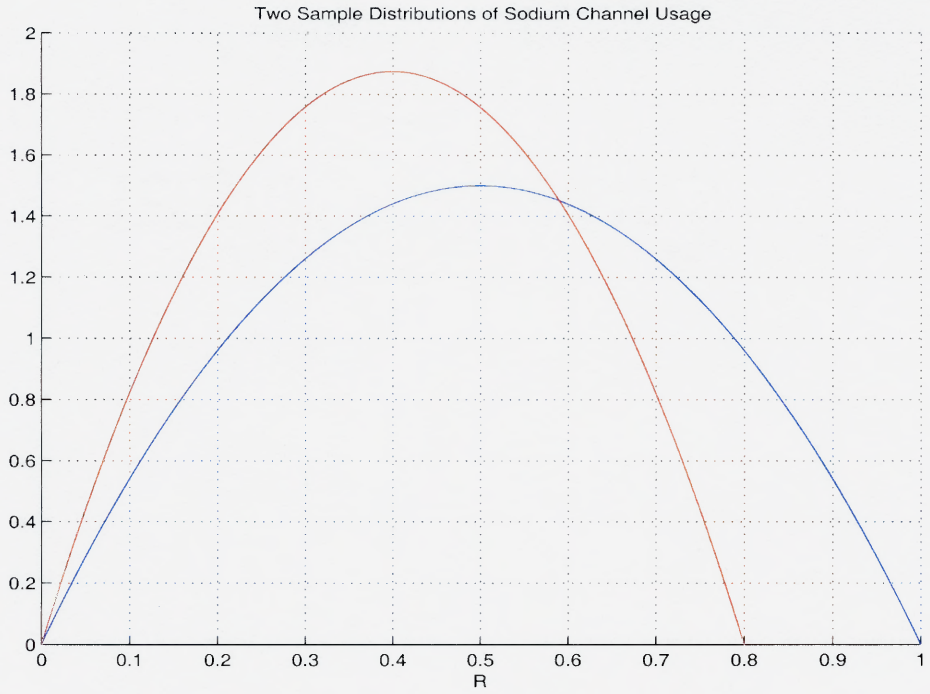

Figure 5.13 Two Distributions of Sodium Channel Usage. For the blue graph, the cell has all of its channels available, $R = 1$. For the red graph, the cell does not have all of its sodium channels at its disposal, $R = 0.8$. Changes in R affect the height of the distribution. The maximum of each graph is centered around $R/2$.

The probability that all or none of the sodium channels are used approaches zero. The underlying assumption here is that it would not make sense for a cell to use all of its sodium channels, in case it needs to quickly generate another action potential, and if the cell used none of its sodium channels, it wouldn't produce action potentials. Note that the value of R varies, as the number of recovered sodium channels changes.

Using the process described above, the joint density $\Delta(u, v)$ can be found:

$$\Delta(u,v) = \begin{cases} \frac{36\gamma^2 g_0^{*2}}{R_1^3 R_2^3 m^2} e^{\gamma(u+2v)} \left(\frac{g_0^* e^{\gamma(u+v)} - g_n}{m}\right)\left(\frac{g_0^* e^{\gamma v} - g_n}{m}\right) \left(R_1 - \frac{g_0^* e^{\gamma(u+v)} - g_n}{m}\right)\left(R_2 - \frac{g_0^* e^{\gamma v} - g_n}{m}\right) & \text{if } u \in \left[\frac{1}{\gamma}\ln\left(\frac{g_n}{g_0^*}\right) - v, \frac{1}{\gamma}\ln\left(\frac{g_n + mR_1}{g_0^*}\right) - v\right] \\ & v \in \left[\frac{1}{\gamma}\ln\left(\frac{g_n}{g_0^*}\right), \frac{1}{\gamma}\ln\left(\frac{g_n + mR_2}{g_0^*}\right)\right] \\ 0 & \text{otherwise} \end{cases} \quad (5.19)$$

Simpson's Method of integration can be used to calculate the double integral, given by (5.17). A MATLAB program for doing this is given in Appendix C.

Now, consider two cells that have just fired and have received a dose of inhibition from an undepressed inhibitory synapse ($g_n = g_{imax}$). The cells receive the same amount of inhibition, but each has a different value of E. Using (5.19) and integrating that joint pdf, the probability of the precision, $P = \frac{1}{P_\Delta}$, can be found.

5.7.2 Quantifying Time Compression

Between doses of inhibition, as time progresses, both g and E begin to decay, according to (A.6) and (5.1). Figure 5.14 depicts how the cells move in the $g - E$ phase plane.

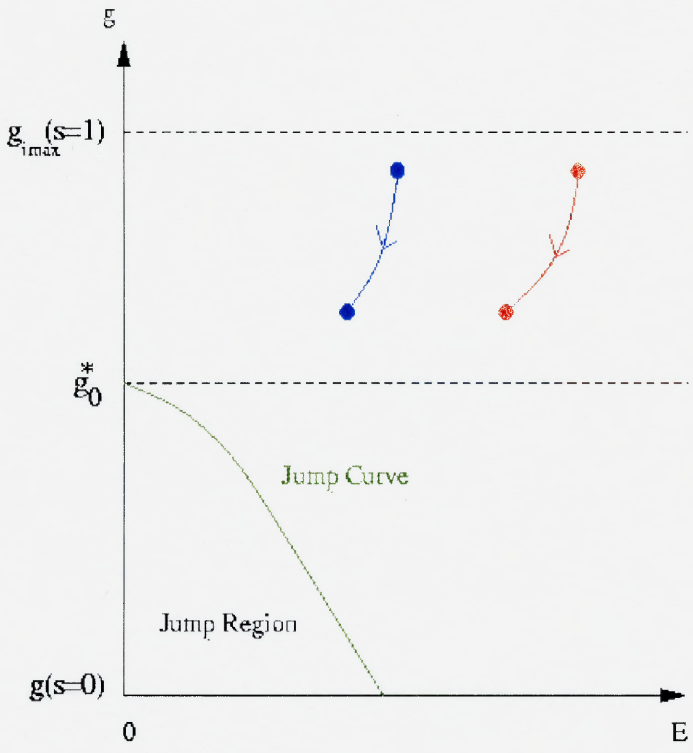

Figure 5.14 An example of how the pyramidal cells move in the $g - E$ phase plane between doses of inhibition.

Using (5.10), the time distance between two cells can be measured as

$$D_t(g_n, E_{1,i}, E_{2,i}) = |\tau_2 - \tau_1| = \frac{1}{\gamma}\left|\ln\left(\frac{g_n - mE_{1,i}}{g_n - mE_{2,i}}\right)\right|, \tag{5.20}$$

since (5.10) measures the time for each cell to reach a knee to fire. The variables $E_{1,i}$ and $E_{2,i}$ are the E values right after the previous inhibition, corresponding to i^{th} action potential produced by cell 1 and cell 2, respectively.

This time distance, D_t, decreases as time increases. Using (5.20), consider

$$D_t(g, E_{1,i}, E_{2,i}) = \begin{cases} \frac{1}{\gamma} \ln \frac{g+mE_{1,i}}{g+mE_{2,i}} & \text{if } E_{1,i} > E_{2,i} \\ -\frac{1}{\gamma} \ln \frac{g+mE_{1,i}}{g+mE_{2,i}} & \text{if } E_{1,i} < E_{2,i} \end{cases} \tag{5.21}$$

Its time derivative, $\frac{dD_t}{dt} = \frac{dg}{dt}\frac{\partial D_t}{\partial g} + \frac{dE_{1,i}}{dt}\frac{\partial D_t}{\partial E_{1,i}} + \frac{dE_{2,i}}{dt}\frac{\partial D_t}{\partial E_{2,i}}$, may be computed using (A.6), (5.1) and (5.21) to obtain

$$\begin{aligned} \frac{dD_t}{dt} &= \frac{mg_0^2|E_{1,i}^0 - E_{2,i}^0|e^{-\gamma t}}{(g_0 + mE_{1,i}^0)(g_0 + mE_{2,i}^0)} - \frac{mg_0|E_{1,i}^0 - E_{2,i}^0|}{(g_0 + mE_{1,i}^0)(g_0 + mE_{2,i}^0)} \\ &= \frac{mg_0|E_{1,i}^0 - E_{2,i}^0|}{(g_0 + mE_{1,i}^0)(g_0 + mE_{2,i}^0)} \left(g_0 e^{-\gamma t} - 1\right), \end{aligned} \tag{5.22}$$

where g_0, $E_{1,i}^0$ and $E_{2,i}^0$ are the initial values of the independent variables between doses of inhibition. Since g_0 and $e^{-\gamma t}$ are both less than 1 and the other quantities are positive, $\frac{dD_t}{dt} \leq 0$ and the time distance decreases as time evolves between inhibitions.

By taking the ratio between the time distance right after receiving the $(n-1)^{st}$ and right before the n^{th} inhibition, a compression factor can be found, given by

$$\nu_n^e = \left| \frac{\ln\left(\frac{g_n^{T_{in}} - mE_{1,i}^{T_{in}}}{g_n^{T_{in}} - mE_{2,i}^{T_{in}}}\right)}{\ln\left(\frac{g_n - mE_{1,i}}{g_n - mE_{2,i}}\right)} \right|, \tag{5.23}$$

where $E_{1,i}^{T_{in}}$ and $E_{2,i}^{T_{in}}$ are the E values of the respective cells after T_{in} time.

When the interneuron applies inhibition to the pyramidal cells, they instantaneously jump from $g_n^{T_{in}}$ to g_{n+1}, while keeping the same values of E. See Figure 5.15 for an example of this in the $g - E$ phase plane.

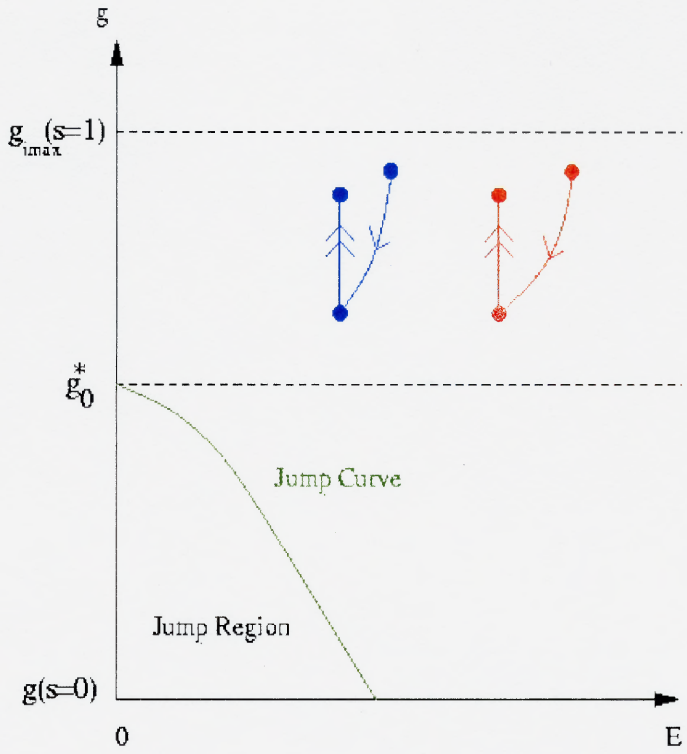

Figure 5.15 An example of how the pyramidal cells move in the $g - E$ phase plane when receiving a dose of inhibition.

During the n^{th} dose of inhibition, as for previous inhibitions, the cells will compress in time. The time distance before and after the jump due to inhibition:

$$\nu_n^j = \left| \frac{\ln\left(\frac{g_{n+1} - mE_{1,i}^{T_{in}}}{g_{n+1} - mE_{2,i}^{T_{in}}}\right)}{\ln\left(\frac{g_{T_{in}}^n - mE_{1,i}^{T_{in}}}{g_{T_{in}}^n - mE_{2,i}^{T_{in}}}\right)} \right| \tag{5.24}$$

The product of these compression factors, ν_n^e and ν_n^j, for each cycle of inhibition, produces the ultimate compression factor for when the cells fire.

A few details need to be discussed. The above analysis assumes the cells fire together between inhibitions. Thus, the cells need to be less than T_{in} close in time for them to fire together. Otherwise, one cell will fire first and the other cell will receive more inhibition and must wait until it decays again to a point at which it can fire.

This may be the next cycle or later cycles. Section 5.6 discusses how to improve the pyramidal cell's ability to fire between inhibitions.

The next detail addresses the last compression factor before the cells fire. The formula (5.23) does not apply because the cells will fire before they receive another dose of inhibition. Thus, the last compression factor is

$$\nu_{last} = \left| \frac{\ln\left(\frac{g_n^{t_1^*} - mE_{1,i}^{t_1^*}}{g_n^{t_2^*} - mE_{2,i}^{t_2^*}}\right)}{\ln\left(\frac{g_n - mE_{1,i}}{g_n - mE_{2,i}}\right)} \right|, \tag{5.25}$$

where t_1^* and t_2^* are the times when cell 1 and cell 2 fire.

The final compression factor is represented as a product of each compression factors:

$$\begin{aligned} \nu_{fin} &= \left| \frac{\ln\left(\frac{g_0^{T_{in}} - mE_{1,i}^{T_{in}}}{g_0^{T_{in}} - mE_{2,i}^{T_{in}}}\right)}{\ln\left(\frac{g_0 - mE_{1,i}}{g_0 - mE_{2,i}}\right)} \right| \left| \frac{\ln\left(\frac{g_1 - mE_{1,i}^{T_{in}}}{g_1 - mE_{2,i}^{T_{in}}}\right)}{\ln\left(\frac{g_0^{T_{in}} - mE_{1,i}^{T_{in}}}{g_0^{T_{in}} - mE_{2,i}^{T_{in}}}\right)} \right| \cdots \left| \frac{\ln\left(\frac{g_N^{t_1^*} - mE_{1,i}^{NT_{in}+t_1^*}}{g_N^{t_2^*} - mE_{2,i}^{NT_{in}+t_2^*}}\right)}{\ln\left(\frac{g_N - mE_{1,i}^{NT_{in}}}{g_N - mE_{2,i}^{NT_{in}}}\right)} \right| \\ &= \left| \frac{\ln\left(\frac{g_N^{t_1^*} - mE_{1,i}^{NT_{in}+t_1^*}}{g_N^{t_2^*} - mE_{2,i}^{NT_{in}+t_2^*}}\right)}{\ln\left(\frac{g_0 - mE_{1,i}}{g_0 - mE_{2,i}}\right)} \right| \end{aligned}$$

It may be non-trivial to find t_1^* and t_2^*, so an upper bound on the final compression factor might be more practical. Using this reasoning,

$$\nu_{fin} \leq \hat{\nu}_{fin} = \left| \frac{\ln\left(\frac{g_N - mE_{1,i}^{NT_{in}}}{g_N - mE_{2,i}^{NT_{in}}}\right)}{\ln\left(\frac{g_0 - mE_{1,i}}{g_0 - mE_{2,i}}\right)} \right|, \tag{5.26}$$

which represents the compression after the last application of inhibition directly before the cells fire.

Various parameters affect the final compression factor in different ways. It seems reasonable to assume that if the pyramidal cell receives more application of inhibition

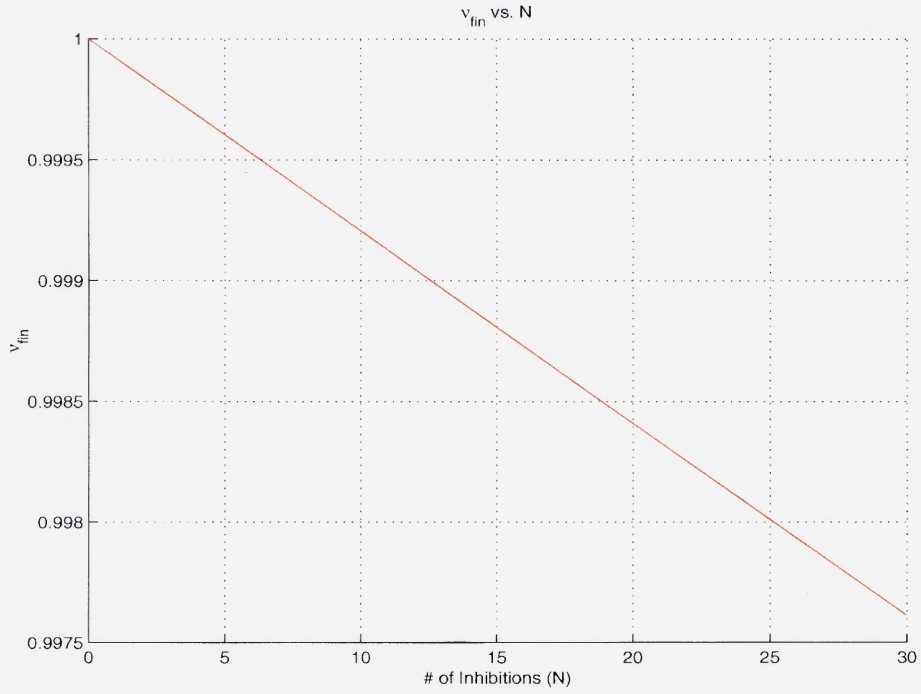

Figure 5.16 Compression Increases as the Number of Cycles of Inhibition Increases. In this simulation, $\gamma = 0.5$ msec^{-1}, $\tau_a = 100$ msec, $T_{in} = \frac{1}{200}$ msec, $\tau_b = 5$ msec and $g_{syn} = 0.04\frac{mS}{cm^2}$. The starting amounts of E for Cell 1 and Cell 2 were 0 and 1, respectively. The parameter N was varied from 0 to 30.

(more N), the final compression factor $\hat{\nu}_{fin}$ should decrease. Figure 5.16 supports this conclusion, as more doses of inhibition cause the cells to jump more, providing more opportunities for time compression.

The rate constant τ_a has the opposite effect of N. If τ_a is increased, $\hat{\nu}_{fin}$ increases, providing less compression. For higher values of τ_a, D recovers more slowly and therefore g_n decreases more rapidly. Each time the cells receive inhibition, they jump to a lower value of g_n than if D *did* recover. Therefore, there is less compression during each jump. Figure 5.17 agrees with this line of reasoning.

As the inhibition period, T_{in} increases, compression increases. This makes sense, since a longer time between inhibitions allows D to recover more and the jumps from $g_n^{T_{in}}$ to g_{n+1} are larger, providing more compression during each jump. Figure 5.18 demonstrates this result.

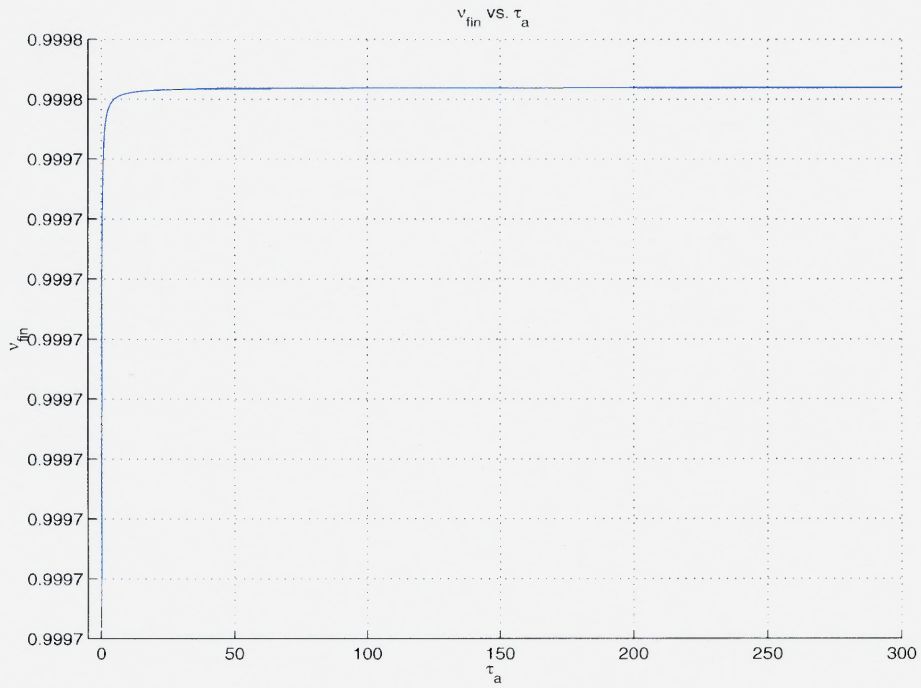

Figure 5.17 Compression Decreases as τ_a Increase. In this simulation, $\gamma = 0.5$ msec^{-1}, $N = 5$, $T_{in} = \frac{1}{200}$ msec, $\tau_b = 5$ msec and $g_{syn} = 0.04\frac{mS}{cm^2}$. The starting amounts of E for Cell 1 and Cell 2 were 0 and 1, respectively. The parameter τ_a was varied from 0.1 to 300 msec.

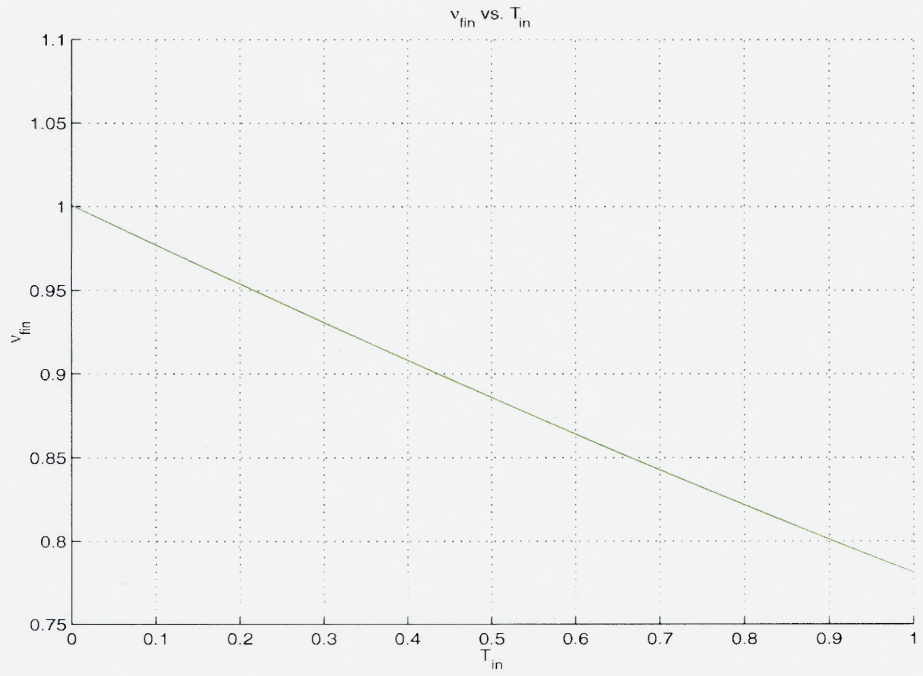

Figure 5.18 Compression Increases as T_{in} Increases. In this simulation, $\gamma = 0.5$ msec^{-1}, $N = 5$, $\tau_a = 100$ msec, $\tau_b = 5$ msec and $g_{syn} = 0.04\frac{mS}{cm^2}$. The starting amounts of E for Cell 1 and Cell 2 were 0 and 1, respectively. The parameter T_{in} was varied from 0.001 to 1 msec.

In Figures 5.16 and 5.17, even though compression can be improved by correctly varying N and τ_a, respectively, the improvement shown is minimal. This is due to an assumption made earlier, in Section 5.6. It was assumed that $\frac{1}{\tau_k} = \frac{1}{\tau_{rec}} = \gamma$ so a time to fire could be derived. In order to see the effects of sodium channel inactivation, τ_{rec} needs to be made sufficiently large. However, according to the condition given by (4.13), ρ must be less than 1 for compression to occur. Using the parameter values given in Chapter 3, particularly the choice for τ_a, the time compression is small. In order for the compression to be more pronounced, τ_a would need to be smaller, but by the condition mentioned above, τ_k would need to be smaller as well and the effects of sodium channel inactivation would become negligible. Cases without the assumption, $\frac{1}{\tau_k} = \frac{1}{\tau_{rec}} = \gamma$, are left for future work.

Table 5.1 Summary of How Time Compression is Affected by Varying Certain Parameters

Parameter	*Effect*	*Why*
Increasing N	Compression Increases	More inhibitions provide more time compressions
Increasing τ_a	Compression Decreases	Weaker synaptic strengths due to depression cause less time compression
Increasing T_{in}	Compression Increases	Long time between inhibitions allows for more synaptic recovery and therefore more time compression when the inhibition is applied

By modulating the parameters, the randomness of the initial time distance can be overcome and the cells can be made to fire at any time distance. The marginal density for u, as calculated in Section 5.7.1, provides a distribution for the initial time distances, depending on the available amount of sodium channels, as depicted in Figure 5.19 for the sample distribution (5.18).

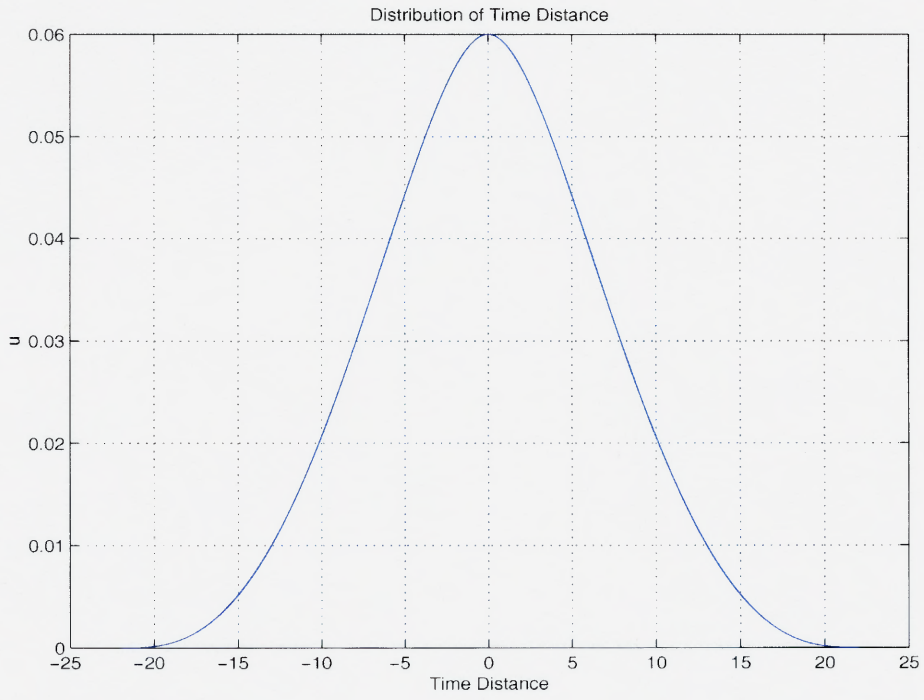

Figure 5.19 The marginal density for initial time distances between cells. Both cells start with all available channels $E_1 = E_2 = 1$ and maximum inhibition $g_n = 1$. The area under the curve from -1 to 1 is the probability that the cells will fire within 1 msec of each other, for the distribution (5.18).

This will determine the probability that the two cells will fire within a given time interval. As an example, using the density described in (5.18), the cells have a 95% chance of firing within 18.275 msec of each other (calculated using the MATLAB program in Appendix D). A 95% confidence interval that the cells will fire within 1 msec of each other is desired. The parameters need to be chosen in such a way so that $18.275\hat{\nu}_{fin} = 1$.

Biologically, the correct parameter combination may be found through some sort of feedback from the pyramidal cells to the interneurons. Therefore, the interneurons are able to cause these changes in "biological parameters" and affect pyramidal cell timing.

CHAPTER 6

CONCLUSION

The Sharp Wave-Associated Ripple is thought to have powerful impact on post-hippocampal targets, due to the amount of excitation involved in its formation [50]. It is possible that some sort of information processing is occurring during the SPWR that may be passed beyond the CA1 region. How information is encoded in neuronal spike trains is a fundamental question of neuroscience. Two theories dominate the debate of how this occurs. One school of thought insists information is embedded in the mean rate of firing of a neuron. The opposite paradigm suggests that the information is represented by the precise temporal structure of the signal [39]. If one agrees with the latter theory, it may be important to show how two or more pyramidal cells can synchronize in time. This dissertation is devoted to addressing that topic.

As with many tasks, it is sensible to start small and work towards a loftier goal. In this spirit, the PIP network, a simplified, subnetwork of the CA1 region, was considered. The PIP network reproduced several natural characteristics of the CA1 architecture. Interneurons synapse onto the pyramidal cells. The pyramidal cell layer within the CA1 region has very sparse connectivity when compared with the CA3 region [8], so the pyramidal cells where not connected. Additionally, the inhibitory synapses were depressing. Each pyramidal cell also contained simulated, intracellular noise, mimicking results shown in [30]. The noise was attributed to sodium channel inactivation, as discussed in [25, 31, 17].

During simulations, the interneuron applied high-frequency inhibition to the pyramidal cells and it was wondered whether the pyramidal cells would synchronize. Results showed that the cells did indeed synchronize, and they fired twice synchronously. It was hypothesized that as the Sharp Wave excitation inundated the interneurons, the frequency of inhibition applied to the pyramidal cells prevented

them from firing at first, and the cell synchronized below threshold. When the excitation reached the pyramidal cells, it caused them to fire for the first time, due to the rapid excitatory input. However, when the cells fired, intracellular noise was introduced into the system, due to the sodium channel inactivation. Additionally, the pyramidal cell were again being bombarded by high-frequency inhibition. While recovering below threshold, the pyramidal cells synchronize again, but this time, due to synaptic depression, the pyramidal cells can fire a second time before the Sharp Wave excitation leaves the area. The question was whether these observed synchronous solutions existed analytically and whether they were stable.

Initially, it was proven that, without intrinsic noise, two stable, synchronous, periodic solutions exist in the PIP network. The type of periodic solution depended on the presence of depressing synapses and the frequency of the inhibition. The first periodic orbit is sub-threshold, and the pyramidal cells never fire. The second periodic solution produces action potentials and can be further divided into two subtypes, depending on the rate of recovery of the depressing synapse. One subtype oscillates at the intrinsic frequency of the pyramidal cells. The other subtype of the action potential-producing periodic solutions must wait for the synaptic strength to decay sufficiently before being able to fire at the intrinsic frequency. Thus, it was shown that the high-frequency inhibition applied during the SPWR affects the pyramidal cells' spike timing and their ability to fire. Similar results were shown in [33], where fast, periodic input modulated a slower rhythm within the stomatogastric system of the *Cancer borealis* crab.

Several factors have been proposed that affect the firing times of action potentials: non-linear properties of dendrites [23] and dynamic membrane properties of neurons, such as sodium channel inactivation. If sodium channel inactivation is factored into the pyramidal cells' cellular processes, the sub-threshold, periodic solution was still shown to exist and be stable, because the noise produced by sodium

channel inactivation would decay if the pyramidal cells never fired. If the pyramidal cells were able to produce action potentials, more machinery was needed to describe the synchrony between pyramidal cells, due to the source of intrinsic noise added each time the cells fired. Confidence intervals for firing times between pyramidal cells were derived, in general and for a particular distribution of sodium channel usage. Time compression between the intrinsically noisy pyramidal cells while receiving repeated inhibition was also quantified. Furthermore, it was shown that the effects of intracellular noise were reduced (i.e. reliability of the cells was improved) by modulating synaptic depression. This is supported by [14, 15].

Depressing synapses have become a important topic in neuroscience. Depressing synapses have been shown to increase signal-to-noise ratios in small integrate-and-fire networks [51], as well as being able to discriminate coherent information from spike trains produced by networks of neurons [40]. It is shown in this dissertation that depressing synapses actually aid in producing action potentials, both in the presence of and in the absence of intracellular noise. Also, depression is shown to improve the reliability of spike generation among pyramidal cells. Articles by Fukai and Kanemura [14, 15] support this conclusion. They demonstrated that depressing synapses suppress noise in networks of inhibitory and excitatory, integrate-and-fire neurons.

The story of the Sharp Wave-Associated Ripple does not end here. There are many questions that still need to be answered. For example, while stable periodic orbits were found in the PIP subnetwork, a more realistic model would include many more neurons, of both interneurons and pyramidal cells. Also, while connectivity between pyramidal cells is sparse in the CA1 region, there are certainly many connections leading from the pyramidal cells to the interneurons. With these additions to the network architecture, do stable synchronous solution still exist? If the CA1 region is sufficiently represented, they must, since we observe the ripple

experimentally. However, is the ripple a function of a particular network structure or can any population of randomly connected interneurons and pyramidal cells produce the same result? In [13, 27], for networks of reciprocally connected excitatory and inhibitory neurons, with synaptic delays, "doublets" fired by interneurons have been shown to synchronize the network.

While studying synchronization among neurons, it is easy to neglect spatial characteristics of the brain. As briefly discussed in Chapter 1, the pyramidal cells in the CA1 region not only synchronize in time during the ripple, they also synchronize spatially across the CA1 region. The model presented in Chapter 3 ignores synaptic delays, but it is believed it would also hold for very small delays (by continuous dependence on parameters). Realistically, larger delays may occur between pyramidal cells in different parts of the CA1 region. So, how do larger synaptic delays affect the previous analysis? For small networks of mutually coupled, self-inhibiting neurons, long synaptic delays have been shown to produce stable, synchronous oscillations [1, 29].

Besides pyramidal cells, the interneurons also synchronize during the ripple, both temporally and spatially. Additionally, they do this in a very short interval of time, during the beginning of the ripple. Computational investigations of networks of heterogeneous, mutually inhibitory neurons [49] suggest that, at high oscillation frequencies, these types of networks lead to non-synchronous (asynchronous) behavior. Non-chemical connections called *gap junctions* (direct links between neurons that allow ions to flow freely from one neuron to another) have been proposed to bring about the synchronization [16]. Gap junction were considered a candidate for synchronization due to observed absence of ripples in the presence of halothane [50], which depresses excitatory synaptic transmissions [35]. Also, numerical studies have shown that strong electrotonic coupling by gap junctions will tend to synchronize cells, while weak coupling will help move cells to non-synchronous configurations

[7, 41]. Despite promising modeling results, gene knock-out experiments have shown that ripples are still produced, despite the absence of gap junctions [10, 22]. Could a combination of both types of connections rapidly synchronize the CA1 interneurons? Or, perhaps the cells coordinate through a different mechanism altogether?

Lastly, pyramidal cells and interneurons are not identical throughout the brain. How would the results of this dissertation hold under heterogeneity among the pyramidal cells. In one article [34], it is shown that for networks of heterogeneous, excitatory, spiking neurons synchrony is more stable than for networks of inhibitory neurons, at low firing rates. However, at high firing rates, the excitatory networks are unable to stay synchronized. Strong internal and external inputs enhance synchrony at high firing rates for inhibitory networks. Another reference [49] proposes that, for networks of heterogeneous, mutually inhibited neurons, the level of synchrony depends on the ratio of synaptic decay time versus the period of repetitive action potentials.

The purpose and mechanisms of the Sharp Wave-Associated Ripple may elude scientists for the near future. However, history shows us that discovery is a series of steps, sometimes leaps, sometimes tip-toes. Neuroscience has advanced a long way since the days of phrenology and aggregate field theory. This researcher has enormous faith that someday the mysteries of the SPWR and the brain itself will be revealed.

APPENDIX A

DERIVATION OF THE SEQUENCE $\{g_n\}$

Recall from Section 3.2 that g_n depends on D, the amount of synaptic resources. Assume initially that $D = D_0 > 0$ so that $s = s_0 > 0$ or $g = g_0 > 0$, and the cell cannot access a knee to fire before more inhibition is applied. Recall that $D_0 \in [0, 1]$. While the interneuron is above the synaptic threshold, D decays according to

$$\frac{dD}{dt} = -\frac{D}{\tau_b},$$

as introduced in (3.18). When the interneuron becomes silent, the new value of D is $\hat{D} = D_0 e^{-B}$, where $B = \frac{\Delta t_f}{\tau_b}$ and Δt_f is the time the interneuron spends above threshold, as described in Section 3.5. It must be noted that while the pyramidal cell is analyzed in the singular limit, the interneuron must spend a non-zero amount of time in the active phase for the analysis below to be valid. Otherwise, if the interneuron produced infinitely sharp action potentials, D would never decay and the synapse would not depress.

When silent, D recovers according to

$$\frac{dD}{dt} = \frac{1 - D}{\tau_a},$$

which has a solution $D(t) = 1 - (1 - \hat{D})e^{-\frac{t}{\tau_a}} = 1 - e^{-\frac{t}{\tau_a}} + \hat{D}e^{-\frac{t}{\tau_a}}$. Since the period of the interneuron, T_{in}, is approximately equal to the time it spends in the silent phase, $D_1 = 1 - e^{-A} + D_0 e^{-B} e^{-A}$, where $A = \frac{T_{in}}{\tau_a}$. By iterating this, a sequence $\{D_n\}$ emerges:

$$\begin{aligned} D_1 &= 1 - e^{-A} + D_0 e^{-B} e^{-A} \qquad \text{(A.1)} \\ D_2 &= 1 - e^{-A} + e^{-B} e^{-A} - e^{-B} e^{-2A} + D_0 e^{-2B} e^{-2A} \\ D_3 &= 1 - e^{-A} + e^{-B} e^{-A} - e^{-B} e^{-2A} + e^{-2B} e^{-2A} - e^{-2B} e^{-3A} + D_0 e^{-3B} e^{-3A} \\ &\vdots \end{aligned}$$

The sequence can be represented as

$$\begin{aligned} D_1 &= 1 - \left(e^B + D_0\right) e^{-(A+B)} \\ D_n &= 1 - \left(e^B - D_0\right) e^{-n(A+B)} - \left(e^B - 1\right) \sum_{k=1}^{n-1} e^{-k(A+B)}. \end{aligned} \tag{A.2}$$

for $n = 2, 3, \ldots$.

The sequence $\{D_n\}$ is decreasing since $B > 0$, $e^B > 1 \geq D_0 \geq 0$, and each term in the series is positive. The finite sum can be readily calculated to obtain

$$\begin{aligned} D_n &= 1 - \left(e^B - 1\right)\left(\frac{1 - e^{-n(A+B)}}{1 - e^{-(A+B)}} - 1\right) - \left(e^B - D_0\right) e^{-n(A+B)} \\ &= \frac{1 - e^{-A} + e^{-n(A+B)}\left[D_0(1 - e^{-(A+B)}) + e^{-A} - 1\right]}{1 - e^{-(A+B)}}, \end{aligned} \tag{A.3}$$

and it is clear that $D_n \to \frac{1-e^{-A}}{1-e^{-(A+B)}}$, as $n \to \infty$.

Now, it is possible to address Theorem 1. Each time the interneuron moves above threshold, s is set equal to D_n, and $g = g_n$, where $g_n = g_{syn} D_n = g_{syn} s$. So,

$$g_n = g_{syn}\left(\frac{1 - e^{-A} + e^{-n(A+B)}\left[D_0(1 - e^{-(A+B)}) + e^{-A} - 1\right]}{1 - e^{-(A+B)}}\right), \tag{A.4}$$

and as $n \to \infty$, $g_n \to g_\infty$, where

$$g_\infty = g_{syn} \frac{1 - e^{-A}}{1 - e^{-(A+B)}}. \tag{A.5}$$

The variable $g = g_{syn} s$ decays according to the equation

$$\frac{dg}{d\tau} = -\frac{g}{\tau_k}, \tag{A.6}$$

so that $g(\tau) = g_{syn} s e^{-\frac{\tau}{\tau_k}} = g e^{-\frac{\tau}{\tau_k}}$. After T_{in} time, while the interneuron is in its silent phase, $g_n(T_{in}) \equiv g_n^{T_{in}} = g_n e^{-K}$, where $K = \frac{T_{in}}{\tau_k}$.

Therefore, during each cycle of inhibition, g decays to

$$g_n^{T_{in}} = g_{syn} e^{-K}\left(\frac{1 - e^{-A} + e^{-n(A+B)}\left[D_0(1 - e^{-(A+B)}) + e^{-A} - 1\right]}{1 - e^{-(A+B)}}\right). \tag{A.7}$$

And, as $n \to \infty$, $g_n^{T_{in}} \to g_\infty^{T_{in}}$, where

$$g_\infty^{T_{in}} = g_{syn} e^{-K} \frac{1 - e^{-A}}{1 - e^{-(A+B)}}. \tag{A.8}$$

If $D_0 = 1$, meaning that initially the synapse has all of its resources at its disposal, then

$$g_n = g_{syn} \left[\frac{1 - e^{-A} + e^{-A} e^{-n(A+B)} (1 - e^{-B})}{1 - e^{-(A+B)}} \right] \tag{A.9}$$

and

$$g_n^{T_{in}} = g_{syn} e^{-K} \left[\frac{1 - e^{-A} + e^{-A} e^{-n(A+B)} (1 - e^{-B})}{1 - e^{-(A+B)}} \right]. \tag{A.10}$$

However, they still approach the same steady states given in (A.5) and (A.8), respectively.

APPENDIX B

PROOF OF THREE T_{in} INTERVALS IN THEOREM 1

Proof. Written in expanded form, (4.8) can be expressed as:

$$\Omega(T_{in}) = g_{syn} e^{-\frac{T_{in}}{\tau_k}} \frac{1 - e^{-\frac{T_{in}}{\tau_a}}}{1 - e^{-\frac{T_{in}}{\tau_a}} e^{-B}} - g^* > 0. \tag{B.1}$$

The range for T_{in} is $[0, \infty]$. As $T_{in} \to \infty$, $\Omega \to -g^*$, and as $T_{in} \to 0$, $\Omega \to -g^*$. Thus, Ω decreases to a negative number at both endpoints of the T_{in} domain.

Now consider $\Omega'(T_{in})$:

$$\Omega'(T_{in}) = \frac{g_{syn} e^{-\frac{T_{in}}{\tau_k}}}{1 - e^{-\frac{T_{in}}{\tau_a}} e^{-B}} \left[\frac{e^{-\frac{T_{in}}{\tau_a}} - 1}{\tau_k} + \frac{e^{-\frac{T_{in}}{\tau_a}}}{\tau_a} \frac{1 - e^{-B}}{1 - e^{-\frac{T_{in}}{\tau_a}} e^{-B}} \right]. \tag{B.2}$$

The local extrema occur when

$$\frac{e^{-\frac{T_{in}}{\tau_a}} - 1}{\tau_k} + \frac{e^{-\frac{T_{in}}{\tau_a}}}{\tau_a} \frac{1 - e^{-B}}{1 - e^{-\frac{T_{in}}{\tau_a}} e^{-B}} = 0, \tag{B.3}$$

or when

$$\tau_a \left(e^{-\frac{T_{in}}{\tau_a}} - 1 \right) \left(1 - e^{-\frac{T_{in}}{\tau_a}} e^{-B} \right) + \tau_k e^{-\frac{T_{in}}{\tau_a}} \left(1 - e^{-B} \right) = 0. \tag{B.4}$$

By letting $x = e^{-\frac{T_{in}}{\tau_a}}$ and using the quadratic equation, two values of T_{in} satisfy (B.4),

$$T_{in} = \tau_a \ln \left[\frac{2e^{-B}}{1 + e^{-B} + \frac{\tau_k}{\tau_a}(1 - e^{-B}) \pm \sqrt{\left(1 + e^{-B} + \frac{\tau_k}{\tau_a}(1 - e^{-B})\right)^2 - 4e^{-B}}} \right]. \tag{B.5}$$

By inspection, the "positive" root, T_{in}^+, is negative (and outside the acceptable range for T_{in}), since the denominator inside the natural logarithm is greater than $2e^{-B}$.

The "negative" root, T_{in}^-, is positive, as demonstrated in the following argument. Consider the terms under the square root. They can be re-written as

$$\left(1 - \frac{\tau_k}{\tau_a}\right)^2 e^{-2B} - 2\left(1 + \left(\frac{\tau_k}{\tau_a}\right)^2\right) e^{-B} + \left(1 + \frac{\tau_k}{\tau_a}\right)^2. \tag{B.6}$$

The smallest value that (B.6) can equal, that of 0, occurs when $B = 0$. When $B > 0$, (B.6) must be positive. Therefore, if (B.6) is written as

$$\left(1+e^{-B}+\frac{\tau_k}{\tau_a}\left(1-e^{-B}\right)\right)^2\left(1-\frac{4e^{-B}}{\left(1+e^{-B}+\frac{\tau_k}{\tau_a}\left(1-e^{-B}\right)\right)^2}\right), \tag{B.7}$$

the fractional term is less than 1. Factoring out $\left(1+e^{-B}+\frac{\tau_k}{\tau_a}\left(1-e^{-B}\right)\right)^2$ from underneath the square root, the denominator for the T_{in}^- in (B.5) can be expressed as

$$1+e^{-B}+\frac{\tau_k}{\tau_a}\left(1-e^{-B}\right)- \tag{B.8}$$
$$\left(1+e^{-B}+\frac{\tau_k}{\tau_a}\left(1-e^{-B}\right)\right)\sqrt{1-\frac{4e^{-B}}{\left(1+e^{-B}+\frac{\tau_k}{\tau_a}(1-e^{-B})\right)^2}}.$$

Using a Taylor series for the square root term, (B.8) becomes

$$\frac{2e^{-B}}{\left(1+e^{-B}+\frac{\tau_k}{\tau_a}\left(1-e^{-B}\right)\right)^2}-\frac{2e^{-2B}}{\left(1+e^{-B}+\frac{\tau_k}{\tau_a}\left(1-e^{-B}\right)\right)^4}+\ldots, \tag{B.9}$$

which, by inspection, is less than

$$\frac{2e^{-B}}{\left(1+e^{-B}+\frac{\tau_k}{\tau_a}\left(1-e^{-B}\right)\right)^2}. \tag{B.10}$$

Therefore, since the denominator for T_{in}^- in (B.5) is less than (B.10), the whole fraction is greater than 1 and T_{in}^- is positive.

Having shown that there exists a single extrema in the domain for T_{in}, it is next shown to be a maximum. Consider (B.2) again. Suppose $T_{in} = \delta$, then δ clearly can be chosen to satisfy $0 < \delta < T_{in}^-$ and $\delta \ll 1$. Hence, $e^{-\frac{T_{in}}{\tau_a}} = e^{-\frac{T_{in}}{\tau_k}} \approx 1$ and

$$\Omega' \approx \frac{g_{syn}}{\tau_a\left(1-e^{-B}\right)} > 0. \tag{B.11}$$

Therefore, the slope for values less than T_{in}^- is greater than 0.

Now, suppose $T_{in} \to \infty$. This implies that $e^{-\frac{T_{in}}{\tau_a}} = e^{-\frac{T_{in}}{\tau_k}} \approx \delta$ (another arbitrarily small, positive number) and (B.2) becomes

$$\begin{aligned} \Omega' &\approx \frac{g_{syn}\delta}{1-\delta}\left[\frac{\delta-1}{\tau_k} + \frac{\delta}{\tau_a}\frac{1-e^{-B}}{1-\delta}\right] \\ &\approx -\delta\frac{g_{syn}}{1-\delta} < 0. \end{aligned} \tag{B.12}$$

The slope for values of $T_{in} > T_{in}^{-}$ is negative. Therefore, T_{in}^{-} is a maximum.

The last condition needed to prove there exists three intervals for T_{in} is that a portion of $\Omega(T_{in})$ must be positive. If $g^* = 0$, $\Omega > 0$ for all $T_{in} > 0$. Since Ω depends continuously on g^* in a linear fashion, as g^* increases from 0, there will be portions of Ω that will be greater than 0. This will occur for values of $g^* < \Omega(T_{in}^{-})$.

Having shown that Ω has a single maximum, whose value is positive, and that on either side of this maximum, Ω approaches a negative value, then there must be two roots for Ω, dividing the T_{in} domain into three intervals. □

APPENDIX C

MATLAB CODE #1

This is the first MATLAB code. The program divides the region of integration into a grid and uses Simpson's Method to do the double integration. The output is the percent confidence that the cells fire within a certain time interval of each other.

```
clear all
format long

global gam m E1 E2 gn g0 u1 u2 v1 v2

gam=0.05;
m=input ('Enter m:');
E1=input ('Enter E1:');
E2=input ('Enter E2:');
gn=input ('Enter gn:');
g0=input ('Enter g0:');
tint=input ('Enter time interval:');
uleft=-tint;
uright=tint;
step=input ('Steps?');

% Defines the region of integration.

u1=(1/gam)*log(gn/g0);
u2=(1/gam)*log((gn+(m*E1))/g0);
```

```
v1=(1/gam)*log(gn/g0);
v2=(1/gam)*log((gn+(m*E2))/g0);

u=linspace(uleft,uright,step);

v=linspace(v1,v2,step);

% The function to be integrated.

c1=6/(E1^3);
c2=6/(E2^3);
a=c1*c2*(gam^2)*(g0^2)/(m^2);

% Step Sizes

hu=(uright-uleft)/step;
hv=(v2-v1)/step;

% Defines a matrix equivalent to Simpson's Integration

trapz=2*ones(1,step)/2;
trapz(1,1)=trapz(1,1)/2;
trapz(1,step)=trapz(1,step)/2;
trapz;

% Determines which portions of the integration region equal 0
```

```
for i=1:step
    for j=1:step
        su=uleft+(i-1)*hu;
        sv=v1+(j-1)*hv;
        d1=((g0*exp(gam*(su+sv)))-gn)/m;
        d2=((g0*exp(gam*sv))-gn)/m;
        r=exp(gam*(su+(2*sv)));
        if (su>(u1-sv))&(su<(u2-sv))&(sv<v2)&(sv>v1)
            h(i,j)=a*r*(E1-d1)*(E2-d2)*d1*d2;
        else
            h(i,j)=0;
        end
    end
end

% Simpson's Integration in the v-direction

clear i j
for i=1:step
    uh(i)=hv*h(i,:)*trapz';
end

% Simpson's Integration in the u-direction

utot=hu*uh*trapz';

perc=utot*100
```

APPENDIX D

MATLAB CODE #2

This is the second MATLAB code. It does the opposite of the MATLAB code in Appendix C. It asks for a certain percent confidence and it outputs the corresponding time interval for which both cells will fire together with the given percent confidence. The program uses an iterative method by which it takes an initial guess for the time interval, uses the Simpson's Integration Method to determine the percent confidence for the initial guess, and if the percentage is not within a certain tolerance of the desired percentage, it reduces its search interval by half and repeats the process.

```
clear all
format long

gam=0.05;

gn=input ('Enter gn:');
gsyn=0.5;

perct1=input ('Enter percentage of confidence:');
perct=perct1/100;
int1=input ('Enter initial guess of interval:');
int2=0;
int3=21;
m=input ('Enter m:');
E1=input ('Enter E1:');
E2=input ('Enter E2:');
gstar=input ('Enter gstar:');
```

```
count=0;

step=input ('Steps of Integration?');

tol=0.0001;
toltest=1;

% Defines the region of integration.

u1=(1/gam)*log(gn/gstar);
u2=(1/gam)*log((gn+(m*E1))/gstar);

v1=(1/gam)*log(gn/gstar);
v2=(1/gam)*log((gn+(m*E2))/gstar);
v=linspace(v1,v2,step);

% Main loop that occurs while outside of tolerance

while abs(toltest)>tol

    count=count+1;

    uleft=-int1;
    uright=int1;
    u=linspace(uleft,uright,step);

    % Function to be integrated
```

```
c1=6/(E1^3);
c2=6/(E2^3);
a=c1*c2*(gam^2)*(gstar^2)/(m^2);

% Step Sizes

hu=(uright-uleft)/step;
hv=(v2-v1)/step;

% Simpson's Integration Matrix

trapz=2*ones(1,step)/2;
trapz(1,1)=trapz(1,1)/2;
trapz(1,step)=trapz(1,step)/2;
trapz;

% Determines which portion of the integration region equal 0

for i=1:step
    for j=1:step
        su=uleft+(i-1)*hu;
        sv=v1+(j-1)*hv;
        d1=((gstar*exp(gam*(su+sv)))-gn)/m;
        d2=((gstar*exp(gam*sv))-gn)/m;
        r=exp(gam*(su+(2*sv)));
        if (su>(u1-sv))&(su<(u2-sv))&(sv<v2)&(sv>v1)
```

```
            h(i,j)=a*r*(E1-d1)*(E2-d2)*d1*d2;
        else
            h(i,j)=0;
        end
    end
end

% Simpson's Integration in the v-direction

clear i j
for i=1:step
    uh(i)=hv*h(i,:)*trapz';
end

% Simpson's Integration in the u-direction

utot=hu*uh*trapz';

% Checking to see if the result is within tolerance

toltest=utot-perct;

utottol=[utot toltest]
ep=[int2 int1 int3]

if toltest>0
    int3=int1;
```

```
        int1=(int1+int2)/2;
    else
        int2=int1;
        int1=(int3+int1)/2;
    end


    if count>100
        break
    end

end
```

APPENDIX E

XPP PROGRAM

The simulation results presented in this paper were computed using the program XPP, developed by Bard Ermentrout [12].

```
# ICs
i i1=-70
i p1=-70
i p2=-70
i wp1=0.4
i wp2=0.4
i d1=1 si1p1=0
i d2=1 si1p2=0
i R1=1
i E1=0
i scp1=0
i R2=1
i E2=0
i scp2=0



# Parameters
p Cp=1 Ci=1
p gNap=100 gNai=100
p VNap=50 VNai=50
p gKp=80 gKi=80
p VKp=-100 VKi=-100
```

```
p gLp=0.05 gLi=0.05

p VLp=-66.65 VLi=-63.8

p Ip1=0  Ip2=0 Ii1=0.35

p SWp1=2  SWp2=2 SWi1=12

p gi1p1=0.04 gi1p2=0.04

p Vesyn=0 Visyn=-80


# Rate of decay for s and d while on the right

p taub=5


# Rate of decay for s       while on the left

p tauk=100


# Rate of recovery for d    while on the left

p taua=100


p di1p1=0 di1p2=0

p taurec=100

p swsi=250 swipeak=280

p swsp=260 swepeak=275

p varr=0.5  ryn=0 ryn1=0 ryn2=0 ryn3=0


# Global Flags


global 1 {t-0.001} {E1=ran(0.4)}

global 1 {t-0.002} {R1=1-E1}

global 1 {t-0.001} {E2=ran(0.4)}
```

```
global 1 {t-0.002} {R2=1-E2}

global 1 {t-0.001} {scp1=ran(R1)}

global 1 {t-0.001} {scp2=ran(R2)}

global 1 {p1} {scp1=ran(R1)}

global 1 {p2} {scp2=ran(R2)}

global 1 {p1} {E1=E1+scp1*R1}

global 1 {p1} {R1=R1*(1-scp1)}

global 1 {p2} {E2=E2+scp2*R2}

global 1 {p2} {R2=R2*(1-scp2)}

global 1 {i1} {si1p1=d1}

global 1 {i1} {si1p2=d2}

global 1 {t-swsi} {SWi=1}

global 1 {t-swei} {SWi=0}


# Tables


table randm r0.tab

table randm1 r1.tab

table randm2 r2.tab

table randm3 r3.tab



# Equations


swei=swsi+100

swep=swsp+80
```

```
H(v)=heav(v)

am(v)=0.32*(54+v)/(1-exp(-(v+54)/4))
bm(v)=0.28*(v+27)/(exp((v+27)/5)-1)
minf(v)=am(v)/(am(v)+bm(v))

hg(n)=(1-1.25*n)*H(1-1.25*n)

an(v)=0.032*((v+53.75)/(1-exp(-(v+53.75)/5)))
bn(v)=0.5*exp(-(58.75+v)/40)

s(v)=1+tanh(v/4)

randy=ryn*varr*randm(t)+ryn1*varr*randm1(t)+
    ryn2*varr*randm2(t)+ryn3*varr*randm3(t)



# ODEs

SWi'=0
SWe'=H(t-swsp)/(swepeak-swsp)-H(t-swepeak)*(1/(swepeak-swsp)+
    1/(swep-swepeak))+H(t-swep)/(swep-swepeak)

i1'=(Ii1+SWi1*SWi-gLi*(i1-VLi)-gKi*(ni1^4)*(i1-VKi)-
    gNai*(minf(i1)^3)*hg(ni1)*(i1-VNai))/Ci
ni1'=an(i1)*(1-ni1)-bn(i1)*ni1
si1p1'=-(1/taub)*si1p1*s(i1)-(1/tauk)*si1p1*s(-i1)
```

```
d1'=-(1/taub)*d1*s(i1)+(1/taua)*(1-d1)*s(-i1)
si1p2'=-(1/taub)*si1p2*s(i1)-(1/tauk)*si1p2*s(-i1)
d2'=-(1/taub)*d2*s(i1)+(1/taua)*(1-d2)*s(-i1)

p1'=(randy+Ip1+SWp1*SWe-gLp*((p1-E1)-VLp)-gKp*(wp1^4)*((p1-E1)-VKp)-
    gNap*(minf((p1-E1))^3)*hg(wp1)*((p1-E1)-VNap)-
    gi1p1*delay(si1p1,di1p1)*((p1-E1)-Visyn))/Cp
wp1'=an(p1)*(1-wp1)-bn(p1)*wp1

p2'=(randy+Ip2+SWp2*SWe-gLp*((p2-E2)-VLp)-gKp*(wp2^4)*((p2-E2)-VKp)-
    gNap*(minf((p2-E2))^3)*hg(wp2)*((p2-E2)-VNap)-
    gi1p2*delay(si1p2,di1p2)*((p2-E2)-Visyn))/Cp
wp2'=an(p2)*(1-wp2)-bn(p2)*wp2

# Sodium Channels

R1'=E1/taurec
E1'=-E1/taurec
scp1'=0

R2'=E2/taurec
E2'=-E2/taurec
scp2'=0

# Auxiliary Equation

aux random=randy
```

```
# Xpp Settings

@ Dt=0.01, total=600, maxstor=550000, bounds=50000
@ nplot=3, xp1=t, yp1=p1, xp2=t, yp2=p2, xp3=t, yp3=i1
@ nmesh=200, delay=1000
```

BIBLIOGRAPHY

[1] A. Bose and S. Kunec, *Synchrony and frequency regulation by synaptic delay in networks of self-inhibiting neurons*, Neurocomputing, 38-40 (2001), pp. 505–513.

[2] A. Bose, Y. Manor, and F. Nadim, *Bistable oscillations arising from synaptic depression*, SIAM Journal of Applied Mathematics, 62 (2001), pp. 706–727.

[3] A. Bragin, G. Jando, Z. Nadasdy, J. Hetke, K. Wise, and G. Buzsaki, *Gamma (40-100 Hz) oscillation in the hippocampus of the behaving rat*, Journal of Neuroscience, 15 (1995), pp. 47–60.

[4] G. Buzasaki and J. Chrobak, *Temporal structure in spatially organized neuronal ensembles: A role for interneuronal networks*, Curr. Opin. Neurobiol., 5 (1995), pp. 504–510.

[5] G. Buzsaki, *Two-stage model of memory trace formation: A role for "noisy" brain states*, Neuroscience, 31 (1989), pp. 551–570.

[6] G. Buzsaki, Z. Horvath, R. Urioste, J. Hetke, and K. Wise, *High-frequency network oscillation in the hippocampus*, Science, 256 (1992), pp. 1025–1027.

[7] C. C. Chow and N. Kopell, *Dynamics of spiking neurons with electrical coupling*, Neural Comp., 12 (2000), pp. 1643–1678.

[8] E. P. Christian and F. E. Dudek, *Electrophysiological evidence from glutamate microapplications for local excitatory circuits in the CA1 area of the rat hippocampal slices*, Journal of Neurophysiology, 59 (1988), pp. 110–123.

[9] J. Csicsvari, H. Hirase, A. Czurko, A. Mamiya, and G. Buzasaki, *Oscillatory coupling of hippocampal pyramidal cells and interneurons in the behaving rat*, Journal of Neuroscience, 19 (1999), pp. 274–287.

[10] M. R. Deans, J. R. Gibson, C. Sellito, B. W. Connors, and D. L. Paul, *Synchronous activity of inhibitory networks in neocortex requires electrical synapses containing Connexin36*, Neuron, 31 (2001), pp. 477–485.

[11] H. Eichenbaum, *Using olfaction to study memory*, Annals of the New York Academy of Science, 855 (1998), pp. 657–669.

[12] B. Ermentrout, *Simulating, Analyzing, and Animating Dynamical Systems: A Guide to XPPAUT for Researchers and Students*, SIAM, 2002.

[13] G. Ermentrout and N. Kopell, *Fine structure of neural spiking and synchronization in the presence of conduction delays*, Proc. Natl. Acad. Sci. USA, 95 (1998), pp. 1259–1264.

[14] T. Fukai and S. Kanemura, *Precisely timed transient synchronization by depressing synapses*, Neurocomputing, 32-33 (2000), pp. 133–140.

[15] ——, *Noise-tolerant stimulus discrimination by synchronization with depressing synapses*, Biol. Cybernetics, 85 (2001), pp. 107–116.

[16] M. GALARRETA AND S. HESTRIN, *Electrical synapses between GABA-releasing interneurons*, Neuroscience, 2 (2001), pp. 425–433.

[17] D. HENZE AND G. BUZSAKI, *Action potential threshold of hippocampal pyramidal cells* in vivo *is increased by recent spiking activity*, Neuroscience, 105 (2001), pp. 121–130.

[18] A. HODGKIN AND A. HUXLEY, *The components of membrane conductance in the giant axon of* loligo, Journal of Physiology (London), 116 (1952), pp. 473–496.

[19] ——, *Currents carried by sodium and potassium ions through the membrane of the giant axon of* loligo, Journal of Physiology (London), 116 (1952), pp. 449–472.

[20] ——, *The dual effect of membrane potential on sodium conductance in the giant axon of* loligo, Journal of Physiology (London), 116 (1952), pp. 497–506.

[21] ——, *A quantitative description of membrane current and its application*, Journal of Physiology (London), 117 (1952), pp. 500–544.

[22] S. G. HORMUZDI, I. PAIS, F. E. LEBEAU, S. K. TOWERS, A. ROZOV, E. H. BUHL, M. A. WHITTINGTON, AND H. MONYER, *Impaired electrical signaling disrupts gamma frequency oscillations in Connexin 36-deficient mice*, Neuron, 31 (2001), pp. 487–495.

[23] D. JAEGER, E. DE SCHUTTER, AND J. M. BOWER, *The role of synaptic and voltage-gated currents in the control of Purkinje cell spiking: A modeling study*, Journal of Neuroscience, 17 (1997), pp. 91–106.

[24] D. JOHNSTON AND S. M.-S. WU, *Foundations of Cellular Neurophysiology*, The MIT Press, 1999.

[25] H.-Y. JUNG, T. MICKUS, AND N. SPRUSTON, *Prolonged sodium channel inactivation contributes to dendritic action potential attentuation in hippocampal pyramidal neurons*, Journal of Neuroscience, 17 (1997), pp. 6639–6646.

[26] E. R. KANDEL, J. H. SCHWARTZ, AND T. M. JESSELL, *Principles of Neural Science*, Appleton & Lange, 1991.

[27] J. KARBOWSKI AND N. KOPELL, *Multispikes and synchronization in a large neural network with temporal delays*, Neural Computation, 12 (2000), pp. 1573–1606.

[28] C. KING, D. HENZE, X. LEINEKUGEL, AND G. BUZSAKI, *Hebbian modification of a hippocampal population pattern in the rat*, The Journal of Physiology, 521 (1999), pp. 159–167.

[29] S. KUNEC AND A. BOSE, *The role of synaptic delay in organizing the behavior of networks of self-inhibting neurons*, Physical Review E, 63 (2001), pp. 0219081–13.

[30] Z. F. MAINEN AND T. J. SEJNOWSKI, *Reliability of spike timing in neocortical neurons*, Science, 268 (1995), pp. 1503–1506.

[31] T. MICKUS, H.-Y. JUNG, AND N. SPRUSTON, *Properties of slow, cumulative sodium channel inactivation in rat hippocampal CA1 pyramidal neurons*, Biophysical Journal, 76 (1999), pp. 846–860.

[32] E. MISHCHENKO AND N. ROZOV, *Differential Equations with a Small Parameter and Relaxation Oscillations*, Plenum Press, New York, 1980.

[33] F. NADIM, Y. MANOR, M. P. NUSBAUM, AND E. MARDER, *Frequency regulation of a slow rhythm by a fast periodic input*, Journal of Neuroscience, (1998).

[34] L. NELTNER, D. HANSEL, G. MATO, AND C. MEUNIER, *Synchrony in heterogeneous networks of spiking neurons*, Neural Computation, 12 (2000), pp. 1607–1641.

[35] K.-I. NISHIKAWA AND M. B. MACIVER, *Membrane and synaptic actions of halothane on rat hippocampal pyramidal neurons and inhibitory interneurons*, Journal of Neuroscience, 20 (2000).

[36] J. O'KEEFE AND J. DOSTROVSKY, *The hippocampus as a spatial map*, Brain Research, 34 (1971), pp. 171–175.

[37] J. RUBIN AND D. TERMAN, *Geomeeric analysis of population rhythms in synaptically coupled neuronal networks*, Neural Computation, 12 (2000), pp. 597–645.

[38] ——, *Handbook of Dynamical Systems: Toward Applications*, vol. 3, Elsevier, Forthcoming, ch. Geometric Singular Perturbation Analysis of Neuronal Dynamics.

[39] R. V. RULLEN AND S. J. THORPE, *Rate coding versus temporal order coding: What the retinal ganglion cells tell the visual cortex*, Neural Computation, 13 (2001), pp. 1255–1283.

[40] W. SENN, I. SEGEV, AND M. TSODYKS, *Reading neuronal synchrony with depressing synapses*, Neural Computation, 10 (1998), pp. 815–819.

[41] A. SHERMAN AND J. RINZEL, *Rhythmogenic effects of weak electrotonic coupling in neuronal models*, Proc. Natl. Acad. Sci. USA, 89 (1992), pp. 2471–2474.

[42] D. SOMERS AND N. KOPELL, *Rapid synchronization through fast threshold modulation*, Biol. Cybern., 68 (1993), pp. 393–407.

[43] D. TERMAN, N. KOPELL, AND A. BOSE, *Dynamics of two mutually coupled slow inhibitory neurons*, Physica D, 117 (1998), pp. 241–275.

[44] R. F. THOMPSON, *The Brain: A Neuroscience Primer*, Worth Publishers, third ed., 2000.

[45] R. TRAUB AND R. MILES, *Neuronal Networks of the Hippocampus*, Cambridge Press, 1991.

[46] R. D. TRAUB AND A. BIBBIG, *A model of high-frequency ripples in the hippocampus based on synaptic coupling plus axon-axon gap junctions between pyramidal cells*, Journal of Neuroscience, 20 (2000), pp. 2086–2093.

[47] M. K. TSODYKS AND H. MARKRAM, *The neural code between neocortical pyramidal neurons depends on neurotransmitter release probability*, in Proc. Natl. Acad. Sci. USA, vol. 94 of Neurobiology, 1997, pp. 719–723.

[48] F. VARGAKHADEM, D. GADIAN, K. WATKINS, A. CONNELLY, W. VAN PAESSCHEN, AND M. MISHKIN, *Differential effects of early hippocampal pathology on episodic and semantic memory*, Science, 277 (1997), pp. 276–280.

[49] J. A. WHITE, C. C. CHOW, J. RITT, C. SOTO-TREVINO, AND N. KOPELL, *Synchronization and oscillatory dynamics in heterogeneous, mutually inhibited neurons*, Journal of Computational Neuroscience, 5 (1998), pp. 407–420.

[50] A. YLINEN, A. BRAGIN, Z. NADASDY, G. JANOD, I. SZABO, A. SIK, AND G. BUZSAKI, *Sharp wave-associated high-frequency oscillation (200 hz) in the intact hippocampus: Network and intracellular mechanisms*, Journal of Neuroscience, 15 (1995), pp. 30–46.

[51] L. ZALANYI, F. BAZSO, AND P. ERDI, *The effect of synaptic depression on stochastic resonance*, Neurocomputing, 38-40 (2001), pp. 459–465.